The Radio Science Bulletin

ISSN 1024-4530

INTERNATIONAL
UNION OF
RADIO SCIENCE

UNION
RADIO-SCIENTIFIQUE
INTERNATIONALE

No 324
March 2008

Publié avec l'aide financière de l'ICSU
URSI, c/o Ghent University (INTEC)
St.-Pietersnieuwstraat 41, B-9000 Gent (Belgium)

Contents

Front cover: A photo showing a meteor with aurora in the background. Towards the end, the meteor was seen to twinkle at least three times. Assuming that the strong trail was some 30 km long, the twinkles would occur within a distance of 4-5 km along the path (photo: Torbjörn Lövgren, Kiruna). See the paper by Asta-Pellinen-Wannberg, Gudmund Wannberg, Johan Kero, Csilla Szasz, and Assar Westman (pp. 17-28).

For information, please contact :
The URSI Secretariat
c/o Ghent University (INTEC)
Sint-Pietersnieuwstraat 41, B-9000 Gent, Belgium
Tel.: (32) 9-264 33 20, Fax: (32) 9-264 42 88
E-mail: info@ursi.org
http://www.ursi.org

Editorial

Our Papers

Spherical-multipole expansions have found wide use in both analytical and numerical methods for solving electromagnetic problems. Analytically, such expansions allow the fields to be expressed in terms of functions that can be more readily manipulated into tractable forms than can some other formulations. Numerically, series acceleration techniques, integral transforms, and parallel methods can make the resulting series quite efficient to evaluate. Ludger Klinkenbusch has provided a very nice invited *Review of Radio Science* from Commission B on the use spherical-multipole expansions. He illustrates the applications of such expansions to scattering by a semi-infinite circular cone, near-field-to-far-field transformations, and definitions of shielding effectiveness.

However, this paper also includes a very important, fundamental, new result. It is shown that if the electric or magnetic field at a single point and in a small neighborhood about that point in an arbitrary homogeneous domain is regular and known, then the electromagnetic field is regular and uniquely determined throughout the domain. Furthermore, the proof of this theorem is constructive: it provides a recipe for uniquely constructing the field through out the homogeneous domain from the field at a point and a small neighborhood around the point, using a spherical-multipole expansion. This result may have important implications for a variety of applications, including inverse scattering problems, measurements of scatterers and radiators, and numerical techniques for scattering and radiation.

The efforts of Karl Langenberg, Associate Editor for Commission B, and Phil Wilkinson in bringing us this review are gratefully acknowledged.

Observations of meteors have been a rich source of information about interplanetary matter for a long time. Historically, much of this data was obtained using specular meteor radars, primarily recording echoes from the trails of meteors. More recently, high-power large-aperture (HPLA) radars have been able to record echoes from the heads of meteors, providing much more information. In their invited *Review of Radio Science* from Commission G, Asta Pellinen-Wannberg, Gudmund Wannberg, Johan Kero, Csilla Szasz, and Assar Westman provide a very interesting review of both methods of meteor observation, with an emphasis on the important role now played by HPLA observations. They describe the process of observing meteors using both methods, and take a careful look at the observational parameters involved. They then explain the radio meteor ceiling effect, and its implications for meteor observations. They describe the HPLA method in detail, tracing its development. EISCAT, the European Incoherent Scatter facility, is presented as an in-depth example of how the method can be used. The results that been obtained using the HPLA method are reviewed. Finally, a description is given for the prospects of future planned HPLA facilities.

The efforts of Michael Rietveld, Associate Editor for Commission G, and Phil Wilkinson in bringing us this review are appreciated.

The analysis of a hologram in terms of an equivalent set of Fresnel zone plates has long been known, and is a commonly used qualitative method of explaining many of the properties of a hologram. Both holograms and Fresnel zone plates can also be used for imaging, spatial power combining, and for antenna applications. However, a quantitative comparison of the performance of holograms and Fresnel zone plates for such applications has not previously been available. Aldo Petosa and Apisak Ittipiboon provide just such a comparison in their paper. They begin with a nice summary of the analysis of the properties of elementary holograms and Fresnel zone plates. They then provide a quantitative comparison of the focal fields for the two structures, and they compare the far-field patterns. The comparisons show that Fresnel zone plates have somewhat better resolution and up to a 2 dB increase in focal power compared to the elementary hologram. When compared as antennas, Fresnel zone plates offer a 2.3 dB improvement in directivity and better sidelobe levels compared to holograms. The authors then look at the effects of the discretization often associated with manufacturing microwave and millimeter-wave holograms. They show that a hologram based on quantizing the phase results in better directivity than a hologram based on quantizing the amplitude.

Our Other Contributions

In his column on "Radio-Frequency Radiation Safety and Health," Jim Lin provides a critical review of recent studies of lymphoma-prone mice exposed to GSM cell-phone radiation. This is interesting both because of the results of the studies, and because of the various factors that affect these results and must be properly controlled.

Peter Watson has brought us a new set of dissertation abstracts in radio science. Please encourage those are about

to complete or have recently completed doctoral work in radio science to send in an abstract of their dissertation.

Sadly, in this issue we also have an "In Memoriam" for Wilbur Norman (Chris) Christiansen. He was a former President of URSI, and a pioneer in world radio astronomy.

The XXIX General Assembly of URSI

If you have not registered for and made reservations to attend the URSI General Assembly in Chicago, August 7-16, 2008, now is the time to do so. This will be an outstanding scientific meeting: over 1500 papers have been received. The Hyatt Regency Chicago Hotel venue is ideal for a General Assembly, with all of the session rooms on the same floor, near to each other. The hotel is also located a block from what is know as the Magnificent Mile, one of the most famous shopping streets in the world. It is a few blocks or less from most all of the major sights in one of the most interesting, vibrant cities in the United States. Registration and hotel information are available at

http://www.ece.uic.edu/2008ursiga

I urge you to make your plans to attend now!

Ross

Please note that the Radio Science Bulletin is freely available on the web. From the September 2002 issue onwards, it is possible to download our magazine (in .pdf format) from http://www.ursi.org/RSB.htm

Brief Review of Spherical-Multipole Analysis in Radio Science

L. Klinkenbusch

Abstract

This contribution briefly surveys several historical and modern developments of spherical-multipole analysis in electromagnetics. Three different examples of recent applications are described: The electromagnetic scattering by a circular cone by means of a double Green's function approach, a multipole-based near-to-far-field transform for frequency- as well as for time-domain methods, and new definitions of the shielding effectiveness for the case of high-frequency and transient fields. In addition, a theorem is presented that states that the field at any point in an arbitrary homogeneous domain is uniquely determined by the knowledge of the electric or magnetic field at one single point and its immediate surroundings. The proof, which is based on repeatedly performed spherical-multipole expansions, includes a recipe of how to reconstruct that field.

1. Introduction

Multipole expansions have been employed in many areas of theoretical and applied physics, including astro, plasma, and nuclear physics. In particular, they are well known in the theory of classical electromagnetic fields. Basically, the term "multipole expansion" is related to electrostatics: Each part of a suitable infinite-series expansion of the characteristic kernel, $|\mathbf{r}-\mathbf{r}'|^{-1}$ (that is, the reciprocal distance between the source and the observation points), can be physically interpreted as a multipole term. Using spherical coordinates, the leading term represents the field belonging to a spherical monopole (a point charge), the second term belongs to a set of spherical dipoles (three orthogonal point dipoles), the third term belongs to a set of quadrupoles, and so forth, while all of these spherical multipoles are located at $r = 0$. The radial dependence of the corresponding electrostatic potential behaves $\sim r^{-(n+1)}$, where $n = 0$ stands for the monopole part, $n = 1$ stands for the dipole parts, $n = 2$ stands for the quadrupole parts, etc. Hence, in the far field (that is, at a distance sufficiently far away from the source region), the field of any localized charge distribution with non-zero total charge is asymptotically a monopole field. In contrast to electrostatics, the far field of electrodynamic sources shows a fundamentally different behavior: The radial dependence of the (similarly derivable) spherical-multipole expansion of the electromagnetic field is described by spherical Bessel functions (including the spherical Hankel function) and their derivatives. In the far field, all electrodynamic spherical-multipole terms have the same radial decay, $\sim 1/r$.

Historically, the development of (electromagnetic) spherical-multipole expansions was closely connected to the problem of electromagnetic scattering and diffraction by a sphere. Probably the first mathematically rigorous investigation of light scattering by a sphere was done by A. Clebsch in 1861 (published in 1863 in [1], before Maxwell introduced his theory on electromagnetic fields [2]). Clebsch solved the boundary-value problem for the already-known elastic-wave equations (i.e., scalar wave equations for both the longitudinal and the transverse components) by the method of separation of variables. He ended up with an expansion of waves, each consisting of products of surface spherical harmonics and spherical Bessel functions. The latter functions were not known at that time, and he had to investigate them and develop appropriate series representations.

Particularly after the introduction of Maxwell's theory, the mathematical investigation of light scattering by a sphere attracted many other researchers, including L. Lorenz [3], Lord Rayleigh [4], G. Mie [5], P. Debye [6], and J. Nicholson [7]. An excellent (and exciting) historical review on the theory of scattering by a sphere can be found in [8].

Ludger Klinkenbusch is with the Institut für Elektrotechnik und Informationstechnik, Christian-Albrechts-Universität zu Kiel, Kaiserstr. 2, D- 24143 Kiel, Germany; Tel: +49 431 880 6252; Fax: +49 431 880 6253; E-mail: klinkenbusch@ieee.org.

This is an invited *Review of Radio Science* from Commission B.

The first electric term (that is, the dipole term) in the spherical-multipole expansion of the electromagnetic field was theoretically analyzed by Hertz in his famous paper [9]. Hertz introduced the infinitesimally short alternating-current element, and related it mathematically to the known electrostatic point dipole ("*elektrischer Doppelpunkt*").

Among the early papers on electromagnetic scattering, the paper by Bromwich [10] is of particular importance. It contains a general approach to systematically construct elementary solutions of Maxwell's equation in curvilinear (including spherical) coordinates. Hansen [11] formulated a concise form of these "vector wave functions" (denoted as "multipole functions" in this paper), which Stratton further developed and extensively used in his brilliant monograph [12]. Many other authors included multipole expansions in their works, using different coordinate systems (e.g., Cartesian, cylindrical, spherical, sphero-conal). Several examples (without a claim of completeness) are listed in [13-25].

Among further applications of spherical-multipole expansions are a matrix formulation of electromagnetic scattering [26], and the probe-corrected near-to-far-field transformation technique for antenna near fields measured on a spherical surface [27, 28]. The more recently proposed and very successful "fast multipole method," and its generalization for computational electromagnetics, uses elements from spherical-multipole analysis. For numerical reasons, the main parts are formulated through Cartesian components, that is, in terms of plane waves [29-31].

The present paper deals with a brief introduction and several developments recently achieved in the context of spherical-multipole analysis. In Section 2, we shall give a short derivation of the spherical-multipole expansion valid outside the sources in a homogenous domain. Section 3 deals with a theorem that states that the electromagnetic field in any homogenous domain, V, is uniquely determined by the knowledge of the electric or magnetic field at one single point and its immediate (infinitesimal) surroundings in V. The proof is based on repeatedly performed spherical-multipole expansions, and thus includes an explicit recipe of how to reconstruct that field. Finally, in Section 4, three quite different applications of spherical-multipole analysis introduced in the last few years are briefly summarized. First, a recently proposed method, based on two dyadic Green's functions, is used to solve the boundary-value problem of electromagnetic scattering by a perfectly conducting semi-infinite circular cone. It will then be shown how multipole expansions can be profitably employed to perform near-to-far-field transformations for time-harmonic as well as for transient near fields. Finally, spherical-multipole expansions are used to derive new definitions of the shielding effectiveness for high-frequency and for transient fields. These are thought to better characterize the electromagnetic behavior of shielded enclosures than the conventional definitions.

2. Spherical-Multipole Expansion of the Electromagnetic Field

For a homogeneous domain, the time-harmonic Maxwell's equations can be easily decoupled to the vector partial differential equation:

$$\vec{\nabla}\times\vec{\nabla}\times\mathbf{E}(\mathbf{r})-k^2\mathbf{E}(\mathbf{r})=-j\omega\mu\mathbf{J}_e(\mathbf{r})\cdot \qquad (1)$$

Here, $\mathbf{E}(\mathbf{r})$ and $\mathbf{J}_e(\mathbf{r})$ represent the space-dependent phasors of the electric-field intensity and electric-current density, respectively. A time factor of $\mathrm{e}^{j\omega t}$ is assumed. The wave number is defined by

$$k=\omega\sqrt{\varepsilon\mu}\,, \qquad (2)$$

where ε and μ denote the complex-valued permittivity and permeability, respectively. From Equation (1), it immediately follows that in a homogeneous medium and outside the sources, the electric field is divergence-free. The corresponding homogeneous equation has a fundamental system represented by the solenoidal vector spherical-multipole functions [11]:

$$\mathbf{M}(\mathbf{r})=\left(\mathbf{r}\times\vec{\nabla}\right)\Psi(\mathbf{r})\,, \qquad (3)$$

$$\mathbf{N}(\mathbf{r})=\frac{1}{k}\vec{\nabla}\times\mathbf{M}(\mathbf{r})\,.$$

$\Psi(\mathbf{r})$ is any suitable solution of the scalar homogeneous Helmholtz equation,

$$\Delta\Psi(\mathbf{r})+k^2\Psi(\mathbf{r})=0\,, \qquad (4)$$

in spherical coordinates r,θ,ϕ. $\hat{r},\hat{\theta},\hat{\phi}$ symbolize the corresponding unit vectors. If the positive polar axis ($\theta=0$) is part of the solution domain, a regular elementary solution of Equation (4) can be written as

$$\Psi_{\nu,\chi}(\mathbf{r})=z_\nu(kr)Y_{\nu,\chi}(\theta,\phi)\,. \qquad (5)$$

Here, $z_\nu(kr)$ are spherical Bessel functions, while the $Y_{\nu,\chi}(\theta,\phi)$ are referred to as the surface spherical harmonics [12]. The latter functions consist of appropriately normalized products of associated Legendre functions of the first kind, $\mathrm{P}_\nu^\chi(\cos\theta)$, and harmonic functions, $\mathrm{e}^{j\chi\phi}$. Thus, the vector spherical-multipole functions can be represented as

$$\mathbf{M}_{\nu,\chi}(\mathbf{r})=z_\nu(kr)\mathbf{m}_{\nu,\chi}(\theta,\phi),$$

$$\mathbf{N}_{\nu,\chi}(\mathbf{r}) = -\frac{z_\nu(kr)}{kr}\nu(\nu+1)Y_{\nu,\chi}(\theta,\phi)\hat{r} \qquad (6)$$

$$-\frac{1}{kr}\frac{d}{dr}\left[rz_\nu(kr)\right]\mathbf{n}_{\nu,\chi}(\theta,\phi).$$

The transverse spherical multipole functions are given by

$$\mathbf{m}_{\nu,\chi}(\theta,\phi) = -\frac{1}{\sin\theta}\frac{\partial Y_{\nu,\chi}(\theta,\phi)}{\partial\phi}\hat{\theta} + \frac{\partial Y_{\nu,\chi}(\theta,\phi)}{\partial\theta}\hat{\phi}, \qquad (7)$$

$$\mathbf{n}_{\nu,\chi}(\theta,\phi) = \frac{\partial Y_{\nu,\chi}(\theta,\phi)}{\partial\theta}\hat{\theta} + \frac{1}{\sin\theta}\frac{\partial Y_{\nu,\chi}(\theta,\phi)}{\partial\phi}\hat{\phi}.$$

Finally, the spherical-multipole expansion can be written as [24]

$$\mathbf{E}(\mathbf{r}) = \sum_{\nu,\chi} A_{\nu,\chi}\mathbf{N}_{\nu,\chi}(\mathbf{r}) + \frac{Z}{j}\sum_{\nu',\chi'} B_{\nu',\chi'}\mathbf{M}_{\nu',\chi'}(\mathbf{r}) \qquad (8)$$

$$\mathbf{H}(\mathbf{r}) = \frac{j}{Z}\sum_{\nu,\chi} A_{\nu,\chi}\mathbf{M}_{\nu,\chi}(\mathbf{r}) + \sum_{\nu',\chi'} B_{\nu',\chi'}\mathbf{N}_{\nu',\chi'}(\mathbf{r}).$$

In Equation (8), the intrinsic impedance of the medium is defined by

$$Z = \sqrt{\frac{\mu}{\varepsilon}}. \qquad (9)$$

Note that the square roots in Equations (2) and (9) have to be extracted correctly, according to physical considerations [32].

The coefficients $A_{\nu,\chi}$ (measured in V/m) and $B_{\nu,\chi}$ (measured in A/m) of the multipole expansion in Equation (8) are referred to as the electric and magnetic multipole amplitudes, respectively. Furthermore, the duality of electric and magnetic quantities, which can be expressed by the dual (or *Fitzgerald*) transform, is extended to multipole expressions, and finally reads [24]

$$\mathbf{E} \to \mathbf{H} \qquad \mathbf{H} \to -\mathbf{E}$$

$$\mathbf{J}_e \to \mathbf{J}_{mag} \qquad \mathbf{J}_{mag} \to -\mathbf{J}_e \qquad (10)$$

$$\varepsilon \to \mu \qquad \mu \to \varepsilon$$

$$A_{\nu,\chi} \to B_{\nu,\chi} \qquad B_{\nu,\chi} \to -A_{\nu,\chi}$$

($\mathbf{J}_{mag}$ represents a fictitious magnetic current density.) Note that the values of ν, ν', χ, χ' in Equation (8) have to be chosen such that the boundary and continuity conditions of the electromagnetic field are satisfied. For a domain unbounded in θ, ϕ (e.g., in free space), it is seen that $\nu = n \in \mathbb{N}$ and $-n \le \chi = m \le +n$ with $m \in \mathbb{Z}$. We shall denote this case as the "free-space type" in the following.

Moreover, for a certain class of problems (including those discussed later in this paper), an explicit solution of Equation (1) can be formulated by means of the integral representation

$$\mathbf{E}(\mathbf{r}) = jkZ\iiint_V \tilde{\Gamma}(\mathbf{r},\mathbf{r}')\bullet\mathbf{J}_e(\mathbf{r}')dv'$$

$$+\oiint_{S(V)}\begin{Bmatrix}\left[\vec{\nabla}'\times\tilde{\Gamma}(\mathbf{r},\mathbf{r}')\right]\bullet\left[\mathbf{n}'\times\mathbf{E}(\mathbf{r}')\right] \\ -\tilde{\Gamma}(\mathbf{r},\mathbf{r}')\bullet\left[\mathbf{n}'\times\vec{\nabla}'\times\mathbf{E}(\mathbf{r}')\right]\end{Bmatrix}ds'. \qquad (11)$$

Outside the sources, the dyadic Green's function, $\tilde{\Gamma}(\mathbf{r},\mathbf{r}')$, in Equation (11) may be constructed in a "bilinear" form, that is, in terms of dyads consisting of vector spherical-multipole functions:

$$\tilde{\Gamma}(\mathbf{r},\mathbf{r}') = jk\begin{Bmatrix}\sum_{\nu,\chi}\dfrac{\mathbf{N}_{\nu,\chi}^{I^*(II)}(\mathbf{r})\mathbf{N}_{\nu,\chi}^{II(I^*)}(\mathbf{r}')}{\nu(\nu+1)} \\ +\sum_{\nu',\chi'}\dfrac{\mathbf{M}_{\nu',\chi'}^{I^*(II)}(\mathbf{r})\mathbf{M}_{\nu',\chi'}^{II(I^*)}(\mathbf{r}')}{\nu'(\nu'+1)}\end{Bmatrix}, \qquad (12)$$

$$r < r' \,(r > r').$$

The index I stands for the use of a spherical Bessel function of the first kind, $z_\nu(kr) = j_\nu(kr)$, while II indicates the use of a spherical Hankel function of the second kind, $z_\nu(kr) = h_\nu^{(2)}(kr)$. The asterisk denotes complex conjugation.

3. A Uniqueness Theorem in Electromagnetics

Consider a homogeneous source-free three-dimensional simply or multiply connected domain, V. (We understand that V can be built up by means of a finite or infinite number of spherical domains, each of non-

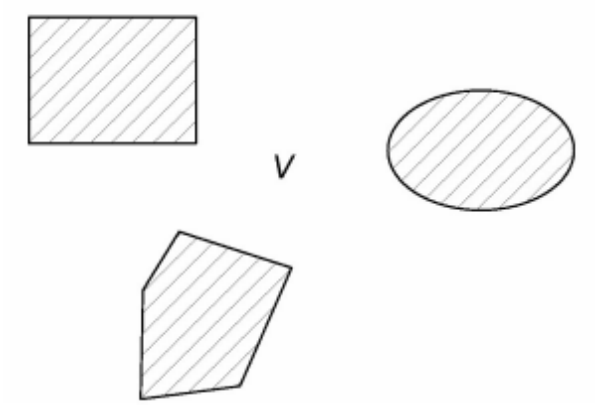

Figure 1. A non-simply connected homogeneous domain V .

vanishing radius.) In particular, V may be unbounded or bounded, and may enclose other arbitrary domains, as sketched in Figure 1. Consider further that in V there may exist a regular (that is, square-integrable over any finite part of V) time-harmonic electromagnetic field, described by the phasors of the electric and magnetic field intensities, $\mathbf{E}(\mathbf{r})$ and $\mathbf{H}(\mathbf{r})$, respectively. Then, the following assertion holds [33]:

Theorem. Let V be a simply or multiply connected three-dimensional homogeneous domain. If the electric or the magnetic field is regular and known at one single point and its immediate surroundings, V_ε ($V_\varepsilon \subseteq V$), then the electromagnetic field is regular and uniquely determined everywhere in V .

Proof. We denote the aforementioned single point P_1, and choose it to be at the origin of a spherical-multipole expansion, Equation (8), by which we first reconstruct the field around P_1. This expansion must be of the "free-space type," that is, we have $\nu = n \in \mathbb{N}$ and $-n \le \chi = m \le +n$ ($m \in \mathbb{Z}$), and it is valid in any homogeneous spherical domain concentrically around P_1. Moreover, since the electromagnetic field at P_1 is considered to be regular, we have to choose spherical Bessel functions of the first kind, $z_n(kr) = j_n(kr)$. In particular, the *known* tangential electric field on a spherical surface (radius r_ε) lying within V_ε can be expressed by means of

$$\mathbf{E}_{tan}(r_\varepsilon,\theta,\phi) = \sum_{n=1}^{\infty}\sum_{m=-n}^{+n}\left[\begin{array}{l} -A_{n,m}\dfrac{1}{kr_\varepsilon}\dfrac{d}{dr}\left[r j_n(kr)\right]\Big|_{r_\varepsilon}\mathbf{n}_{n,m}(\theta,\phi) \\ +\dfrac{Z}{j}B_{n,m}\,j_n(kr_\varepsilon)\,\mathbf{m}_{n,m}(\theta,\phi)\end{array}\right] \quad (13)$$

Since the transverse spherical-multipole functions form an orthogonal set on a closed spherical surface, according to

$$\int_{\theta=0}^{\pi}\int_{\phi=0}^{2\pi}\mathbf{m}_{n,m}\bullet\mathbf{m}^*_{n',m'}\sin\theta\,d\theta\,d\phi$$

$$=\int_{\theta=0}^{\pi}\int_{\phi=0}^{2\pi}\mathbf{n}_{n,m}\bullet\mathbf{n}^*_{n',m'}\sin\theta\,d\theta\,d\phi \quad (14)$$

$$=\begin{cases} n(n+1) & \text{if } n=n' \text{ and } m=m', \\ 0 & \text{else}\end{cases}$$

$$\int_{\theta=0}^{\pi}\int_{\phi=0}^{2\pi}\mathbf{m}_{n,m}\bullet\mathbf{n}^*_{n',m'}\sin\theta\,d\theta\,d\phi = 0\,,$$

we can uniquely determine all of the multipole amplitudes, $A_{n,m}$ and $B_{n,m}$, from

$$A_{n,m} = -\frac{1}{n(n+1)}\frac{1}{\dfrac{1}{kr_\varepsilon}\dfrac{d}{dr}\left[r j_n(kr)\right]\Big|_{r=r_\varepsilon}}$$

$$\int_{\theta=0}^{\pi}\int_{\phi=0}^{2\pi}\mathbf{E}(r_\varepsilon,\theta,\phi)\bullet\mathbf{n}^*_{n,m}\sin\theta\,d\theta\,d\phi\,, \quad (15)$$

$$\frac{Z}{j}B_{n,m} = \frac{1}{n(n+1)}\frac{1}{j_n(kr_\varepsilon)}$$

$$\int_{\theta=0}^{\pi}\int_{\phi=0}^{2\pi}\mathbf{E}(r_\varepsilon,\theta,\phi)\bullet\mathbf{m}^*_{n,m}\sin\theta\,d\theta\,d\phi$$

Likewise, the multipole amplitudes can be found from the tangential components of the magnetic field or from the normal (radial) components of the electric and magnetic fields, each of these on that spherical surface with radius r_ε (within V_ε). Because of the behavior of the spherical Bessel functions of the first kind and their derivatives, there always (for any circular frequency, ω) can be found an "electrical radius," kr_ε , which is small enough that the concerned fractions in Equation (15) remain regular for any value of n . Once we have obtained the multipole amplitudes for that spherical-multipole expansion centered at P_1, we may use it to describe the exact electromagnetic field in any homogeneous spherical domain concentrically around P_1. The extent of that homogeneous spherical domain, D_1, around P_1 is limited by the boundary next to P_1 (see Figure 2). However, in that case, we can choose any point, P_2 , within D_1 as the origin of a new spherical domain, D_2 , and repeat the procedure as described above to come to the unique field expansion around P_2 . Consequently, repeating this procedure as often as necessary, the field at any point in V can be uniquely reconstructed. In particular, all boundary values are uniquely reconstructed, as well. In the case of a

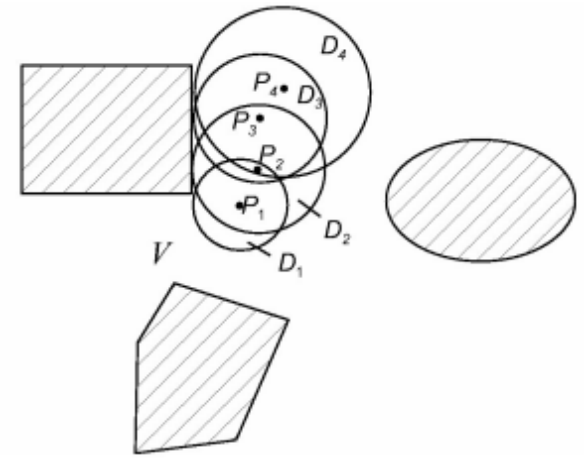

Figure 2. Consecutively defined spherical domains D_i *(* $i = 1,2,3,4$ *) with centers at* P_i *.*

scattering or radiation problem, the far field can also be uniquely evaluated. We may explicitly include the radiation condition, since (by the aforementioned method) we do have the exact field on any spherical *Huygens* surface enclosing all inhomogeneities.

Obviously, first consequences of this theorem are:

- If within a simply- or multiply-connected homogeneous domain there exists a plane electromagnetic wave at a single point (and its immediate surroundings), then that plane wave exists everywhere in the domain (see Booysen [34], for an illustrative two-dimensional example).
- If within a simply- or multiply-connected homogeneous domain the electric or magnetic field identically vanishes at a single point and its immediate surroundings, then the electromagnetic field identically vanishes everywhere in the domain.
- All the information related to the electromagnetic field in a simply- or multiply-connected homogeneous domain is present at each single point (and its immediate surroundings) in the domain.

Finally, it should be emphasized that this theorem is valid within classical (continuum) electrodynamics. The influence of the discretization of (electromagnetic) energy in quantum theory has to be further investigated.

4. Examples of Recent Applications

4.1 Scattering by a Semi-Infinite Circular Cone

Electromagnetic scattering by semi-infinite cones is of particular interest for radio scientists because cones have a tip. The electromagnetic field at that geometrical singularity becomes infinite, and an evaluation of the related diffracted and scattered field may help to understand the influence of the tip on the field. Moreover, the isolated field scattered by the tip can serve as a further canonical extension of certain scattering theories, such as the Geometrical Theory of Diffraction or the Uniform Theory of Diffraction. The literature on scattering by cones is extensive. It has been discussed in [20] and [24]. A few (of the many) other references are listed in [35-43].

Consider a PEC (perfectly electrically conducting) semi-infinite circular cone located around the negative z axis, as sketched in Figure 3. In terms of spherical coordinates, the cone is described by the coordinate surface $\theta = \theta_0$, with $\pi/2 < \theta_0 < \pi$. The cone is illuminated by a plane electromagnetic wave, incident from the direction θ^{inc}, ϕ^{inc}. The total electromagnetic field, $\mathbf{E}^{total}$, $\mathbf{H}^{total}$ can be found by means of the representation in Equation (11), with the dyadic Green's function of the circular cone given by Equation (12) for $r < r'$. The corresponding values of χ, χ' have to be integral numbers ($\chi = m$, $\chi' = m'$), while the values of ν, ν' are chosen such that the tangential electric field on the PEC cone's surface vanishes. Moreover, it can be shown that the following holds: $|m| \le \nu$ for all valid (ν, m) pairs, and $|m'| \le \nu'$ for all valid (ν', m') pairs.

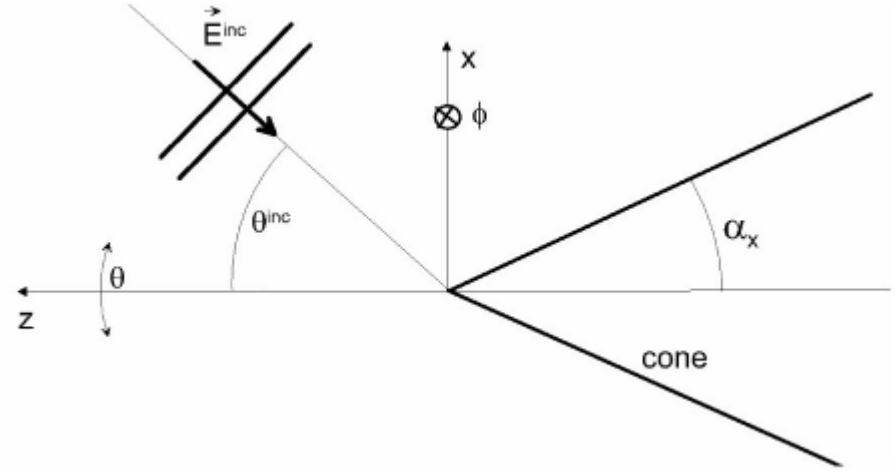

Figure 3. A PEC circular cone with half-cone angle α_x *illuminated by a plane wave* $\mathbf{E}^{inc}$ *(from [43], © 2007 American Geophysical Union).*

We choose a Hertzian dipole located at infinity as the electric current density in Equation (11), and normalize the corresponding multipole expansion of the total electromagnetic field according to an incident plane wave [46, 40]. The multipole amplitudes of this total-field expansion will be denoted as $a_{\nu,m}$, $b_{\nu',m'}$. The exact electric surface current induced on the circular cone is determined from the tangential magnetic field by $\mathbf{J}_{S,e} = \mathbf{H}^{total} \times \hat{\theta}\Big|_{\theta=\theta_0}$. Clearly, $\mathbf{J}_{S,e}$ serves as the source of the scattered far field, which can be again found through an appropriate application of Equation (11). Here, we choose the free-space type of the dyadic Green's function, Equation (12), with integer values of ν, ν', χ, χ', as described above. Thus, the result finally obtained for the scattered electric far field can be written in the form of the multipole expansion

$$\mathbf{E}^{sc}(\mathbf{r}) = \frac{\mathrm{e}^{-jkr}}{kr} \sum_{n,m} j^n \begin{bmatrix} -A^{sc}_{n,m} \mathbf{n}_{n,m}(\theta,\phi) \\ +ZB^{sc}_{n,m} \mathbf{m}_{n,m}(\theta,\phi) \end{bmatrix} \quad (16)$$

The corresponding multipole amplitudes read

$$A^{sc}_{n,m} = -\bar{P}^m_n(\cos\theta_0)$$

$$\left\{ j \sin\theta_0 \sum_{\nu} a_{\nu,m} \frac{d\bar{P}^m_\nu(\cos\theta)}{d\theta}\Big|_{\theta_0} \int_0^\infty j_n(kr)\, j_\nu(kr)\, dkr \right.$$

$$\left. + m \sum_{\nu'} Z b_{\nu',m} \bar{P}^m_{\nu'}(\cos\theta_0) \right.$$

$$\left. \int_0^\infty \begin{bmatrix} -j_n(\kappa r) \dfrac{\left[r j_{\nu'}(kr)\right]'}{kr} \\ +\dfrac{\nu'(\nu'+1)}{n(n+1)} j_{\nu'}(kr) \dfrac{\left[r j_n(kr)\right]'}{kr} \end{bmatrix} dkr \right\}, \quad (17)$$

$$B^{sc}_{n,m} = j \frac{\bar{P}^m_n(\cos\theta)}{d\theta}\Big|_{\theta_0} \sin\theta_0 \frac{1}{n(n+1)}$$

$$\sum_{\nu'} \left\{ \begin{matrix} b_{\nu',m} \bar{P}^m_{\nu'}(\cos\theta_0) \nu'(\nu'+1) \\ \times \int_0^\infty j_n(kr) \dfrac{\left[r j_{\nu'}(kr)\right]'}{kr} dkr \end{matrix} \right\} \quad (18)$$

Here, the $\bar{P}^m_n$ are the normalized associated Legendre functions of the first kind. The semi-infinite integrals over r in Equations (17) and (18) are of the *Weber-Schafheitlein* type; they exist and can be solved analytically [44]. Moreover, their results reveal that for any given value of n, m in Equations (17), (18) the series in ν and ν' do converge.

Finally, the electric far field can be written by means of a scattering matrix, $\ddot{D}$, as

$$\begin{bmatrix} E^{sc}_\theta(\theta,\phi) \\ E^{sc}_\phi(\theta,\phi) \end{bmatrix} = \frac{e^{-jkr}}{kr} \begin{bmatrix} D_{\theta\theta} & D_{\theta\phi} \\ D_{\phi\theta} & D_{\phi\phi} \end{bmatrix} \begin{bmatrix} E^{inc}_\theta(\theta^{inc},\phi^{inc}) \\ E^{inc}_\phi(\theta^{inc},\phi^{inc}) \end{bmatrix}. \quad (19)$$

Note that the elements of the scattering matrix (the scattering coefficients) each depend on the angles of observation (θ,ϕ), as well as on the angles of incidence $(\theta^{inc},\phi^{inc})$.

Although each of the multipole amplitudes $A^{sc}_{n,m}$ and $B^{sc}_{n,m}$ in Equations (17), (18) can be evaluated with arbitrary accuracy, the attempt to simply sum up the spherical-multipole expansion of Equation (16) with respect to n, m fails, since the series does not converge. In fact, the corresponding partial-sum sequences show an alternating behavior as a function of n. (Note that for each n, the summation in m is a finite sum, according to $-n \le m \le n$.) That lack of convergence may be explained by there being no convergence-enforcing n-dependent functions in the final expressions. This is due to the fact that a) the source point (of the incident plane wave) as well the observation points are at infinity, and b) that the scattering structure is of infinite extent. Following a more physical explanation, one may argue that the final result is given in terms of spherical waves with decay $\sim 1/r$. The amplitude of the illuminating plane wave is constant, while the corresponding wave parts scattered by an infinite or semi-infinite structure may have either the (constant) plane-wave behavior, a cylindrical-wave decay $\sim 1/\sqrt{R}$ (with R being the cylindrical coordinate), or the mentioned spherical-wave characteristics. Clearly, in terms of spherical waves, the plane and cylindrical scattered waves must become infinite in the far field. As the spherical-multipole expansion does not explicitly include these (plane or cylinder wave) singularities of the scattered field within the multipole functions, the only chance to represent them is through an infinite number of multipole terms. That finally ends up in the observed non-convergent behavior of the multipole expansion, not only at the directions of the singularities. (One finds a similar although mathematically not identical behavior in trying to numerically evaluate a completeness relation at points apart from the location of the δ peak.) On the other hand, at directions where only nonsingular spherical-wave terms do exist, the spherical-multipole expansion should contain all of the information about the correct scattering coefficient, and one may try to find out that information from a limited number of (i.e., the first) multipole terms.

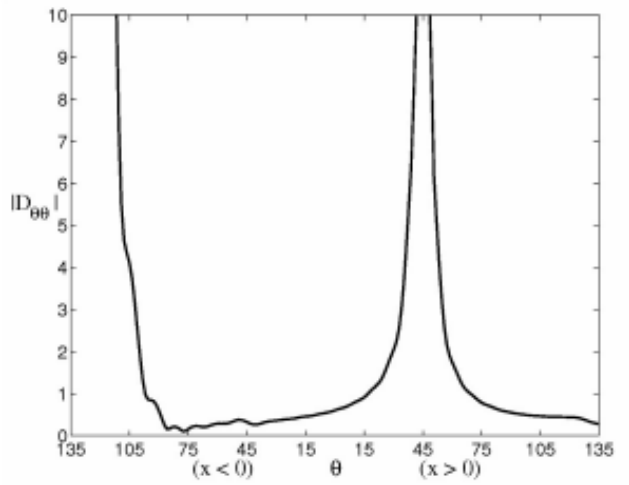

Figure 4a. The amplitudes of the scattering coefficients in the xz plane for a PEC circular cone with a half-cone angle $\alpha_x = 45°$, illuminated by a plane wave $\mathbf{E}^{inc}$ from $\theta^{inc} = 45°, \phi^{inc} = 0°$ and polarized in the xz plane (from [43], © 2007 American Geophysical Union).

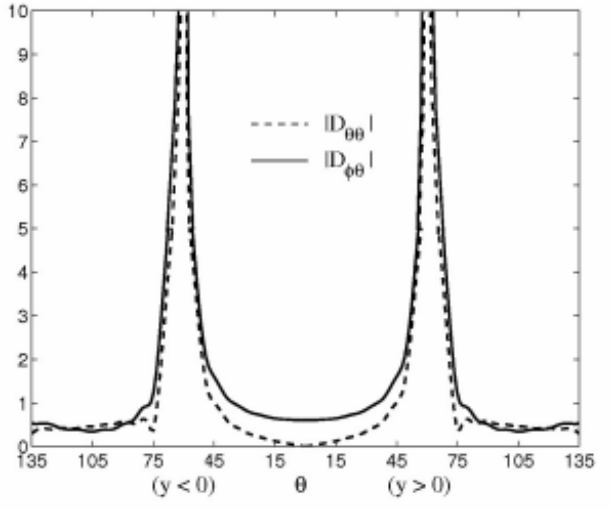

Figure 4b. The amplitudes of the scattering coefficients in the yz (Figure 4b) plane for a PEC circular cone with a half-cone angle $\alpha_x = 45°$, illuminated by a plane wave $\mathbf{E}^{inc}$ from $\theta^{inc} = 45°, \phi^{inc} = 0°$ and polarized in the xz plane (from [43], © 2007 American Geophysical Union).

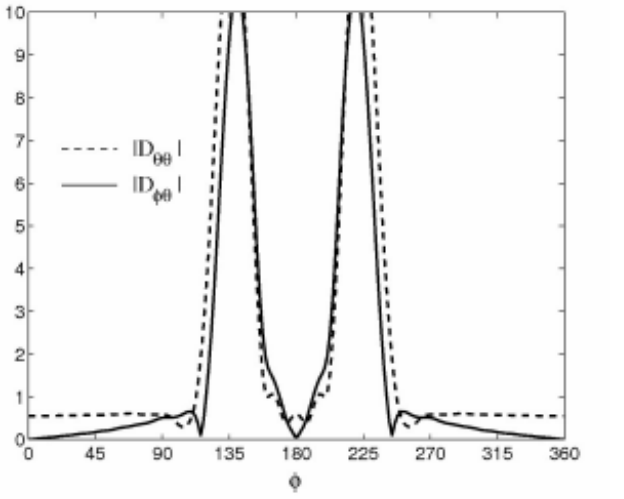

Figure 4c. The amplitudes of the scattering coefficients in the xy plane for a PEC circular cone with a half-cone angle $\alpha_x = 45°$, illuminated by a plane wave $\mathbf{E}^{inc}$ from $\theta^{inc} = 45°, \phi^{inc} = 0°$ and polarized in the xz plane (from [43], © 2007 American Geophysical Union).

For such cases, mathematicians have developed a number of sequence transforms with the aim of converting a non-convergent (alternating) sequence into a convergent sequence [45]. Among these approaches, linear methods have been proven to be generally consistent: If a transformed partial-sum sequence is convergent, then the obtained limiting value is the correct value. For the series in question, we have applied the very simple but effective *Césaro* transform, which delivers the transformed partial-sum sequence, s_n', for a given s_n by the instruction

$$s_n' = \frac{s_0 + s_1 + s_2 + \cdots + s_n}{n+1}. \qquad (20)$$

Other linear methods include those due to *Fejér* and to *Euler*. The nonlinear methods, most noticeable that one due to *Shanks*, can be more effective and generally show faster convergence. However, nonlinear methods have been proven to be consistent only for certain classes of *model sequences*, where the sequences in question do not count to.

By means of the described approach (including a simply or multiply applied *Césaro* transform), we have numerically evaluated the scattering coefficient for a PEC circular cone with a half cone opening angle $\alpha_x = 45°$ (see Figure 3). The cone was illuminated by a plane wave incident from $\theta^{inc} = 45°$, $\phi^{inc} = 0°$, and polarized in the xz plane. The scattering coefficients in the three main planes are represented in Figures 4a-4c. For all computations, we applied a double *Césaro* transform to the results obtained with multipole amplitudes up to $n = 40$.

4.2 Spherical-Multipole Based Near-to-Far Field Transformation

Most of the numerical methods employed for solving scattering and antenna problems do not directly deliver the scattered or radiated far field. Instead, they either solve Maxwell's equations within finite discretized domains (e.g., the Finite-Element, Finite-Difference, and finite-integration methods), or they yield (equivalent) current densities on discretized surfaces (e.g., most integral-equation methods). In each of these cases, it is necessary to perform a near-to-far-field transformation to obtain the radiated or scattered far field. Usually, for this purpose the closed form of the free-space dyadic Green's function,

$$\tilde{\Gamma}(\mathbf{r},\mathbf{r}') = -\frac{1}{4\pi}\left[\tilde{I} + \frac{1}{k^2}\vec{\nabla}\vec{\nabla}\right]\frac{\exp\left(-jk|\mathbf{r}-\mathbf{r}'|\right)}{|\mathbf{r}-\mathbf{r}'|}, \qquad (21)$$

($\tilde{I}$ represents the unity dyad), or the corresponding time-domain expression, is employed. The use of that $|\mathbf{r}-\mathbf{r}'|$-

dependent kernel involves the need to repeat the evaluation of the integral of Equation (11) for each new observation point, $\mathbf{r}$. This might be the method of choice if the far field is needed for only a few observation points. However, it can become a time-consuming and inefficient task if evaluations for many far-field directions have to be performed, or if even the global far-field information is needed. In such cases, it can be advisable to use the bilinear form of the free-space dyadic Green's function, Equation (12), instead. To this end, we insert Equation (12) into Equation (11), asymptotically evaluate the Hankel functions of the second kind for large values of kr, and end up at the electric far-field expansion

$$\mathbf{E}_\infty(\mathbf{r}) = \frac{\mathrm{e}^{-jkr}}{kr}\sum_{n,m} j^n \Big[-A_{n,m}\mathbf{n}_{n,m}(\theta,\phi) + ZB_{n,m}\mathbf{m}_{n,m}(\theta,\phi)\Big] \quad (22)$$

For a given *electric* current density, we obtain the multipole amplitudes as

$$A_{n,m} = -k^2 Z \frac{(-1)^m}{n(n+1)} \iiint_V \mathbf{N}^I_{n,-m}(\mathbf{r}')\bullet\mathbf{J}_e(\mathbf{r}')\,dv', \quad (23)$$

$$\frac{Z}{j}B_{n,m} = -k^2 Z \frac{(-1)^m}{n(n+1)} \iiint_V \mathbf{M}^I_{n,-m}(\mathbf{r}')\bullet\mathbf{J}_e(\mathbf{r}')\,dv'$$

By applying the duality relations of Equation (10), the multipole amplitudes for a given *magnetic* current density are found to be

$$A_{n,m} = jk^2 \frac{(-1)^m}{n(n+1)} \iiint_V \mathbf{M}^I_{n,-m}(\mathbf{r}')\bullet\mathbf{J}_{mag}(\mathbf{r}')\,dv', \quad (24)$$

$$\frac{Z}{j}B_{n,m} = jk^2 \frac{(-1)^m}{n(n+1)} \iiint_V \mathbf{N}^I_{n,-m}(\mathbf{r}')\bullet\mathbf{J}_{mag}(\mathbf{r}')\,dv'$$

Obviously, the evaluation of the multipole amplitudes can be performed by a single integration over the sources, independently of the observation point, $\mathbf{r}$. Hence, for a given electric and magnetic current density (including equivalent currents) the formulae of Equations (22)-(24) constitute a frequency-domain spherical-multipole-based near-to-far-field transformation. To come to a representation that is more adjusted to common discretization schemes, the electric and magnetic current densities have been replaced by a sufficient number of equivalent electric and magnetic elementary (Hertzian and Fitzgerald) dipoles according to [47]

$$\mathbf{J}_e(\mathbf{r}) = \sum_{i=1}^{N_e} \mathbf{C}_e^{[i]}\delta\left(\mathbf{r}-\mathbf{r}_e^{[i]}\right), \quad (25)$$

$$\mathbf{J}_{mag}(\mathbf{r}) = \sum_{i=1}^{N_{mag}} \mathbf{C}_{mag}^{[i]}\delta\left(\mathbf{r}-\mathbf{r}_{mag}^{[i]}\right).$$

$\mathbf{C}_e$ and $\mathbf{C}_{mag}$ are referred to as the electric and magnetic current moments (with dimensions Am and Vm, respectively) of the elementary dipoles. For instance, they can be obtained from given tangential field components on an appropriately discretized *Huygens* surface by

$$\mathbf{C}_e = (\mathbf{n}\times\mathbf{H})\Delta f\,, \quad (26)$$

$$\mathbf{C}_{mag} = -(\mathbf{n}\times\mathbf{E})\Delta f\,.$$

Here, Δf is the area of the corresponding surface element, and $\mathbf{n}$ denotes the related normal unit vector. We insert Equation (25) into Equations (23) and (24) and are lead to the multipole amplitudes

$$A_{n,m} = k^2 \frac{(-1)^m}{n(n+1)}\Bigg[-Z\sum_{i=1}^{L_e}\mathbf{N}^I_{n,-m}\left(\mathbf{r}_e^{[i]}\right)\bullet\mathbf{C}_e^{[i]} + j\sum_{i=1}^{L_{mag}}\mathbf{M}^I_{n,-m}\left(\mathbf{r}_{mag}^{[i]}\right)\bullet\mathbf{C}_{mag}^{[i]}\Bigg] \quad (27)$$

$$\frac{Z}{j}B_{n,m} = k^2 \frac{(-1)^m}{n(n+1)}\Bigg[-Z\sum_{i=1}^{L_e}\mathbf{M}^I_{n,-m}\left(\mathbf{r}_e^{[i]}\right)\bullet\mathbf{C}_e^{[i]} + j\sum_{i=1}^{L_{mag}}\mathbf{N}^I_{n,-m}\left(\mathbf{r}_{mag}^{[i]}\right)\bullet\mathbf{C}_{mag}^{[i]}\Bigg]$$

The method has also been extended to obtain near-to-far-field transformation directly in the time domain [48, 49]. To this end, first the time-domain electric far field follows from an inverse Fourier transform of Equation (22), as

$$\mathbf{e}_\infty(\mathbf{r},t) = \frac{1}{r}\sum_{n,m}\Bigg[-a_{n,m}\left(t-\frac{r}{v_c}\right)\mathbf{n}_{n,m}(\theta,\phi) + Zb_{n,m}\left(t-\frac{r}{v_c}\right)\mathbf{m}_{n,m}(\theta,\phi)\Bigg] \quad (28)$$

where $v_c = \omega/k$ is the velocity of light. Consequently, the time-domain spherical-multipole amplitudes are found from Equation (27) as convolutions:

$$a_{n,m}(t)=\frac{(-1)^m}{n(n+1)}\left[Z\sum_{i=1}^{L_e}\int_{-\infty}^{\infty}\boldsymbol{\alpha}_{n,m}^{[i]}(t-t')\bullet\mathbf{c}_e^{[i]}(t')dt'\right.$$

$$\left.+\sum_{i=1}^{L_{mag}}\int_{-\infty}^{\infty}\boldsymbol{\beta}_{n,m}^{[i]}(t-t')\bullet\mathbf{c}_{mag}^{[i]}(t')dt'\right] \qquad (29)$$

$$b_{n,m}(t)=\frac{(-1)^m}{n(n+1)}\left[\frac{1}{Z}\sum_{i=1}^{L_{mag}}\int_{-\infty}^{\infty}\boldsymbol{\alpha}_{n,m}^{[i]}(t-t')\bullet\mathbf{c}_{mag}^{[i]}(t')dt'\right.$$

$$\left.-\sum_{i=1}^{L_e}\int_{-\infty}^{\infty}\boldsymbol{\beta}_{n,m}^{[i]}(t-t')\bullet\mathbf{c}_{el}^{[i]}(t')dt'\right]$$

Here, $\mathbf{c}_e$ and $\mathbf{c}_{mag}$ denote the time-domain current moments, which, for instance, can be found directly from the near-field outcomes of a Finite-Difference Time-Domain (FDTD) algorithm. The other convolution partners are determined completely analytically. For $|t|\le r^{[i]}/v_c$, we have

$$\boldsymbol{\alpha}_{n,m}^{[i]}=\frac{(-1)^n v_c}{2r^{[i]^2}}P_n\left(\frac{v_c}{r^{[i]}}t\right)\left\{n(n+1)Y_{n,-m}\left(\theta^{[i]},\phi^{[i]}\right)\hat{r}\right.$$

$$\left.+\mathbf{n}_{n,-m}\left(\theta^{[i]},\phi^{[i]}\right)\left(1+t\frac{\partial}{\partial t}\right)\right\},$$

$$\boldsymbol{\beta}_{n,m}^{[i]}=-\frac{(-1)^n}{2r^{[i]}}P_n\left(\frac{v_c}{r^{[i]}}t\right), \qquad (30)$$

$$\mathbf{m}_{n,-m}\left(\theta^{[i]},\phi^{[i]}\right)\frac{\partial}{\partial t},$$

while for $|t|>r^{[i]}/v_c$ the following holds:

$$\boldsymbol{\alpha}_{n,m}^{[i]}=0, \qquad (31)$$

$$\boldsymbol{\beta}_{n,m}^{[i]}=0\cdot$$

In Equations (30) and (31), we have exploited the analytically available inverse Fourier transform of the spherical Bessel functions, which leads to expressions with Legendre polynomials, P_n [51].

The method has been implemented into a three-dimensional FDTD algorithm that delivers the time-domain current moments at certain discrete time steps $t_n=n\Delta t$, $n=0,1,2,\ldots$. To increase the accuracy and the efficiency, a temporal linear interpolation of the current moments in Equation (29) was fully analytically established [48, 49].

4.3 Definitions of the Shielding Effectiveness

Electromagnetic shielding is one of the basic steps to ensure electromagnetic compatibility (EMC) of systems and devices. Common measures to quantify the shielding ability of a shielded enclosure are the electric and magnetic shielding effectiveness (*SE*), defined by [52]

$$SE_e\big|_P=20\log_{10}\frac{\left|\mathbf{E}^{without}\right|_P}{\left|\mathbf{E}^{with}\right|_P}, \qquad (32)$$

$$SE_m\big|_P=20\log_{10}\frac{\left|\mathbf{H}^{without}\right|_P}{\left|\mathbf{H}^{with}\right|_P}.$$

Here, "without" and "with" indicate the absence and the presence of the shield, respectively, while P stands for the point where the SE is defined. These measures are useful, expressive, and practicable (that is, measurable with a reasonable effort) for electrostatic, magnetostatic, and low-frequency fields. However, for shielding problems with high-frequency or transient fields, deriving more suitable definitions that take into account their electromagnetic behavior is recommended.

To this end, first let P be an arbitrary point inside an arbitrary empty shielded enclosure. The field around that point can be expanded by means of a spherical-multipole expansion, Equation (8), centered at P and of the "free-space type," that is, ν and χ are integers. Because the field at P should be regular, we have to choose spherical Bessel functions of the first kind, $j_n(kr)$. From their behavior for $kr\to 0$, it immediately follows that in the representation of the field at P only the first (dipole) terms are needed. Hence, Equation (32) can be represented as

$$SE_e\big|_P=10\log_{10}\frac{\sum_{m=-1}^{1}\left|A_{1,m}^{without}\right|^2}{\sum_{m=-1}^{1}\left|A_{1,m}^{with}\right|^2} \qquad (33)$$

$$SE_m\big|_P=10\log_{10}\frac{\sum_{m=-1}^{1}\left|B_{1,m}^{without}\right|^2}{\sum_{m=-1}^{1}\left|B_{1,m}^{with}\right|^2}.$$

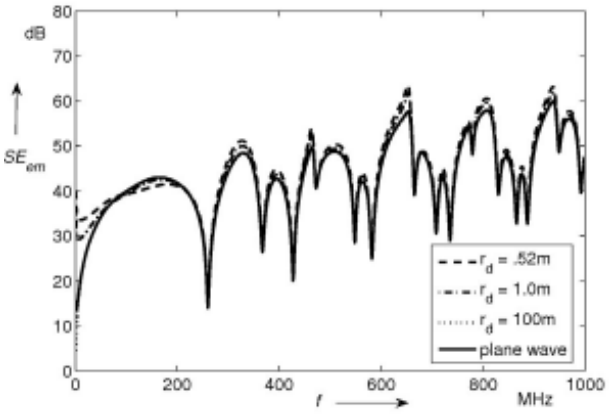

Figure 5. The electromagnetic SE at 10 cm off the center (in direction of the incident wave) of a closed spherical shield (inner radius: 50 cm, thickness: 1 cm, electrical conductivity: 50 S/m), for an incident plane wave and for Hertzian-dipole sources, located at different distances r_d to the center of the spherical shell and polarized perpendicularly to $\mathbf{r}_d$.

Consider next that the shield is not empty, but partly filled with a lossy spherical test load, concentrically located around P. The ratio of the time-averaged electromagnetic input power of the unshielded test load to the power of the shielded test load,

$$\gamma_P = 10\log_{10}\frac{\bar{P}^{without}}{\bar{P}^{with}}, \qquad (34)$$

obviously would be a suitable measure for the ability of the shield to reduce the electromagnetic field. However, the practicability of that definition for EMC measurement is rather limited. In trying to obtain a link between the theoretically ideal definition of Equation (34), and the practical definitions of Equation (32), we first describe the time-averaged power delivered to the test load by means of spherical-multipole expansions. We then let the size of the test load become infinitely small. Both the numerator and the denominator in Equation (34) vanish; however, the ratio does not vanish and exists: It will be referred to as the electromagnetic shielding effectiveness, SE_{em}. For an incident plane wave, we derive the expression [53]

$$SE_{em}\big|_P = 10\log_{10}\frac{2}{\dfrac{\sum_{m=-1}^{1}\left|A_{1,m}^{with}\right|^2}{\sum_{m=-1}^{1}\left|A_{1,m}^{without}\right|^2}+\dfrac{\sum_{m=-1}^{1}\left|B_{1,m}^{with}\right|^2}{\sum_{m=-1}^{1}\left|B_{1,m}^{without}\right|^2}} \qquad (35)$$

The ratios in the denominator of Equation (35) have already occurred in Equation (33). Through Equation (32), they are identified as ratios of electric and magnetic field intensities according to

$$SE_{em}\big|_P = 10\log_{10}\frac{2}{\dfrac{\left|\mathbf{E}^{with}\right|_P^2}{\left|\mathbf{E}^{without}\right|_P^2}+\dfrac{\left|\mathbf{H}^{with}\right|_P^2}{\left|\mathbf{H}^{without}\right|_P^2}} \qquad (36)$$

Note that this final result is both closely related to the (ideal) starting definition, Equation (34), and relatively easily measurable.

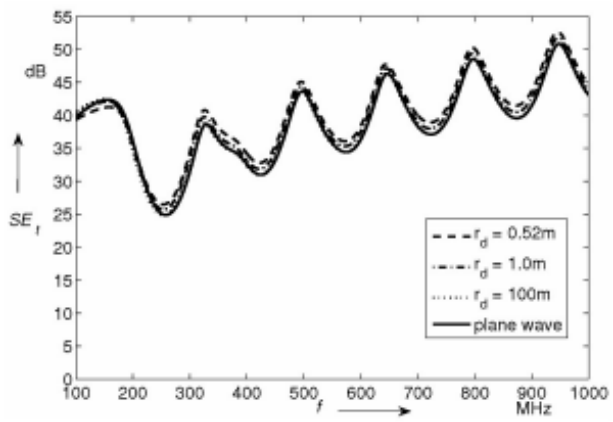

Figure 6a. The transient SE at 10 cm off the center (in direction of the incident wave) of a closed spherical shield (inner radius: 50 cm, thickness: 1 cm, electrical conductivity: 50 S/m), for an incident plane wave and for Hertzian-dipole sources, located at different distances r_d to the center of the spherical shell and polarized perpendicularly to $\mathbf{r}_d$. The spectrum of the incident wave was described by a Gaussian impulse with center frequency f and with decay to 1% of its maximum amplitude at $f \pm 100$ MHz.

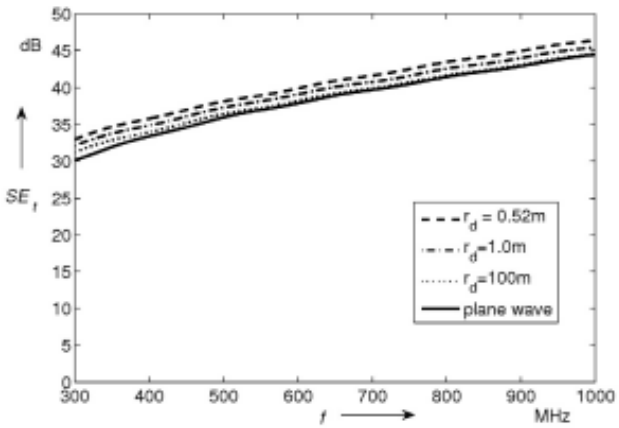

Figure 6b. The transient SE as in Figure 6a, but for the case where the spectrum of the incident wave was described by a Gaussian impulse with center frequency f and with decay to 1% of its maximum amplitude at $f \pm 300$ MHz.

A similar method has been applied to characterize the ability of a shielding enclosure to protect against transient fields. Instead of time-averaged input powers, as in

Equation (34), we start from the ratio of electromagnetic energies absorbed by the test load:

$$\gamma_W = 10\log_{10}\frac{W^{without}}{W^{with}}. \qquad (37)$$

For a transient incident plane wave characterized by its spectral density distribution, $S(\omega)$, a spherical-multipole based approach finally yields the transient shielding effectiveness as [53]

$$SE_t\big|_P = 10\log_{10}\frac{2\int_0^\infty |S(\omega)|^2\,\omega d\omega}{\int_0^\infty |S(\omega)|^2\left[\frac{\left|\mathbf{E}^{with}\right|_P^2}{\left|\mathbf{E}^{without}\right|_P^2}+\frac{\left|\mathbf{H}^{with}\right|_P^2}{\left|\mathbf{H}^{without}\right|_P^2}\right]\omega d\omega} \qquad (38)$$

Note that Equation (38) exactly turns into Equation (36) for a spectral-density distribution that corresponds to a time-harmonic field. The expressions of Equations (36) and (38), which are valid for plane-wave incidence, have been generalized to the case of dipole near-field sources in [54].

By means of a spherical-multipole expansion, we exemplarily investigated the case of a closed spherical shield. The results for the electromagnetic SE and for the transient SE (for a Gaussian-type impulse), each for an incident plane wave and for dipole source located at different distances to the shield, are represented in Figures 5 and Figures 6a and 6b. Note that the resonances of the spherical shield are dominantly present in case of the electromagnetic SE, and that for an increasing bandwidth, we get smoother and hence better comparable results.

5. Conclusions

Spherical-multipole expansions have accompanied the development of modern electromagnetic theory from its beginning. They are more than just an old-fashioned method to analytically solve problems with simple geometries. They can be used as a perfect mathematical tool for analyzing general properties of fields and for enhancing numerical methods. Both their unique mathematical features and their direct physical interpretability allow an insight into wave processes that can be directly exploited for many interesting applications.

Two examples for open problems concern the development of optimal strategies to evaluate slowly converging multipole series (e.g., by means of enhanced series acceleration techniques or by integral transforms), and the analysis of stochastic processes (e.g., in the context of EMC) by means of suitable multipole formulations.

6. Acknowledgements

The author would like to thank Prof. em. Siegfried Blume (Ruhr-Universität Bochum, Germany) for his advice and for his continual encouragement to work on multipole methods in electromagnetic field theory. The author would also like to thank the anonymous reviewers for several helpful and important hints. Part of this work was supported by the *Deutsche Forschungsgemeinschaft* (DFG).

7. References

1. A. Clebsch, "Ueber die Reflexion an einer Kugelfläche," ("On the Reflexion by a Spherical Surface,") *Journal für die reine und angewandte Mathematik (Crelle's Journal)*, **61**, 1863, pp. 195-262.
2. J. C. Maxwell, "A Dynamical Theory of the Electromagnetic Field," *Proc. of the Royal Society (London)*, **13**, 1864, pp. 531-536.
3. L. V. Lorenz, "Sur la lumière réfléchie er réfractée par une sphere transparante," *Vidensk. Selsk. Skrifter,* 6, 1890, pp. 1-62 (original paper in Danish, French translation in *Œuvres Scientifiques de L. Lorenz, Revues et Annotées par H. Valentiner*, Copenhague, Tome Premier, Libraire Lehmann & Stage, 1898, pp. 403-529).
4. Lord Rayleigh, "On the Acoustic Shadow of a Sphere," *Phil. Transactions of the Royal Society*, **203**, 1904, pp. 97-110.
5. G. Mie, "Beiträge zur Optik trüber Medien, speziell kolloidaler Metallösungen," ("On the Optical Behavior of Cloudy Media, in Particular Colloid Fluids,") *Annalen der Physik (4. Folge)*, **25**, 1908, pp. 379-445.
6. P. Debye, "Der Lichtdruck auf Kugeln von beliebigem Material," ("Light Pressure on Spheres of Arbitrary Material,") *Annalen der Physik (4. Folge)*, **30**, 1909, pp. 57-136.
7. J. W. Nicholsen, "The Scattering of Light by a Large Conducting Sphere," *Proc. of the Mathematical Society (London)*, **9**, 1910, pp. 67-80.
8. N. A. Logan, "Survey of Some Early Studies of the Scattering of Plane Waves by a Sphere*," Proceedings of the IEEE*, **53**, 1965, pp. 773-785.
9. H. Hertz, "Die Kräfte elektrischer Schwingungen, behandelt nach der Maxwell'schen Theorie," ("The Forces of Electric Oscillations, Treated by Means of Maxwell's Theory,") *Wiedemanns Annalen*, **36**, 1888, p. 1ff.
10. T. J. I'A Bromwich, "Electromagnetic Waves," *Phil. Magazine*, **38**, 1919, pp. 143-163.
11. W. W. Hansen, "A New Type of Expansion in Radiation Problems," *Physical review*, **47**, 1935, pp. 139-143.
12. J. A. Stratton, *Electromagnetic Theory*, New York, McGraw Hill, 1941.
13. W. Trinks, "Zur Vielfachstreuung an kleinen Kugeln, " ("On Multiple Scattering by Small Spheres,") *Annalen der Physik*, **22**, 1935, pp. 561-590.
14. P. M. Morse and H. Feshbach, *Methods of Theoretical Physics*, New York, McGraw-Hill, 1953.
15. J. J. Bowkamp and H. B. G. Casimir, "On Multipole Expansions in the Theory of Electromagnetic Radiation," *Physica*, **XX**, 1954, pp. 539-554.
16. H. C. van der Hulst, *Light Scattering by Small Particles*, New York, Wiley, 1957.
17. T. B. A. Senior, "A Note on Hansen's Vector Wave Functions," *Canadian Journal of Physics*, **38**, 1960, pp. 1702-1705.

18. M. Kerker (ed.), *Electromagnetic Scattering*, Oxford, Pergamon Press, 1963.
19. D. S. Jones, *The Theory of Electromagnetism*, New York, Macmillan, 1964.
20. J. J. Bowman, T. B. A. Senior, and P. L. E. Uslenghi, *Electromagnetic and Acoustic Scattering by Simple Shapes*, Amsterdam, North-Holland, 1969.
21. C.-T. Tai, *Dyadic Green's Functions in Electromagnetic Theory*, Scranton, Intext Educational Publishers, 1971.
22. J. D. Jackson, *Classical Electrodynamics, Second Edition*, New York, Wiley, 1975.
23. R. E. Collin, *Field Theory of Guided Waves*, New York, IEEE Press, 1991.
24. S. Blume and L. Klinkenbusch, "Spherical Multipole Analysis in Electromagnetics," in D. W. Werner and R. Mittra (eds.), *Frontiers in Electromagnetics*, New York, IEEE Press, 1999, pp. 553-608.
25. R. E. Raab and O. L. de Lange, *Multipole Theory in Electromagnetism*, Oxford University Press, 2005.
26. P. C. Waterman, "Matrix Formulation of Electromagnetic Scattering," *Proceedings of the IEEE*, **53**, 1965, pp. 805-812.
27. J. E. Hansen (ed.), *Spherical Near-Field Antenna Measurements*, London, Peter Peregrinus, 1988.
28. A. Yaghjian, "**An Overview of Near-Field Antenna Measurements,**" ***IEEE Transactions on Antennas and Propagation*****, AP-34, 1986, pp. 30-45.**
29. V. Rokhlin, "Rapid Solution of Integral Equations of Classical Potential Theory," *Journal of Computational Physics*, **60**, 1985, pp. 187–207.
30. W. C. Chew, J.-M. Jin, E. Michielssen, and J. Song (eds.), *Fast and Efficient Algorithms in Computational Electromagnetics*, Norwood (MA), Artech-House, 2000.
31. T. F. Eibert, "A Diagonalized Multilevel Fast Multipole Method with Spherical Harmonics Expansion of the k-Space Integrals," *IEEE Transactions on Antennas and Propagation*, **AP-53**, 2005, pp. 814-817.
32. R. W. Ziolkowski and E. Heyman, "Wave Propagation in Media having Negative Permittivity and Permeability," *Physical Review E*, **64**, 2001, pp. 056625-1 - 056625-15.
33. L. Klinkenbusch, "Multipole Approach to a Uniqueness Theorem in Electromagnetics," *Proceedings of the 2007 URSI Commission B Symposium on Electromagnetic Theory, and Conference Digest of the 2007 North American Radio Science Meeting,* July 22-28, 2007, Ottawa, Canada.
34. R. Booysen, "An Illustrative Equivalence Theorem Example," *IEEE Antennas and Propagation Magazine*, **42**, 2000, pp. 132-135.
35. W. W. Hansen and L. I. Schiff, "Theoretical Study of Electromagnetic Waves Scattered from Shaped Metal Surfaces," Stanford University, Microwave Laboratory, Quarterly Reports 1 to 4, 1948, (Contract W 28-099-333).
36. L. B. Felsen, "Back-Scattering from Wide-Angle and Narrow-Angle Cones," *Journal of Applied Physics*, **26**, 1955, pp. 138-151.
37. K. M. Siegel, J. W. Crispin, and C. E. Schensted, "Electromagnetic and Acoustical Scattering from a Semi-Infinite Cone," *Journal of Applied Physics*, **26**, 1955, pp. 309-313.
38. L. Kraus and L. M. Levine, "Diffraction by an Elliptic Cone," *Communications on Pure and Applied Mathematics*, **XIV**, 1961, pp. 49-68.
39. S. Blume and G. Kahl, "The Physical Optics Radar Cross Section of an Elliptic Cone," *IEEE Transactions on Antennas and Propagation*, **AP-35**, 1987, pp. 457-460.
40. S. Blume, L. Klinkenbusch, and U. Uschkerat, "The Radar Cross Section of the Semi-Infinite Elliptic Cone," *Wave Motion*, **17**, 1993, pp. 365-389.
41. V. M. Babich and V. P. Smyshlyaev, D. B. Dementiev, and B. A. Samokish, "Numerical Calculation of the Diffraction Coefficients for an Arbitrary Shaped Perfectly Conducting Cone," *IEEE Transactions on Antennas and Propagation*, **AP-44**, 1996, pp. 740-747.
42. S. Blume and V. Krebs, "Numerical Evaluation of Dyadic Diffraction Coefficients and Bistatic Radar Cross Sections for a Perfectly Conducting Semi Infinite Elliptic Cone," *IEEE Transactions on Antennas and Propagation*, **AP-46**, 1998, pp. 414-424.
43. L. Klinkenbusch, "Electromagnetic Scattering by Semi-Infinite Circular and Elliptic Cones," *Radio Science*, 2007, in press.
44. G. N. Watson, *A Treatise on the Theory of Bessel Functions (reprint of Second Edition)*, Cambridge, UK, Cambridge University Press, 1995.
45. G. H. Hardy, *Divergent Series*, Oxford, Clarendon Press, 1963.
46. L. Klinkenbusch, "Scattering of an Arbitrary Plane Electromagnetic Wave by a Finite Elliptic Cone," *Archiv für Elektrotechnik (Electrical Engineering)*, **77**, 1994, pp. 315-325.
47. L. Klinkenbusch, "A Spherical-Multipole Interface for Numerical Methods in Electromagnetic Field Theory," *Proceedings of the Latsis Symposium on Computational Electromagnetics*, Zurich 1995, pp. 242-247.
48. C.-C. Oetting and L. Klinkenbusch, "Near-to-Far-Field Transformation by a Time-Domain Spherical-Multipole Analysis," *IEEE Transactions on Antennas and Propagation*, **AP-53**, 2005, pp. 2054-2063.
49. L. Klinkenbusch and C.-C. Oetting, "Correction to: Near-to-Far-Field Transformation by a Time Domain Spherical-Multipole Analysis," *IEEE Transactions on Antennas and Propagation*, 2007, in press.
50. J. Adam and L. Klinkenbusch, "Argument Recursive Computation of Legendre Polynomials with Applications in Computational Electromagnetics," 2006 IEEE International Symposium on Antennas and Propagation *Digest*, Albuquerque (NM), 2006.
51. M. A. Abramowitz and I. A. Stegun, *Handbook of Mathematical Functions*, New York, Dover Publications, 1970.
52. H. Kaden, *Wirbelströme und Schirmung in der Nachrichtentechnik (Eddy Currents and Shielding in Communications)*, Berlin, Springer, 1959.
53. L. Klinkenbusch, "On the Shielding Effectiveness of Enclosures," *IEEE Transactions on Electromagnetic Compatibility*, **47**, 2005, pp. 589-601.
54. C. Möller and L. Klinkenbusch, "Electromagnetic and Transient Shielding Effectiveness for Near-Field Sources," *Advances in Radio Science*, **5**, 2007, pp. 57-62.

The Impact of High-Resolution Radar on Meteor Studies: The EISCAT Perspective

A. Pellinen-Wannberg
G. Wannberg
J. Kero, C. Szasz
A. Westman

Abstract

Meteors – i.e., meteoroids interacting with the atmosphere – provided a vast amount of knowledge about interplanetary matter already long before the space era. Using what is today known as specular meteor radars (SMR), a great body of data on meteors was accumulated, mainly through recording echoes from the meteor trails. However, due to the specular requirement and the ceiling effect, this method only detects a subset of the meteor population. By contrast, the high-power large-aperture (HPLA) radar method can observe head echoes from meteors passing through the radar beam at almost arbitrary aspect angles. The very high power densities available at typical HPLA installations allow millisecond time resolution and spatial resolution in the range of tens of meters to be routinely achieved. In special cases, interference between echoes from two meteors has made it possible to achieve centimeter-scale spatial resolution, thus allowing the deduction of an upper limit on the effective target size. Vector quantities, such as meteor velocity and deceleration, providing mass and orbit estimates, can be recorded by phased arrays with interferometric capability, as well as by multi-static radars. A case in point is the tri-static EISCAT UHF radar system, which provides a unique capability for monitoring head echoes over a very wide range of aspect angles. A recent analysis of data from the UHF system confirmed that head-echo targets are essentially spherical in the forward direction. The next generation of HPLA systems is exemplified by the EISCAT_3D multi-static phased-array radar concept. We discuss how this system will affect temporal and spatial resolution, sensitivity, and rate of statistics in meteor observations.

1. Introduction

Shooting stars, or meteors, have long whetted people's curiosity about what is really happening with the tiny pieces of extraterrestrial matter entering and interacting with the Earth's atmosphere. For a long time, the naked eye was the instrument with the best dynamic range to see variations in meteor behavior. Meteors can be seen coming from various directions with apparently different velocities; the trails can look like straight or curved lines, especially if they persist for a while, and have different nuances of color. The luminosity can be seen to vary along the trail. It is often strongest towards the end of the trail, and can twinkle a few times, as can be seen in Figure 1.

Figure 1. A photo showing a meteor with aurora in the background. Towards the end, the meteor was seen to twinkle at least three times. Assuming that the strong trail was some 30 km long, the twinkles would occur within a distance of 4-5 km along the path (photo: Torbjörn Lövgren, Kiruna).

Asta Pellinen-Wannberg is with the Umeä University, Swedeish Institute of Space Physics, Box 812, SE-98128 Kiruna, Sweden.
Gudmund Wannberg, Johan Kero, and Csilla Szasz are with the Swedish Institute of Space Physics, Box 812, SE-98128 Kiruna, Sweden; e-mail: asta.pellinen-wannberg@irf.se, gudmund.wannberg@irf.se, johan.kero@irf.se, csilla.szasz@irf.se.

Assar Westman is with the EISCAT Scientific Association, Box 812, SE-98128 Kiruna, Sweden; e-mail: assar.westman@eiscat.se.

T his is one of the Commission G invited Reviews of Radio Science.

Both photographic and radio methods for observing meteors were developed in the general development of these techniques in the first half of the 20th century ([1] and references therein). Photos recorded the static features of a meteor, while radars recorded the dynamic process yielding, e.g., the velocity. In 1958, an excellent text book, *Physics of Meteor Flight in the Atmosphere*, by Ernst Öpik [2] described, postulated, and modeled various small-scale processes occurring when a meteoroid enters the atmosphere, such as ablation, vaporization, sputtering, and fragmentation. The interpretation of these was probably based on and related to a profound amount of naked-eye observations, in addition to the visual and radio measurements, theoretical calculations, and assumptions, as well as knowledge of the structure and composition of the atmosphere and the meteoroids: at least meteorites could be thoroughly studied. In fact, the atmosphere was first monitored through the meteoroid interactions. Öpik's description of the small-scale processes was fascinating for its details. At that time, the approach was theoretical, and it was probably not expected that the processes could be recorded. However, today, due to the huge development of signal-processing and data-storage capabilities, more and more details of the meteoric disintegration processes can be revealed.

In this paper, we describe the meteor process in general. We describe how it can be observed with radio methods, starting with the specular meteor radar (SMR), followed by an introduction to the high-power large-aperture (HPLA) radar method. The status of the head-echo scattering models and the potential of HPLA radar trail echoes for better understanding the meteor-atmosphere interactions are discussed. We further discuss the development of one of the high-resolution methods of HPLA radars for observing meteors. We discuss the impact of this method on meteor studies in general, and the unique features offered by the EISCAT facility. Finally, we speculate about possible improvements that could be reached with new HPLA facilities, such as the EISCAT_3D, which is in the design phase.

2. Observing the Meteor Process

When a meteoric body enters the atmosphere, its collisions with the air molecules result in the production of heat, light, and ionization, distributed in the form of a long thin paraboloid with the meteoroid at its head. In this process, the region of ionized gas formed near the meteoroid expands – due to the atmospheric mean free path – instantaneously to a dimension called the initial radius. This is a few centimeters at 85 km, and a few meters at 115 km. Further back, the trail continues to expand at a much slower rate, due to the normal radial ambipolar diffusion process.

Standard ablation theory predicts that the electron line density in the trail is proportional to the mass of the particle. The radial distribution of the ionization within a trail is assumed to be Gaussian in the first approximation. In reality, trails seldom behave so neatly, but also contain more exciting constituents, including massive fragments and ions of both atmospheric and meteoric origin. The amount of these varies with altitude due to differential ablation. Studies of dusty-plasma conditions in meteor trails have even been conducted. What happens to various-size bodies entering the Earth's atmosphere depends on their velocity, structure, and size related to the atmospheric mean free path at various altitudes.

2.1 Observational Parameters

Ordinary meteoroids have velocities ranging from 10 to 80 km/s, and their sizes are from micrometers to centimeters. The faster and/or smaller meteoroids disintegrate at higher altitudes, due to faster heating of the body caused by collisions with the atmospheric constituents. Still smaller particles can pass the atmosphere unaffected, and end up as micrometeorites. Meteoroids have a variety of structures formed by their constituents, consisting of metals, volatile gases, chemical compounds, and minerals with different densities under various circumstances in their history. A dense and solid meteoroid gives a different signature than a porous particle with identical above-atmosphere mass, velocity, and impact angle. The atmosphere is known to have geographical, diurnal, and annual impacts, and it probably also has solar-cycle effects on the meteor process.

The ability to observe a meteor depends on many parameters. These can be divided into natural and observational parameters. For many kinds of observations, the most important natural parameters are the meteoroid's size and velocity: the large and fast meteoroids are most easily seen in passive visual observations. Different impact angles result in different path lengths through the atmosphere, affecting the strength of the interaction within the typical meteor's altitude range of 80-110 km.

Radars observe meteors through radiowave scattering from the target. The transient and strongly Doppler-shifted head echoes are due to coherent scattering, or reflection from ionization created around the meteoroid's body. Trail echoes are due to specular scattering or reflection from the trails formed in the wake of the meteoroid, and are therefore more stationary over time and target location, relatively speaking.

We now consider how different system parameters – such as the operating frequency, antenna size, and transmitter power – govern the sensitivity of a radar system. In general, increasing the antenna's aperture size and/or going to a higher frequency will result in a narrower radar beam and a correspondingly higher power density in the beam.

SMR antenna systems normally comprise a relatively small number of dipole antennas, as in the popular SkiyMET systems [3], for example. Consequently, the SMR beam is

wide and the collecting area at meteor altitudes is very large, while the in-beam power density is several orders of magnitude below that of HPLA radars. It is probably this vast difference in power density in the probing volume that is responsible for the most obvious difference in behavior between SMRs (which mostly only observe trail echoes) and HPLA systems (which nearly see only head echoes). Typical SMR operating frequencies range from 15 to 40 MHz. The lower frequency limit is essentially set by the maximum ionospheric plasma frequency, while the upper frequency limit is set by the quite intricate radio meteor ceiling effect, described below.

Incoherent-scatter HPLA radar operating frequencies range from 46.5 MHz at the Japanese MU radar [4], to 1.29 GHz at the Søndre Strømfjord radar, in Greenland [5]. Furthermore, the ALTAIR system operates at 160 MHz, 422 MHz, 1.32 GHz, and 2.95 GHz [6]. SMRs and HPLA radars show similar trends in their behavior of event rate as a function of frequency: more meteors are seen at lower frequencies, even though the two types of systems record echoes from different parts of the meteoroid disintegration process.

In HPLA radars, the system's noise temperature also plays an important role in determining the system's sensitivity. The total system noise temperature is the sum of receiver noise and sky noise; sky noise is mostly of galactic origin. Using modern semiconductors, the receiver contribution can easily be kept well below 100 K over the whole (50 MHz to 1 GHz) range. However, over this range, the sky noise decreases three orders of magnitude, from several thousand K at 50 MHz to less than 5 K at 1 GHz. Everything else being equal, a higher operating frequency thus results in a more-sensitive system. In addition, when going to higher frequencies, the target-size/radar-wavelength ratio of centimeter- or sub-centimeter-size targets will increase, causing the effective Rayleigh scattering cross sections to increase dramatically. These phenomena together can contribute to surprisingly high head-echo rates at GHz.

If the HPLA system uses a reflector antenna with multiple feeds, or a phased array, interferometry can be used to define the target location, and vector properties such as velocity and deceleration within the observing volume. At present, only ALTAIR, the Jicamarca system [7], and the EISCAT ESR are instrumented to do this.

The location of the instruments can also be considered to be an observational parameter. Optical instruments can be moved fairly easily, while radars are in general not easily relocated. However, SMRs are quite small and cheap, and there is now a good distribution of them around the world. They are very valuable for continuous monitoring of global meteoric flux and its variations on the Earth. HPLA radars are big science projects, and are expensive both to construct and to run. They are sited at strategic locations, selected according to their primary application, such as auroral zone research (AMISR, EISCAT, ESR, Søndre Strømfjord) or along a meridian (Søndre Strømfjord, Millstone, Arecibo, Jicamarca). They employ different hardware, and operate at vastly different frequencies.

Unfortunately, the sheer size of HPLA radars adds yet another parameter, namely, the economic parameter. There are only about ten of these multimillion-Euro facilities in the world, they are expensive to operate, and there is a lot of competition for observing time, thus practically excluding the possibility of running extended meteor campaigns on them.

2.2 The Radio Meteor Ceiling Effect

The ceiling effect is fundamental for the "HF, low-power, and small-aperture" radar method of observing meteors. The three parameters, frequency, power, and aperture, together make the observation conditions optimal for trail echoes. Single dipole antennas (small aperture) have wide beams with large collecting areas. This increases the probability of getting echoes from meteor trails with different orientations. To obtain maximum signal, the trails must be perpendicular to the radar beam for backscatter systems, to maximize the constructive interference from trail structures with lateral dimensions up to a quarter of the probing wavelength. This occurs through the radar wave scattering from the electrons in the expanding trail within a small area, along and across the trail. When the trail diameter reaches half the probing wavelength, the signal disappears, due to destructive interference. Thus, longer wavelengths, or, equally, lower frequencies (HF), down to just above the ionospheric plasma frequencies, are optimum. At the same time, only marginal enhancement from the background ionization level can be observed (low power). These advantages must be simultaneously related to the decreasing density and mean free path of the atmospheric constituents with increasing altitude at the meteor interaction range, to fully understand the limitations of the SMR method.

The geometry is an important factor in meteor radar studies [1]. To be observed, a meteor trail must be oriented almost normal to the scattering bisector. For backscatter systems where the transmitter and receiver are located at the same site, the meteor trail must be normal to the radar beam. The major part of the received signal is scattered by electrons in the first Fresnel zone, centered at that point on the trail that is normal to the radar beam. Over this zone, the phase of the wavefront varies less than $\pi/2$, and the partial wave contributions add constructively, as in a normal diffraction process. For a 50 MHz radar, the first Fresnel zone is about 1.6 km long at a range of 200 km.

The meteor trails are classified as under-dense or over-dense, depending on the electron density within the ionized column [1]. An under-dense trail is one in which the electron density is sufficiently low that a radar wave penetrates the trail, and scattering occurs independently

from free electrons within the trail. Thus, the concepts of under-dense and over-dense also depend on the probing frequency. In an over-dense trail, the electron density is sufficiently large – at least on the trail axis – that coherent scattering dominates. The wave is reflected from the over-dense part of the trail as if from a metallic cylinder. The ionized cylinder expands as the trail diffuses, and the over-dense condition collapses when the electron density on the axis falls below the critical value. As the trail further expands, the phase difference of the contributions from individual electrons distributed across the trail increases, so that the received power decreases exponentially due to destructive interference, as described above. The limiting line density between under-dense and over-dense trails for typical meteor radar frequencies is about 2.4×10^{14} electrons/m [1].

The detection of meteors using SMRs depends on the amplitude and duration of the echo. Of particular interest here is the finite-initial-radius effect on the amplitude of signals scattered from under-dense trails. If the exploring wavelength is comparable to or less than half of the initial diameter of the trail, the received signal is severely attenuated. As the initial radius increases with increasing altitude, this effect determines the radio meteor ceiling for a given wavelength. At VHF, the radio meteor ceiling for under-dense trails is about 105-110 km [1]. It has been suggested that this is one of the main reasons why VHF radars only detect about 3.5% of the meteors they should see, if the mass distribution is continuous [8].

For meter wavelengths, an expanding under-dense meteor trail, formed below the radio meteor ceiling, is observable as a cylindrical column of ionized particles with the growing diameter still less than a half of the exploring wavelength, and longer than the first Fresnel zone from which the main reflection is assumed to occur. When the exploring wavelength is decreased to the centimeter range, the expanding trail remains small compared to the wavelength only for a short time, t [9]. Signals can then be assumed to be reflected only from a small portion of the trail of length vt, which can be modeled as the head (region of maximum curvature) of a paraboloid immediately behind the evaporating meteoroid, moving with velocity v. This effect, together with the initial-radius effect and the equipment sensitivity limitations, define an upper frequency limit for SMRs.

Although the ceiling effect restricts observation of many meteor trails, the SMR method has been the base of understanding the meteor process since its start in the 1940s. Large numbers of valuable scientific results have been published. A very good review of these results is given in [10].

3. The HPLA Method

3.1 Background

John Evans performed some meteor studies at the 430 MHz MIT Millstone Hill Radar as early as in the 1960s. Even though "head echoes" were identified and mentioned in these studies [11, 12], their characteristics as understood today were not highlighted. For the following three decades, dedicated radar studies of meteors thus continued to employ low-VHF specular-reflection meteor radars, and to focus on trail echoes. Meanwhile, meteor echoes were regularly noted at many HPLA facilities, but were regarded more as a nuisance, contaminating ordinary incoherent-scatter data [13].

A new era started in 1990, independently at the EISCAT and Jicamarca incoherent-scatter facilities [14, 15]. While EISCAT operates at 224 MHz and 930 MHz, Jicamarca runs a huge phased-array system at 50 MHz. The first results from the two systems were quite different from each other: EISCAT reported the first modern incoherent-scatter radar head-echo observations, while the studies reported from Jicamarca were on non-specular trail echoes.

As almost all meteor echoes registered at these facilities were coherent, the term "incoherent-scatter radar" was seen to be a misnomer. Instead, the concept HPLA (high-power large-aperture) radar was introduced to distinguish the big systems from the dedicated meteor radars [16]. The HPLA classification has the added advantage of also covering some major defense radar installations occasionally being made available for scientific work, such as the multi-frequency ALTAIR radar system at Kwajalein Atoll [6]. HPLA systems operate with transmitter powers in the multi-MW class, and large antenna apertures of diameters ranging from 30 m to 300 m.

The visit of the 33-year-period parent comet of the Leonid meteor shower, 55P/Tempel-Tuttle, to the central solar system in 1998, and the expected increase of Leonid rates during the years around the perihelion passage, enormously increased the interest in meteor studies. During the 1997 and 1998 Leonid showers, most of the world's incoherent-scatter radars ran dedicated Leonid observations, just to observe that the shower activity – so spectacular when observed optically and with conventional meteor radars – did not produce any significant increase in the observed meteor rates [17, 18, 6]. The power densities of these radars in their small collecting volumes is so high (three to six orders of magnitudes higher than for the most powerful meteor radars [19]) that returns from the numerous sporadic populations of very small grains dominates in rate over the comparatively few (but larger) shower meteor grains that would hit the observing volume.

3.2 An Example of an Instrument: EISCAT Incoherent-Scatter Facility

Most of the world's HPLA-class radar facilities perform meteor studies today. They vary in their frequency, latitude, and antenna types and configurations. These were compared to some extent in [20], but were best described for the meteor application by the primary users themselves [14, 21, 5, 22, 4, 23, 7]. Here, we use the EISCAT radar systems to exemplify how to use an HPLA facility for meteor work.

EISCAT, the European Incoherent Scatter radar facility, comprises three radars, viz., a tri-static 930 MHz UHF system, a dual-antenna monostatic 500 MHz UHF system (the EISCAT Svalbard Radar), and a 224 MHz VHF system. The UHF and VHF transmitters are both located at Ramfjordmoen, near Tromsø, Norway (69.6° N, 19.2° E). The transmitters work at peak powers close to 2 MW. The –3 dB beamwidth of the parabolic 32-m UHF antenna is 0.6°, corresponding to a 1 km half-power beam diameter at 100 km range. The VHF system operates into a (120×40) m^2 parabolic-cylinder antenna, which produces a roughly elliptical $(1.2° \times 1.7°)$ –3 dB beam. This corresponds to a (2×3) km half-power beamwidth at 100 km range. The two remote UHF receivers are located in Kiruna, Sweden (67.9° N, 20.4° E) and Sodankylä, Finland (67.4° N, 26.6° E).

The present EISCAT radars are by no means perfect instruments for meteor studies, but they have many advantages and unique features. During the first observations in 1990 and 1991, the time resolution was two seconds and the spatial resolution was 300 m, which was the best the system could do at that time [14]. For the 1993 observations, a time-slice receiving technique with 10 ms slices was implemented, just to confirm that with this resolution the meteor passage through the radar beam could be observed in several steps [24]. In pace with the huge leaps in data-storage and computational-capacity development, a completely new signal-processing philosophy was developed for the new EISCAT Svalbard radar. Shortly afterwards, the mainland EISCAT UHF and VHF radars were upgraded with the same pulse-modulation and data-processing systems. How these are utilized for meteor studies today is described in Section 3.5.

The EISCAT radars offer three features that are essential for successful meteor studies:

1. With the tri-static UHF system (unique in the world today), radiowave scattering from the meteor heads can be simultaneously monitored at different aspect angles, allowing us to study the head-echo target form [25]. Multi-static observations also allow meteoroid fragmentation to be distinguished from meteoroid rotation [26]. In addition, high-resolution vector velocity and deceleration observations (Figure 2) can be made, giving very good mass and orbit estimates and,

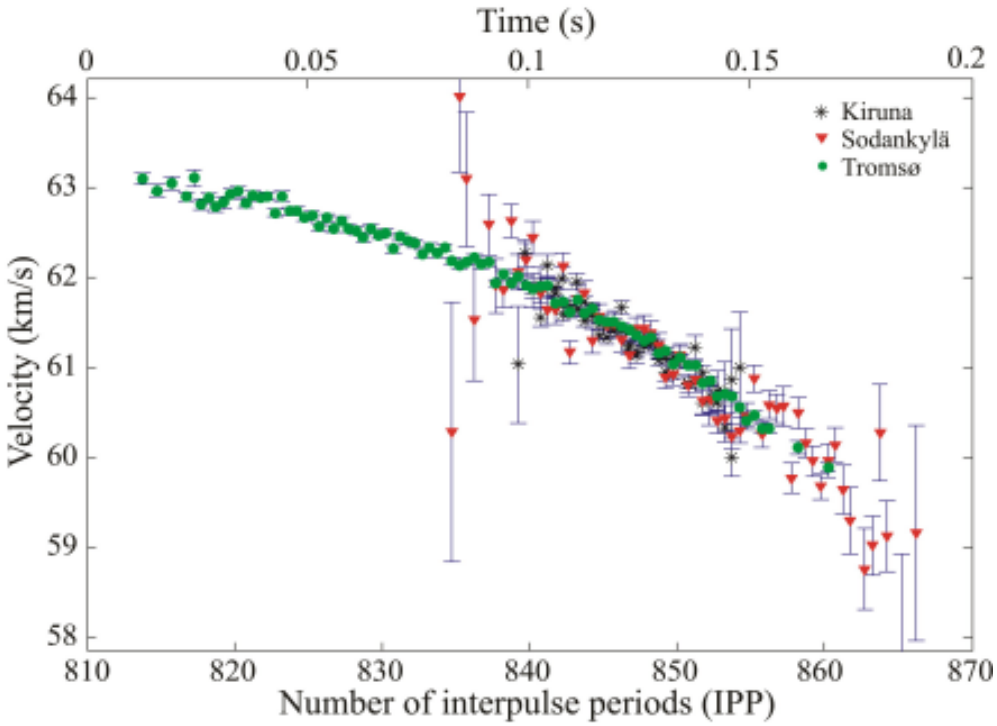

Figure 2. Velocity and deceleration data from a tri-static EISCAT UHF observation. This meteoroid moved quite a long time along the Tromsø radar beam before entering the common volume for the three receivers. The data was plotted as a function of the number of inter-pulse periods (IPP), which gave the location of the event in the data dump. The length of the IPP was 3312 μs.

ultimately, an indication of the origin of the observed meteoroids [27]. These results are comparable to the results from the interferometric method at the Jicamarca radar [7].

2. The VHF and UHF radars have been used together for dual-frequency monitoring of a common interaction volume to observe the scattering from the same meteor at two very different frequencies, 224 MHz and 930 MHz. This sheds some light on the wavelength dependence of the scattering process [24, 28]. At the ALTAIR radars, similar observations have been performed on four different radar frequencies [23]. The results from the two facilities show similar features.
3. Because of the short path through the atmosphere, the location of EISCAT at high northern latitudes offers a good opportunity to study the off-ecliptic meteoroid population related to long-period comets.

3.3 Head echoes

Head echoes have fascinated meteor scientists since the 1940s [29], and about a half-dozen different models have been introduced to explain all their observed features. Jones and Webster [30] presented a thorough analysis of visual and radar studies of meteor-head echoes. They stated that "even after 4 decades there is still no comprehensive theory which explains all the features associated with head echoes." They concluded that a detailed knowledge of the ionized coma in the vicinity of a single meteoric grain would be a prerequisite for a successful theory. Even Steel and Elford [31] concluded, in their paper on radio meteor height distributions, that further experimental work aimed at determining the true height distribution might need to use techniques completely different from those used in meteor radars. A review of the history of head-echo modeling was given in [32] and the references therein.

The very first meteor-head-echo observations with the EISCAT UHF incoherent scatter radar were performed in December 1990 [14]. Following that, head echoes had been reported at least from ALTAIR, Arecibo, Millstone Hill, Jicamarca, MU, and Søndre Strømfjord [21, 22, 4, 23, 7]. All these observations were in good agreement with the definition of a head echo first introduced in [33]: "An instantaneous echo moving with the velocity of a meteor." They were consistent with a scenario where the echoes originate from sharp density gradients in the ionization in the immediate vicinity of the approaching meteors. The disagreements between current competing models are mainly related to whether or not the scattering is truly coherent from over-dense plasma (such as from a conducting sphere), and what really is the effective target size [34, 35]. In Section 3.5, some data from EISCAT supporting the very-small-target hypothesis are presented. The discussion on head echoes will probably still continue for a long time.

3.4 Trail echoes

The very-high-resolution-method features are not relevant for trail-echo studies. Therefore, we just briefly present various kinds of trail-echo types identified up to now, which show different phases of the trail's formation.

Meteors were first identified through specular trail echoes perpendicular to the radar beam, a technique that SMRs have been using during their whole history. In addition, non-specular trail echoes, appearing shortly after the head echo, also called RSTE (range-spread trail echoes), have been observed by many HPLA radars [36, 37]. These are assumed to be caused by plasma-turbulence-generated field-aligned irregularities. The fact that EISCAT has never seen such echoes supports this interpretation, since EISCAT generally observes close to the almost vertical geomagnetic field lines. In a test to come as close to perpendicular to the geomagnetic field as possible (73°), no trails were observed [38].

There are at least two other kinds of observations of meteor trails. Brosch et al. [39] reported trails up to 250 km altitude, and interpreted the origin of these trails as sputtering of atmospheric particles on meteoroids at these altitudes. Also, very high trail-like observations have been done with EISCAT. Pellinen-Wannberg and Wannberg [40] reported a few trails from 135 to 150 km altitude, apparently in thermal equilibrium and with different plasma content than the background ionosphere at these altitudes. The feature is interpreted as incoherent scatter from "old" meteor trails traversing the radar beam. A dusty-plasma approach to this phenomenon has been initiated by the Dusty Plasma Team at the International Space Science Institute, ISSI, in Bern, Switzerland.

3.5 High-Resolution Observations

In ordinary ionospheric observation modes, integration times of the order of seconds are required to raise the received signal to a statistically significant level above the background noise. A spatial resolution of the order of a fraction of the ionospheric scale height (i.e., typically more than a kilometer) is normally sufficient. However, at 100 km altitude, a 35 km/s velocity meteoroid traverses the EISCAT UHF beam in about 30-60 ms. Since good deceleration data are needed for mass estimates, the meteor must be sampled several tens of times during the passage, thus defining the desired time resolution to be something of the order of a millisecond. A fully reliable online analysis system for the meteor experiments is not yet available. In order to allow each echo to be studied interactively after an experiment, the unprocessed complex-amplitude data stream is therefore recorded at the full sampling rate. This technique unfortunately generates a huge volume of data.

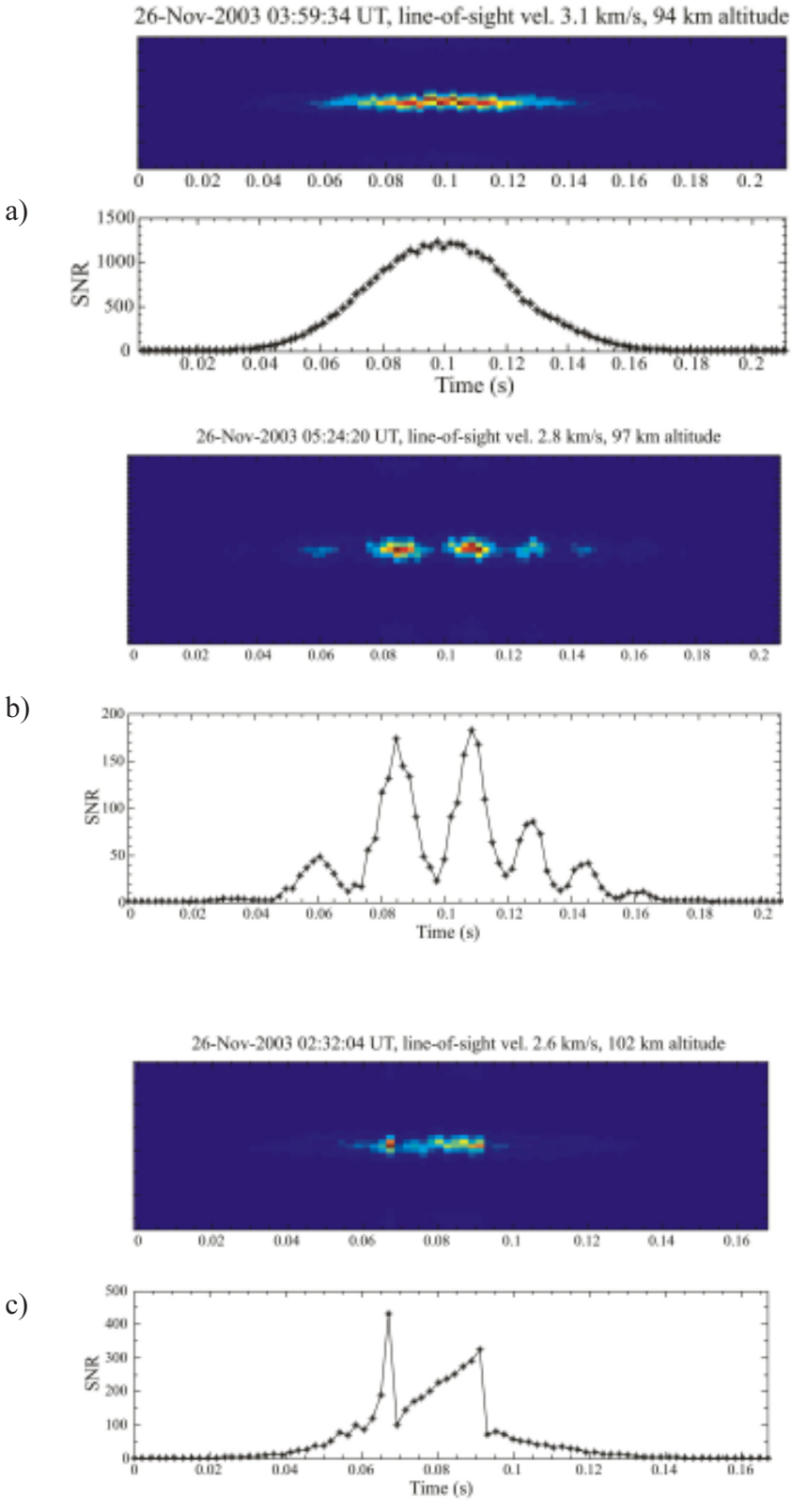

Figure 3. Different kinds of behavior of meteoroids as they pass through a radar beam: (a) shows nice constant disintegration, (b) oscillations, and (c) sudden break-up features. The upper and lower panels show the meteor-aligned range-time intensity plot (upper) and the SNR (lower).

When pulse coding is employed, the sub-pulse length defines the spatial resolution. In a monostatic geometry, 1 μs (the shortest sub-pulse that can sensibly be used at EISCAT) thus corresponds to 150 m, that is, three to four orders of magnitude larger than the (100 μm to 1 mm) meteoroid particle size range typically monitored by EISCAT.

The EISCAT meteor code uses a 32×2.4 μs = 76.8 μs long pulse, where the sub-pulses are binary phase-shift-keying (BPSK) modulated according to a low-sidelobe 32-bit binary pseudo-random sequence [41]. This gives better than –30 dB sidelobe suppression over the range ±1100 meters. The worst sidelobes are approximately –17 dB, but they are further out. On receiving, the signal is sampled at 0.6 μs intervals, corresponding to 90 m range resolution [38]. This allows a very good reconstruction of the meteor's propagation through the radar beam. Figure 3 shows three different kinds of behavior for meteoroids passing through a beam. In a few lucky cases among about 2500 observed events, two meteoroids simultaneously present in the radar beam could be resolved and individually analyzed. An example of this was given in [41].

When the meteoroid interacts with the atmosphere, electrons and neutral as well as ionized atoms and molecules (both from the particle, as well as from the atmosphere) contribute to the meteor "head" plasma cloud and the lagging trail. It is important to understand which parts of this composite target are visible to different observational techniques. SMRs typically only see the trail behind the meteor, and they see that only for as long as its lateral dimensions are less than half a wavelength. Thereafter, the trail with enhanced ionization, continues to expand and recombine until the electron density approaches the background ionospheric density.

HPLA radars generally only observe head echoes. There are different views on how big the part of the plasma cloud that forms the HPLA target really is. If one assumes that the scattering is off over-dense plasma, the target size can be roughly estimated to be in the centimeter range [24]. The full plasma cloud is, of course, larger, but beyond half a radar wavelength, signals scattered from the outermost parts begin to interfere destructively, similarly to what is observed in the trail case. This limits the observable target size to something of the order of a few tens of centimeters for most HPLA radars [34].

As a first approximation, the electron density in the plasma cloud can be assumed to follow a Gaussian distribution [24, 42]. The width of the distribution – which is the parameter of interest connected to the target size – decreases with decreasing mean free path and altitude. In a recent simulation, Dyrud et al. [35] arrived at typical plasma-cloud diameters of tens of meters perpendicular to the meteoroid direction of propagation, and trail-ward extents of hundreds of meters.

The tri-static EISCAT UHF system offers the unique possibility of studying the aspect-angle sensitivity of meteor-head echoes. All observations made during the last few years have been made in a common volume at 96 km altitude, where the UHF system has its average head-echo-rate maximum. The volume is located so as to make the three scattering vectors as linearly independent as possible, given the actual system layout. While meteors can enter the common volume from any direction in the upper hemisphere, the system's geometry only allows observations to be made out to 130° from the direction of meteoroid propagation. A statistical study of a database containing 410 events, comparing the cross section estimates deduced from the simultaneous observations from all the three receivers,

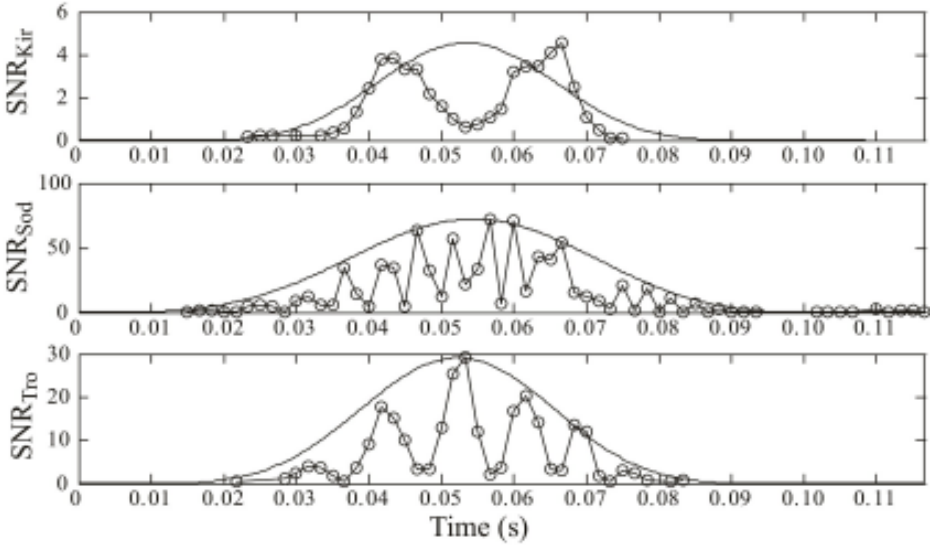

Figure 4. A tri-static observation of an oscillating meteor. The periods of the oscillations from the three sites were different. This was due to constructive and destructive interference between scattered signals from two meteoroid fragments still very close to each other.

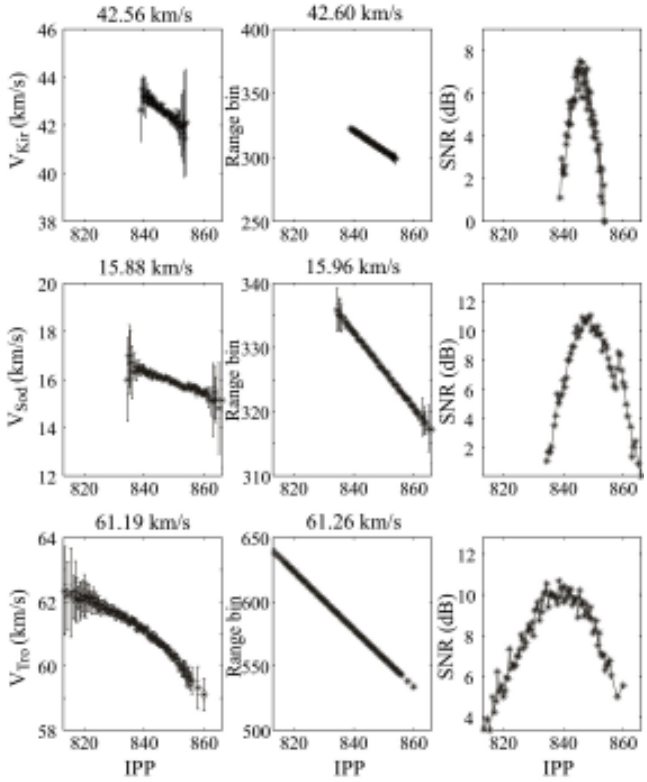

Figure 5. Both Doppler (column 1) and range – with every range bin corresponding to 90 m (column 2) – data, as well as SNR data (column 3) from Kiruna (row 1), Sodankylä (row 2), and Tromsø (row 3) receivers for the meteoroid from Figure 2 passing the common volume monitored by the three antennas.

showed that the cross section was close to isotropic out to the observational limit, consistent with an essentially spherical target [25]. If there is any plasma slipping behind the meteor, it must be restricted to the unobservable 50° cone in the backward direction.

Wave interference is a powerful tool in many studies using electromagnetic waves, from sub-nuclear to astronomical scales. Under favorable conditions, it can also help us to investigate specific aspects of the meteor-atmosphere interaction process. Figure 3b shows the oscillating behavior of a meteor passing through the radar beam. When this kind of behavior is seen from three directions simultaneously with the UHF radar, the true origin of the phenomenon is revealed (Figure 4): The periods of the oscillations as seen at the three sites are different, showing that the oscillations are not coming from the body itself, due to rotation, for example. The period of the oscillations also decreases for every component. This is interpreted as being the result of interference between signals scattered from two meteoroid fragments slowly moving away from each other. Since the composite signal is almost extinguished at the nulls, the two interfering signals must be about equally strong, and so first-order interference is most probable. Thus the observation is interpreted as two fragments, initially separated by only a few centimeters and drifting apart to a distance of some meters [26]. This interpretation strongly supports the over-dense-target hypothesis: the effective target sizes must be smaller than the initial separation for the signal nulls to be so sharp.

The possibility of using wave interference as an analysis tool in the above case was the result of a unique combination of observation conditions, and thus quite fortuitous. However, in phased arrays, where data are separately processed for every individual antenna element or groups of elements, *interferometry* can also be used systematically to get highly increased resolution.

At the EISCAT UHF, signals received from the same meteor by all three receivers have been used to follow its propagation through the common volume with very high resolution [43]. Figure 5 shows an example of such data. This is the same meteor as the one shown in detail in Figure 2. The velocity components above the column 1 panels in Figure 5 come from the average decoded Doppler over the observation range, while the components in column 2 come from the time-of-flight estimates. For the whole data set of 410 tri-static observations, these two ways of estimating the velocity agree very well, as was shown in [41]. The SNR data in column 3 is essential to trace back the meteor path through the radar beam, as shown for six arbitrary tri-static meteors in Figure 6. It shows the position of each single head-echo observation projected perpendicular to the radar beam. There were two meteors crossing almost through the center of the radar beam. Three meteors passed the beam outside the –3 dB limit from the beam center. The strongest one of these scattered echoes even from the sidelobes, while the faintest one of the six meteors was hardly seen through its whole passage within the central lobe.

Since the tri-static data gives the exact position of the meteoroid in the radar beam and the power-density distribution across the beam is well known, the scattering cross section of the meteoroid coma can be estimated with great precision. The absolute visual magnitudes of meteors

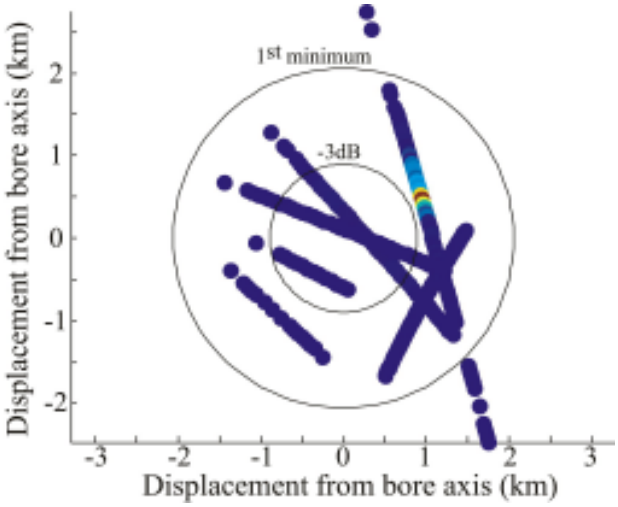

Figure 6. Examples of six different meteor-head echo trajectories through the UHF radar beam.

producing radar head echoes can then be estimated from the cross sections. They are in the range of +9 to +5, and should thus be observable with telescopic CCD cameras [44]. Preliminary results from a joint optical-EISCAT campaign in October 2007 confirmed this [45].

4. Summary

The HPLA radar method for meteor studies has proved to be very powerful. More than 100 meteor-science papers based on ALTAIR, Arecibo, EISCAT, Jicamarca, Millstone, MU, and Søndre Strømfjord radar data have been published since the early 1990s. Most of these installations have always had the raw sensitivity required for these observations, but only with the explosive development in signal-processing, computing-power, and data-storage capabilities over the last two decades has it become possible to use them sensibly for meteor studies.

The most important results contributed by HPLA radars so far are all related to various aspects of the head echoes. Properly analyzed, these carry a lot of information. The orbits of the meteoroids can be estimated from the observed vector velocities, while time-series observations of meteoroid passage through the radar beam allow meteor deceleration (and thus, by extension, meteor mass) to be estimated. Feeding the mass estimates back into the orbit determination makes it possible to correct for the effect of atmospheric drag on the meteoroid on its way to the observation altitude, thus greatly improving the accuracy of the orbit determination [27]. Using the tri-static EISCAT UHF radar, Kero et al. [43] were able to trace the passage of a meteoroid through the radar beam in detail.

Time-series observations through the radar beam reveal a range of features related to different phases of the disintegration process, such as constant vaporization; sudden break-ups, indicating releases of volatile components locked in the body; and small-scale and larger-scale fragmentation. Together with the known orbit of the meteoroid, such data can reveal structure and composition of the meteoroids originating from different populations, such as long-period comets or the solar-system dust cloud.

A lot of observational, theoretical, modeling, and simulation work has gone into trying to understand the radiowave scattering from meteors that is classified as a head echo. There is general agreement that the targets move with the velocity of the meteoroid, and that the head echoes originate from a region of highly increased ionization. The remaining controversies mainly concern the effective size of the target, the ionization distribution, how much of the increased ionization actually contributes to the head-echo power, and the frequency dependence of all these. From EISCAT UHF tri-static observations of small-scale fragmentation events, Kero et al. [26] were able to start to distinguish the fragments already when their separation was only a fraction of the wavelength, 32 cm. Thus, Kero et al. [26] claimed that the size of the head-echo targets must be in the centimeter range, with small variations depending on the HPLA radar frequency.

Some HPLA radar work has also been conducted on trail echoes. Data from non-specular trails promise to be of great interest from the plasma-physics point of view. The diagnostic technique for which these radars were originally built – incoherent scatter – might turn out to be the technique of choice, and of crucial importance for the further study of the high-altitude meteor trails reported in [39] and [40].

5. Future Prospects

The HPLA method can still contribute a lot of new knowledge to meteor-related science. There are still challenges concerning the understanding of the head-echo process, and its applications regarding orbits, origins, and mass fluxes of the meteoroid population, as well as the fate of the disintegrated meteor matter in the atmosphere. For the latter studies, the incoherent-scatter technique could reveal the presence of various heavy ions in the D region, originating from the meteoroids. Multi-static interferometric radar systems, distributed all around the world, would be good for all these topics, and lower frequencies would give higher rates for any kind of studies.

EISCAT_3D is a four-year design study for a new radar facility with greatly enhanced performance, to meet the requirements for meteor studies as well as other space-science issues in the European high-latitude region. The new system will retain and expand on the unique multi-static configuration of the mainland EISCAT UHF system. A central transmitting/receiving core, located close to the Tromsø radar site, will be augmented by four receive-only facilities. Two of these will be located on a baseline pointing southwards from the core site, at ground distances of ~ 90-120 km and ~ 220-280 km from the core, and the other two on an eastwards-pointing baseline. Each receive-only site

will comprise a phased-array antenna with its associated receivers, followed by a beam-former system capable of generating several simultaneous, independently steerable receiving beams.

The design targets for the new system include a tenfold improvement in temporal and spatial resolution relative to the current EISCAT systems, an extension of the instantaneous measurement of full-vector ionospheric-drift velocities from a single point to the entire altitude range of the radar, a beam-pointing resolution of better than 0.625° in two orthogonal planes, and built-in interferometric capabilities, offering a horizontal resolution of better than 20 m at 100 km altitude.

When fully populated, the core array will contain about 16000 elements, each equipped with a dual 300 + 300 watt solid-state power amplifier, a short X Yagi antenna, and a digitizing receiver. The power-amplifier system will be designed for an instantaneous -1 dB power bandwidth of more than 5 MHz, corresponding to a range resolution of about 60 m. Pulse lengths from 0.2 to 2000 ìs and PRFs up to 3000 Hz can be accommodated. It will be possible to steer the beam generated by the central core array out to a maximum zenith angle of $\approx 40°$ in all azimuth directions. At 300 km altitude, the radius of the resulting field-of-view will be approximately 200 km, corresponding to a latitudinal coverage of ±1.80° relative to the transmitter site.

For optimum incoherent-scatter performance in low-electron-density conditions and in the middle atmosphere, the system will use an operating frequency in the high VHF range, somewhere between 220 to 250 MHz. Since the core site is going to be located in Norway, but the receiving stations will be in Finland and Sweden, frequency coordination across national borders will be required. At this time, no firm frequency allocation has been issued by any of the concerned frequency administrations, but it is expected that at least a 5 MHz wide slot will be made available for transmission in Norway.

When EISCAT_3D eventually gets financed and constructed[1] according to the design study, it will offer many improvements for meteor studies. The operating frequency is one important factor: head-echo rates with the present VHF are about ten times higher than for the UHF. Thus, three-dimensional observations can be expected on a much larger population than that observed with the present UHF facility, including smaller and slower meteors. This would dramatically increase the number of meteors for which orbits and probable origins can be determined. Each receive-only phased array will be equipped with several beam formers, permitting the simultaneous generation of a number of independently steerable receiving beams. This will make it possible to use the close-in receiving sites to perform simultaneous and overlapping three-dimensional observations over a range of altitudes in the E region, and this will thus increase the common scattering volume and the rate of meteor statistics by a factor of at least five compared to the present UHF case. At the same time, the "F-region" receiver sites could be dedicated to searching for high-altitude trails. Finally, the interferometric capability could be employed to improve the spatial resolution further, down to something of the order of 10 meters, which should finally make it possible to put a credible upper boundary on the head-echo target size.

The HPLA radar method has already shown parts of its potential for acquiring new knowledge from its meteor observations. Even though there are still discussions about the head-echo scattering process, there is an agreement concerning the general features offering velocity, deceleration, and cross-section estimates of the meteor target. To fill in the gaps in our knowledge in the submicrometer- to centimeter-sized meteor population fluxes on Earth, we need not only instrumental improvements to the HPLA radars in the future, but also joint SMR, HPLA radar, and visual observations of the same meteors.

6. Acknowledgements

We gratefully acknowledge the EISCAT staff for their assistance during the observation campaigns. EISCAT is an international association supported by research organizations from China (CRIPR), Finland (SA), Germany (DFG), Japan (NIPR and STEL), Norway (NFR), Sweden (VR), and the United Kingdom (STFC). The EISCAT_3D Design Project is financed by the EU 6th Framework Programme. Two of the authors (J. K. and C. S.) are financed by the Swedish National Graduate School of Space Technology. We thank Margaret Campbell-Brown, Nicole Kaiser, and Rob Weryk at the University of Western Ontario for preliminary optical results.

7. References

1. D. W. R. McKinley, *Meteor Science and Engineering*, New York, McGraw-Hill, 1961.
2. E. J. Öpik, *Physics of Meteor Flight in the Atmosphere*, New York, Interscience Publishers, Inc., 1958.
3. W. K. Hocking, B. Fuller, and B. Vandepeer, "Real-Time Determination of Meteor-related Parameters Utilizing Modern Digital Technology," *Journal of Atmospheric and Solar-Terrestrial Physics*, **63**, 2001, pp. 155-169.
4. K. Nishimura, T. Sato, T. Nakamura, and M. Ueda, "High Sensitivity Radar-Optical Observations of Faint Meteors," *IEICE Trans. Commun.*, **E84-C**, 12, December 2001.
5. C. J. Heinselman, "Auroral Effects on the Gas Phase Chemistry of Meteoric Sodium," *Journal of Geophysical Research*, **105**, 2000, pp. 12181-12192.
6. S. Close, S. Hunt, M. Minardi, and F. McKeen, "Characterization of Leonid Meteor Head Echo Data Collected Using the VHF/UHF Advanced Research Projects Agency Long-Range and Tracking Radar," *Radio Science*, **37**, 2002, DOI:10.1029/2000RS002602.
7. J. L. Chau and R. F. Woodman, "Observations of Meteor-Head Echoes Using the Jicamarca 50 MHz Radar in Interferometer Mode," *Atmospheric Chemistry and Physics*, **4**, 2004, pp. 511-521.
8. D. Olsson-Steel, and W. G. Elford, "The Height Distribution of Radio Meteors: Observations at 2 MHz," *Journal of Atmospheric and Terrestrial Physics*, **49**, 1987, pp. 243-258.

9. R. von Eshleman, "Meteor Scatter," in D. H. Menzel (ed.), *The Radio Noise Spectrum*, Cambridge, MA, Harvard University Press, 1960.
10. Z. Ceplecha, J. Borovicka, W. G. Elford, D. O. ReVelle, R. L. Hawkes, V. Porubcan, and M. Simek, "Meteor Phenomena and Bodies," *Space Sci. Rev.*, **84**, 1998, pp. 327-471.
11. J. V. Evans, "Radio-Echo Studies of Meteors at 68-Centimeter Wavelength," *Journal of Geophysical Research*, **70**, 1965, pp. 5395-5416.
12. J. V. Evans, "Radar Observations of Meteor Deceleration," *Journal of Geophysical Research*, **71**, 1966, pp. 171-188.
13. M. J. German, and J. D. Mathews, "Interference Detection and Correction Applied to Incoherent Scatter Radar Power Profile Measurements," *Radio Science*, **21**, 1986, pp. 745-751.
14. A. Pellinen-Wannberg, and G. Wannberg, "Meteor Observations with the European Incoherent Scatter UHF Radar," *Journal of Geophysical Research*, **99**, 1994, pp. 11 379-11 390.
15. E. Chapin, and E. Kudeki, "Radar Interferometric Imaging Studies of Long-Duration Meteor Echoes Observed at Jicamarca," *Journal of Geophysical Research*, **99**, 1994, pp. 8937-8949.
16. A. Pellinen-Wannberg, "The High Power Large Aperture Radar Method for Meteor Observations," *Proceedings of the Meteoroids 2001 Conference*, Vol. ESA SP-495, 2001, pp. 443-450.
17. A. Pellinen-Wannberg, A. Westman, G. Wannberg, and K. Kaila, "Meteor Fluxes and Visual Magnitudes from EISCAT Radar Event Rates: A Comparison with Cross Section Based Magnitude Estimates and Optical Data," *Annales Geophysicae*, **16**, 1998, pp. 1475-1485.
18. D. Janches, J. D. Mathews, D. D. Meisel, and Q. Zhou, "Micrometeor Observations Using the Arecibo 430 MHz Radar: I. Determination of the Ballistic Parameters from Measured Doppler Velocity and Deceleration Results," *Icarus*, **145**, 2000, pp. 53-63.
19. W. J. Baggaley, R. G. T. Bennett, D. I. Steel, and A. D. Taylor, "The Advanced Meteor Orbit Radar Facility: AMOR," *Quarterly Journal of Royal Astronomical Society*, **35**, 1994, pp. 293-320.
20. D. Janches, S. Close, and J. Fentzke, "A Comparison of Detection Sensitivity Between ALTAIR and Arecibo Meteor Observations: Can High Power and Large Aperture Radars Detect Low Velocity Meteor Head Echoes," *Icarus*, 2007, DOI: 10.1016/ j.icarus.2007.08.022.
21. Q. Zhou, C. A. Tepley, and M. P. Sulzer, "Meteor Observations by the Arecibo 430MHz Incoherent Scatter Radar – I. Results from Time-Integrated Observations," *Journal of Atmospheric and Terrestrial Physics*, **57**, 1995, pp. 421-431.
22. P. J. Erickson, F. D. Lind, S. M. Wendelken, and M. A. Faubert, "Meteor Head Echo Observations Using the Millstone Hill UHF Incoherent Scatter Radar System," *Proceedings of the Meteoroids 2001 Conference*, Vol. ESA SP-495, 2001, pp. 457-463.
23. S. Close, M. Oppenheim, S. Hunt, and L. Duryd, "Scattering Characteristics of High-Resolution Meteor Head Echoes Detected at Multiple Frequencies," *Journal of Geophysical Research*, **107**, 2002, DOI: 10.1029/2002JA009253.
24. G. Wannberg, A. Pellinen-Wannberg, and A. Westman, "An Ambiguity-Function-Based Method for Analysis of Doppler Decompressed Radar Signals to EISCAT Measurements of Oblique UHF-VHF Meteor Echoes, *Radio Science*, **31**, 1996, pp. 497-518.
25. J. Kero, C. Szasz, G. Wannberg, A. Pellinen-Wannberg, and A. Westman, "On the Meteoric Head Echo Radar Cross Section Angular Dependence," *Geophysical Research Letters*, 35, L07101, doi:10.1029/ 2008GL033402, 2008.
26. J. Kero, C. Szasz, A. Pellinen-Wannberg, G. Wannberg, A. Westman, and D. D. Meisel, "Three Dimensional Radar Observation of a Submillimeter Meteoroid Fragmentation," *Geophysical Research Letters*, **35**, 2008, doi:10.1029/ 2007GL032733.
27. C. Szasz, J. Kero, D. D. Meisel, A. Pellinen-Wannberg, G. Wannberg, and A. Westman, "Orbit Characteristics of the Tristatic EISCAT UHF Meteors, to be submitted to *Monthly Notices of Royal Astronomical Society*, 2008.
28. A. Westman, G. Wannberg, and A. Pellinen-Wannberg, "Meteor Head Echo Height Distributions and the Height Cutoff Effect Studied with the EISCAT HPLA UHF and VHF Radars," *Annales Geophysicae*, **22**, 2004, pp. 1575-1584.
29. J. S. Hey, S. J. Parsons, and G. S. Stewart, "Radar Observations of the Giacobinid Meteor Shower," *Monthly Notices of Royal Astronomical Society*, **107**, 1947, pp. 176-183.
30. J. Jones, and A. R. Webster, A. "Visual and Radar Studies of Meteor Head Echoes," *Planetary and Space Science*, **39**, 1991, pp. 873-878.
31. D. I. Steel, and W. G. Elford, "The Height Distribution of Radio Meteors: Comparison of Observations at Different Frequencies on the Basis of Standard Echo Theory," *Journal of Atmospheric and Terrestrial Physics*, **53**, 1991, pp. 409-417.
32. A. Pellinen-Wannberg, "Meteor Head Echoes – Observations and Models," *Annales Geophysicae*, **23**, 2005, pp. 201-205.
33. P. M. Millman, and D. W. R. McKinley, "A Note on Four Complex Meteor Radar Echoes," *Journal of Royal Astronomical Society in Canada*, **42**, 1949, pp. 121-130.
34. J. D. Mathews, "Radio Science Issues Surrounding HF/VHF/ UHF Radar Meteor Studies," *Journal of Atmospheric and Solar-Terrestrial Physics*, **66**, 3, 2004, pp. 285-299.
35. L. Dyrud, D. Wilson, S. Boerve, J. Trulsen, H. Pecseli, S. Close, C. Chen and Y. Lee, "Plasma and Electromagnetic Wave Simulations of Meteors, *Advances of Space Research*, 2007, doi:10.1016/ j.asr.2007.03.048.
36. Q. H. Zhou, J. D. Mathews, and T. Nakamura, "Implications of Meteor Observations by the MU Radar," *Geophysical Research Letters*, **28**, 2001, pp. 1399-1402.
37. L. P. Dyrud, M. M. Oppenheim, S. Close, and S. Hunt, "Interpretation of Non-Specular Radar Meteor Trails," *Geophysical Research Letters*, **29**, 2002, DOI:10.1029/2002GL015953.
38. J. Kero, C. Szasz, A. Pellinen-Wannberg, G. Wannberg, and A. Westman, "Power Fluctuations in Meteor Head Echoes Observed with the EISCAT VHF Radar," *Earth Moon, and Planets*, **95**, 2004, pp. 633-638.
39. N. Brosch, D Polishook, R. Helled, S. Schijvarg, and M. Rosenkrantz, "Radar and Optical Leonids," *Atmospheric Chemistry and Physics*, **4**, 2004, pp. 1063-1069.
40. A. Pellinen-Wannberg, and G. Wannberg, "Enhanced Ion-Acoustic Echoes from Meteor Trails," *Journal of Atmospheric and Terrestrial Physics*, **58**, 1996, pp. 495-506.
41. G. Wannberg, A. Westman, J. Kero, C. Szasz, and A. Pellinen-Wannberg, "The EISCAT Meteor Code," submitted to *Annales Geophysicae*, 2008.
42. S. Close, M. Oppenheim, S. Hunt, and A. Coster, "A Technique for Calculating Meteor Plasma Density and Meteoroid Mass from Radar Head Echo Scattering," *Icarus*, **168**, 2004, pp. 43-52.
43. J. Kero, C. Szasz, A. Pellinen-Wannberg, G. Wannberg, and A. Westman, "3D Position Determination of Small Coherent Meteor Targets with EISCAT UHF," submitted to *Annales Geophysicae*, 2008.
44. C. Szasz, J. Kero, A. Pellinen-Wannberg, D. D. Meisel, G. Wannberg and A. Westman, "Visual Magnitudes of the EISCAT UHF Micrometeoroids," *Earth, Moon, and Planets*, 2007, DOI: 10.1007/s11038-007-9206-y.
45. R. Weryk, and N. Kaiser, private communication, 2007.

[1] This will probably have to happen rather soon, because the imminent introduction of 3G-type mobile communications services in the 900 MHz GSM band (UMTS900) will make the present EISCAT UHF operating frequency allocation at 926-931 MHz unavailable after the year 2009, effectively killing the tri-static UHF system.

Comparison of an Elementary Hologram and a Fresnel Zone Plate

A. Petosa
A. Ittipiboon

Abstract

The performance of an elementary hologram is compared to that of a Fresnel zone plate for imaging, spatial power combining, or for antenna applications. The focal-field power, resolution, and far-field patterns are computed and compared for various focal lengths. Results show that the Fresnel zone plate offers better resolution, and about a 2 dB increase in both focusing power and in directivity, compared to the elementary amplitude hologram. However, by proper binary discretization of the hologram, identical results can be obtained.

1. Introduction

The field of holography is well established at optical frequencies. It is used in various applications, such as microscopy, imaging, data storage, and interferometry [1-4]. At microwave and millimeter-wave frequencies, holography has been adapted to such applications as synthetic-aperture-radar synthesis and imaging of hidden objects [5-9]. Holographic principles have also been applied to the design of microwave and millimeter-wave antennas [10-21].

In holographic theory, the concept of the elementary hologram is often invoked. These elementary holograms, formed by the interference of a plane wave and a spherical wave, have been likened to Fresnel zone plates [22, 23]. Many of these comparisons have been of a general nature. For example, the maximum diffraction efficiency for an elementary amplitude hologram has been found to be 6.25%, while for a Fresnel zone plate, the value is 10.1% [24-26]. However, direct comparisons of the performance of specific designs appear to be lacking.

This paper investigates the performance of elementary holograms and Fresnel zone plates, designed for imaging, spatial power combining, or for antenna applications. After a brief review of the design principles for constructing elementary holograms and Fresnel zone plates, an analysis is conducted on the focusing and the radiation characteristics for different focal lengths commonly used in antenna designs.

2. Elementary Holograms

A hologram is formed from the interference pattern of two sets of monochromatic waves, usually called a reference wave and an object wave. A hologram can be constructed over any arbitrary surface, but a plane is commonly chosen for ease of fabrication. The example in Figure 1 shows a hologram to be constructed in the plane located at $z = 0$. If the complex amplitude of the reference wave over this plane is denoted by $U_r(x, y)$ and that of the object wave by $U_o(x, y)$, and assuming that the polarizations of the two sets of waves are identical, then the intensity, $I(x, y)$, of the interference pattern can be expressed as

$$I(x,y) = \left|U_r(x,y) + U_o(x,y)\right|^2 \tag{1}$$

$$= \left|U_r\right|^2 + \left|U_o\right|^2 + U_r^* U_o + U_o^* U_r ,$$

where U^* denotes the complex conjugate of U. In one of its simplest forms, the hologram is constructed from the intensity pattern of a spherical wave (object wave) and a plane wave (reference wave). Such a hologram is referred to as an elementary hologram. The spherical wave, arising from a point source located at (x_o, y_o, z_o), will generate a field distribution over the plane at $z = 0$ given by [24]

$$U_o(x,y) = Ae^{\left\{-j\frac{2\pi}{\lambda}\sqrt{(x-x_o)^2+(y-y_o)^2+z_o^2}\right\}}. \tag{2}$$

Aldo Petosa and Apisak Ittipiboon are with the Communications Research Centre Canada, 3701 Carling Ave., Box 11490, Station H, Ottawa, ON, Canada, K2H 8S2; Tel: +1 (613) 991-9352; Fax: +1 (613) 990-8369; E-mail: aldo.petosa@crc.ca, apisak.ittipiboon@crc.ca

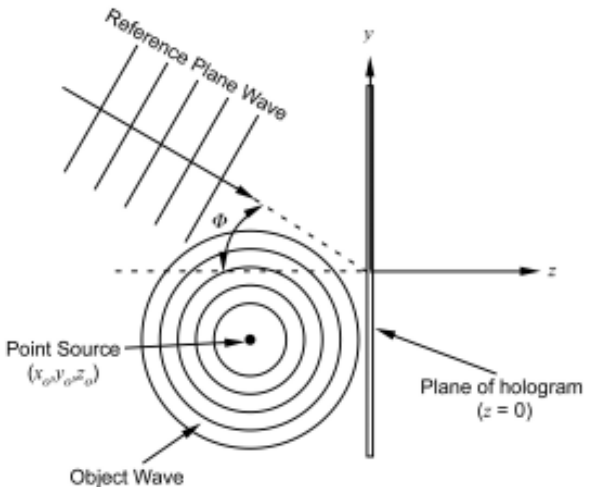

Figure 1. The interference of a plane wave and a point source

If the reference plane wave propagates with an inclination angle of Φ, as defined in Figure 1, then in the plane of the hologram, its field distribution will be

$$U_r(y) = Be^{\left\{-j\frac{2\pi}{\lambda}y\sin\Phi\right\}}. \qquad (3)$$

The complex constants A and B in Equations (2) and (3) represent the amplitude and phase of the object and reference waves, respectively. The real constant λ represents the wavelength of the spherical and plane waves. The intensity pattern of the elementary hologram is obtained by substituting Equations (2) and (3) into Equation (1):

$$I(x,y) = |A|^2 + |B|^2 + A^* e^{-j\alpha} + B^* e^{-j\beta}, \qquad (4)$$

where

$$\alpha = \frac{2\pi}{\lambda}\sqrt{(x-x_o)^2 + (y-y_o)^2 + z_o^2}$$

and

$$\beta = \frac{2\pi}{\lambda} y\sin\Phi .$$

If the complex constants of the two waves are chosen to be $A = B = 1$, and if the reference wave is at normal incidence ($\Phi = 0$) to the plane of the hologram, then Equation (4) reduces to

$$I(x,y) = \cos(\alpha), \qquad (5)$$

where the constants, representing a biasing term, have been omitted. This intensity pattern consists of a set of concentric circular fringes (light and dark rings), centered about (x_o, y_o). The number of fringes in a given area of the hologram is a function of the distance of the point source from the plane of the hologram. Figure 2 shows the effect of varying the point source distance along the z axis. The number of fringes decreases as the point source moves further from the plane of the hologram. These fringe patterns will be compared to Fresnel zone plates, which are examined in the next section.

3. Fresnel Zone Plates

The concept of Fresnel zones on a plane surface can be explained by considering the geometry in Figure 3, where a spherical wave emanating from a point source at O, located on the z axis, impinges on a planar surface at a distance f. The phase of the wave at a point A' on the plane will be related to the distance, R, to the point source. All points on the plane that are equidistance to the source will have the same phase [27]. Contours of constant phase will thus form concentric circles in the plane. The relative phase difference ($\Delta\phi$) over the aperture plane as a function of radius, r, is a function of the path difference ($R - f$), and can be written as

$$\Delta\phi = \left(\sqrt{r^2 + f^2} - f\right)\frac{360}{\lambda_o}, \qquad (6)$$

where the factor ($360/\lambda_o$) is used to express the phase difference in electrical degrees.

Fresnel zones are areas on the aperture plane within which the difference in phase values is limited to 360°.

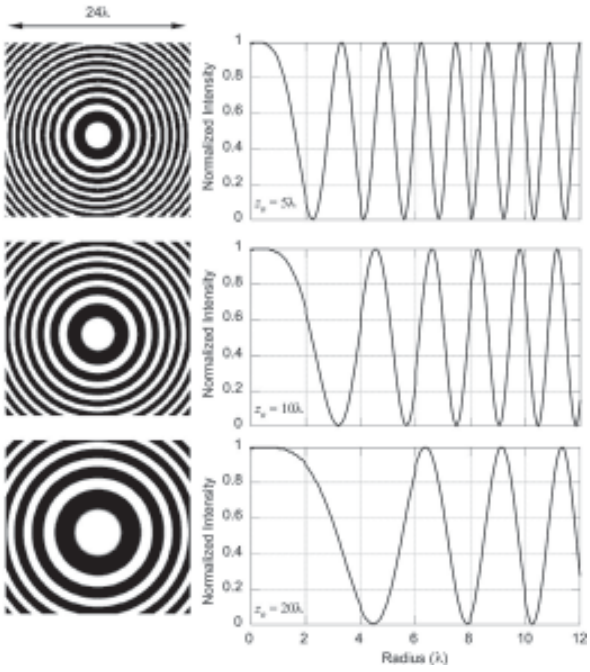

Figure 2. Holograms of a plane wave (normal incidence) and a point source at different distances, z_o, from the hologram plane.

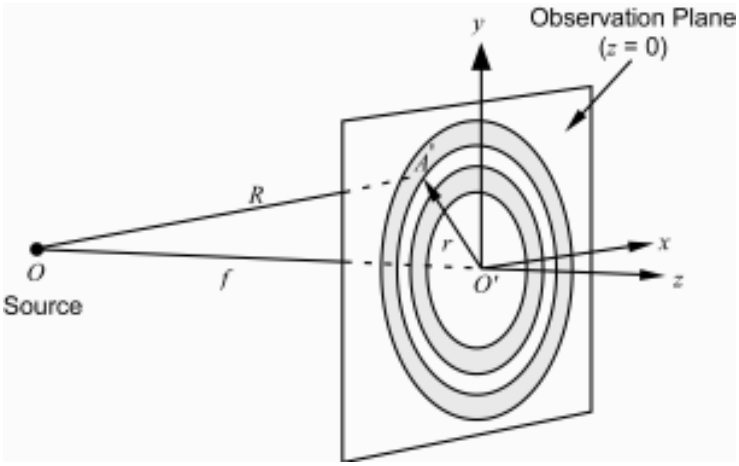

Figure 3. Fresnel zones on a plane surface.

(Sub-zones can also be defined where the phase difference is restricted to a smaller limit.) To determine the radius values (r_i) for the Fresnel zones (or sub-zones), the left-hand side of Equation (6) is set to the desired maximum phase difference ($\Delta\phi_{max}$), and the equation is rearranged to solve for the radii:

$$r_i = \sqrt{\left(i\frac{\lambda_o}{P}\right)^2 + \frac{2fi\lambda_o}{P}}, \quad i = 1, 2, \ldots, \qquad (7)$$

where $P = 360/\Delta\phi_{max}$, and $\Delta\phi_{max}$ is expressed in degrees.

By dividing the aperture plane into sub-zones of 180°, and by making each alternate sub-zone electromagnetically opaque (using either absorbing or reflecting material), the resultant aperture, known as a Fresnel zone plate, will focus the waves from the point source. The transparent regions let pass portions of the incident wave radiated from the feed the relative phase of which at the aperture is between 0° and 180°. The contributions from each of these portions will add constructively to form a focused beam. The opaque rings block (or absorb) the portion of the incident wave the phase of which lies between 180° and 360°, which would have added destructively with the portions of the wave passing through the transparent rings. Fresnel zone plates have found applications in imaging at optical frequencies, and as antennas at microwave and millimeter-wave frequencies [28-31].

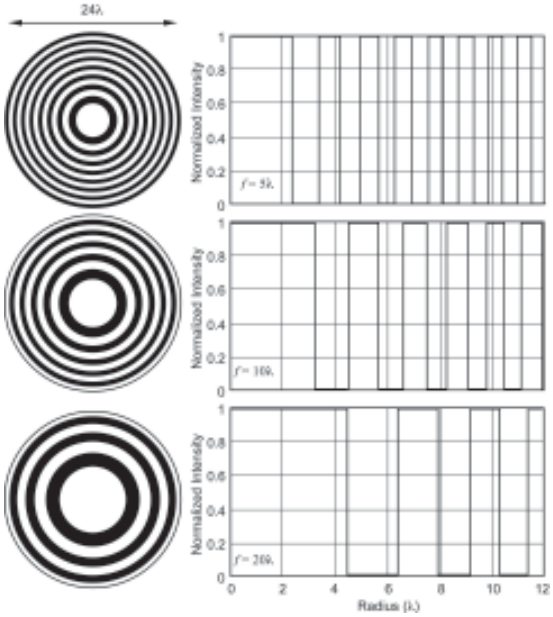

Figure 4. Fresnel zone plates for various focal lengths f

The radii for the Fresnel zone plate are obtained from Equation (7) by setting $P = 2$ ($\Delta\phi_{max} = 180°$). Examples of Fresnel zone plates designed for sources at various focal distances (*f*) are shown in Figure 4. The similarities between the intensity patterns of the holograms in Figure 2 and the Fresnel zone plates of Figure 4 are evident, and were first recognized by Rogers [22]. Quantitative comparisons for specific designs, especially for antenna applications, do not appear to have been carried out (to the authors' knowledge). In the next sections, the elementary hologram and Fresnel zone plate will be compared for the case of normal incidence.

4. Comparison of Focal Fields

The focusing ability of a lens is important in applications such as imaging and spatial power combining. In this section, the focal fields of an elementary hologram will be compared to those of the Fresnel zone plate. The geometry of the problem is shown in Figure 5. The elementary hologram, constructed by a source located at ($0, 0, -f$), is illuminated with a plane wave that is normally incident to the hologram. The magnitude (Ψ) of the fields behind the hologram in an observation plane located at $z = F$ are determined by integrating the intensity pattern over the aperture area (at $z = 0$) of the hologram of radius R_a , using [28, 29]

$$\Psi(x', y', F) \propto \int_0^{2\pi}\int_0^{R_a} \frac{I(r,\phi)}{R} e^{jkR}\,\frac{1}{2}\left(1+\frac{z}{R}\right) r\,dr\,d\phi, \quad (8)$$

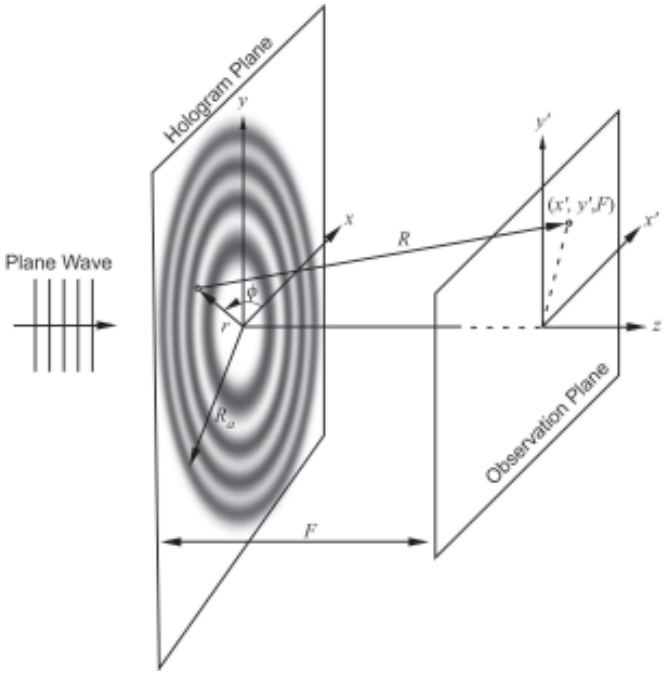

Figure 5. The focal field geometry of the elementary hologram

where

$$R = \sqrt{(r\cos\phi - x')^2 + (r\sin\phi - y')^2 + F^2}\ .$$

The focal field power ($20\log(\Psi)$) for the three holograms of Figure 2 are shown in Figure 6, in the $z = F$ plane. The focusing properties of the hologram were also examined along the *z* axis. Since the hologram is rotationally symmetric about the *z* axis, the double integral in Equation (8) reduces to a single integral:

$$\Psi(z) \propto \pi \int_0^{R_a} \frac{I(r)}{R} e^{jkR}\left(1 + \frac{z}{R}\right) r\,dr\ , \qquad (9)$$

where

$$R = \sqrt{r^2 + z^2}\ .$$

The focal field power along the *z* axis for the three holograms in Figure 2 are plotted in Figure 7.

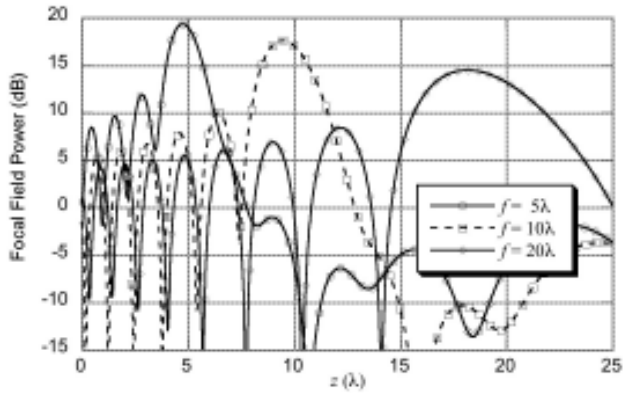

Figure 7. The focal field power along the z axis for the elementary holograms

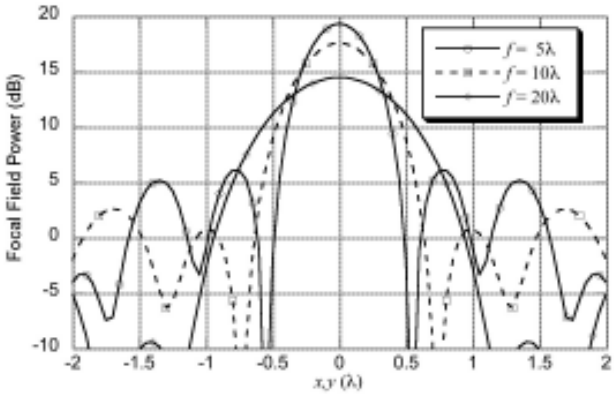

Figure 6. The focal field power in the $z = F$ plane for the elementary holograms.

The amount of focusing achieved by a Fresnel zone plate can also be determined using Equations (8) and (9) by replacing the intensity function for the hologram, $I(r,\phi)$, with a transmission function, $T(r)$:

$$T(r) = \begin{cases} 1, & \text{for transparent (odd) sub-zones} \\ 0, & \text{for opaque (even) sub-zones} \end{cases}\ . \qquad (10)$$

The focal field power for the Fresnel zone plates shown in Figure 4 are plotted in the $z = F$ plane in Figure 8 and along the *z* axis in Figure 9.

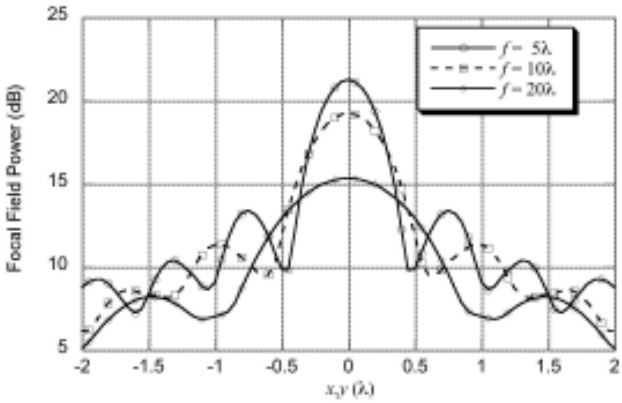

Figure 8. Focal fields in the $z = F$ plane for the Fresnel zone plates.

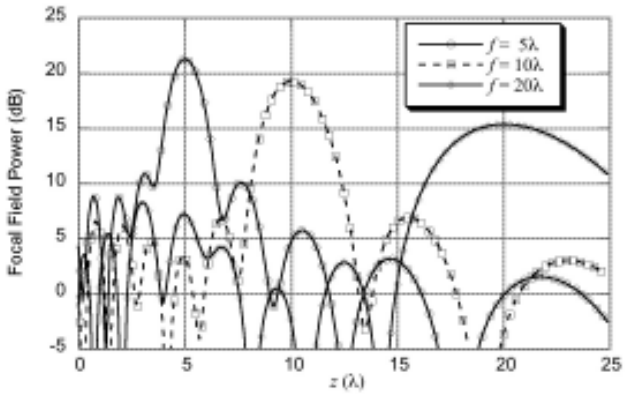

Figure 9. The focal fields along the z axis for the Fresnel zone plates

Designed Focal Distance $f(\lambda)$	Radius $R_A(\lambda)$	Computed Focal Distance $F(\lambda)$		Focal Field Peak Power (dB)		Resolution (λ)	
		Holo	FZP	Holo	FZP	Holo	FZP
5	10.91	4.8	5.0	19.3	21.2	0.58	0.50
10	11.18	9.5	10.0	17.6	19.2	0.82	0.65
20	11.36	18.2	20.0	14.5	15.3	1.40	1.1

Table 1. The focal field comparison (Holo is the elementary hologram; FZP is the Fresnel zone plate)

Table 1 compares the results for the focal fields between the elementary hologram and Fresnel zone plate. The selected values for R_a were chosen to give the Fresnel zone plates an integer number of zones. The resolution (last column in Table 1) was determined from Figures 6 and 8, and is defined as the separation distance between the peak and the first null of the focal field. The values of *F* in Table 1 were determined from the location of the peaks of the focal fields along the z axis (Figures 7 and 9). Ideally, the values of *F* should equal the design focal length (*f*). This is the case for the Fresnel zone plate designs. For the amplitude holograms, the computed focal distance deviated somewhat from the design, with the error increasing as the focal-to-diameter ratio ($f/2R_a$) increased. The comparison indicated that the Fresnel zone plates achieved somewhat better resolution and up to a 2 dB increase in focal power than the elementary amplitude holograms.

The bandwidth performance was investigated by examining the focal fields for the case of the focal length of $f = 5\lambda$, over wavelengths ranging from 0.7λ to 1.35λ. Figure 10 plots the focal power peak location as a function of wavelength for the hologram and the Fresnel zone plate. The focal power behavior for both cases was nearly identical, with the peaks traversing nearly the same range along the *z* axis, and exhibiting nearly the same variation in power levels.

5. Comparison of Far-Field Patterns

Fresnel zone plates and holograms have also been used as antennas at microwave and millimeter-wave frequencies. In this section, the far-field radiation patterns of an elementary hologram and a corresponding Fresnel zone plate antenna are compared.

To calculate the far-field patterns, the fields in the $z = 0$ aperture plane due to a source antenna located at $z = F$ are integrated, using the approach outlined in [32]. The source antenna has an axially symmetric pattern (based on $\cos^N$), and a peak linear gain of $2(N+1)$. In this paper, only the case where the focal point lies on the *z* axis is considered, so that the far-field patterns are rotationally symmetric, and the equations for directivity (*D*) in [32] reduce to

$$D(\theta) = \left(\frac{N+1}{2\lambda^2}\right)\left|\int_0^{2\pi}\int_0^{R_a} IT(r)\,g(r,\theta)\,e^{jkh(r,\phi,\theta)}\,dr\,d\phi\right|^2 \tag{11}$$

where

$$g(r,\theta) = \left[\frac{(F)^{N/2}}{\left(F^2+r^2\right)^{0.5(1+N/2)}}\left(\cos(\theta)+\frac{F}{\sqrt{F^2+r^2}}\right)\right]r$$

and

$$h(r,\theta,\phi) = -\sqrt{F^2+r^2} + r\sin(\theta)\cos(\phi)$$

For the hologram, $IT(r) = I(r)$, and for the Fresnel zone plate, $IT(r) = T(r)$. (r,ϕ) are defined in Figure 5, and θ

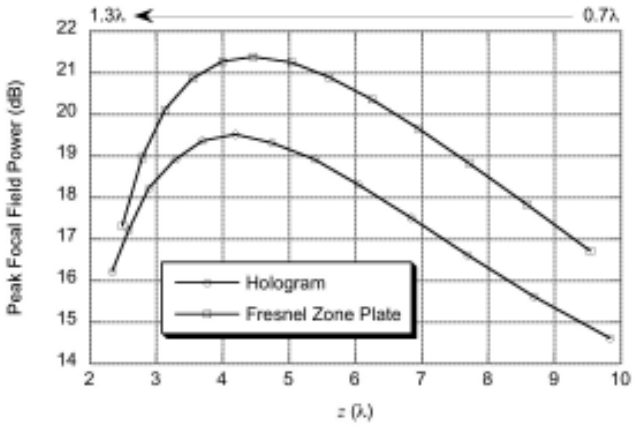

Figure 10. The focal power peaks as a function of wavelength for a focal length of $f = 5\lambda$. The markers denote every 0.05λ.

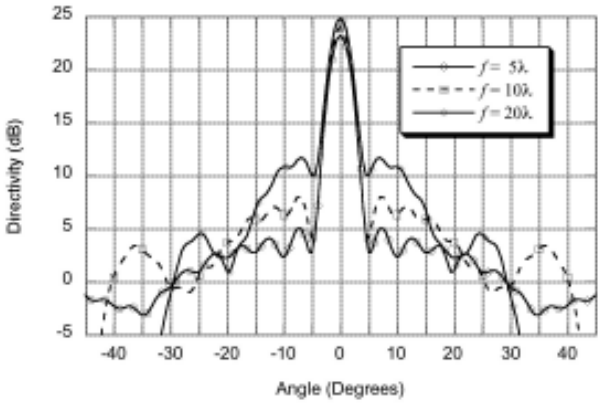

Figure 11. Hologram far-field patterns.

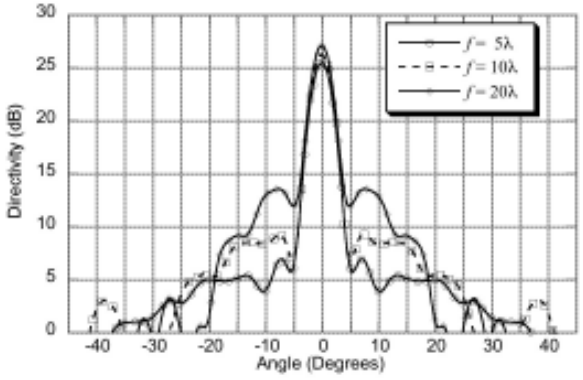

Figure 12. Fresnel zone plate far-field patterns

is the far-field angle measured from the *z* axis. For the three focal lengths chosen, the value of *N* used to define the gain of the feed antenna was selected to optimize the directivity. The directivity patterns for the holograms and the Fresnel zone plates are shown in Figures 11 and 12, respectively. The results are summarized in Table 2. The feeds were located at the computed focal lengths (*F*), listed in Table 1. The Fresnel zone plate was again observed to offer better performance, with up to a 2.3 dB improvement in directivity and better maximum sidelobe levels.

Figure 13 shows the variation in directivity as a function of wavelength for the hologram and the Fresnel zone plate designed with a focal length of $f = 5\lambda$. The 1 dB directivity bandwidth for the two antennas were nearly the same, being about 7%.

6. Hologram Discretization

At optical frequencies, a hologram is usually constructed using photographic film, which records the interference pattern of the reference and object wave and will reproduce the full range of values of the intensity pattern. At microwave frequencies, a practical equivalent to photographic film does not exist, and amplitude holograms are usually synthesized by etching metal patterns on a thin dielectric substrate. A photoengraving technique was proposed in [33] to generate a gray scale corresponding to the required range of amplitude values of the intensity pattern; however, the process is complicated and not often used in practice. In [21], artificial impedance surfaces were used to synthesize the desired intensity pattern; however, a ground plane was required, restricting this method to reflecting-type holograms. A binary amplitude discretization is more commonly used to implement microwave holograms. This discretization will impact the focusing and far-field performance of the hologram. Various digitization schemes have been proposed. In [10, 11], regions where the amplitude of the desired intensity pattern was less than half the peak value were metallized. In [11-13], only regions where the amplitude of the desired intensity pattern was zero were metallized. In [25], a binary coding scheme was used that translated the amplitude of the desired intensity pattern into a corresponding width of metallization.

In this section, the effects of four coding schemes are investigated on the focusing power and far-field directivity of the elementary hologram. The four coding schemes are shown in Figure 14, for the case of an elementary hologram designed with a focal distance of $f = 5\lambda$. The discretization rule used for each case in Figure 14 is listed in the second column of Table 3. The first three rules use different amplitude values of the intensity to set the "1" and "0" levels of the binary hologram. The last rule uses the sign of the phase of the total field ($U = U_r + U_o$) to determine the binary levels. The computed focal field power (using Equations (9) and (10)) and the directivity (using Equation (11)) for the four discretization rules are compared to the original hologram (case "o") in Table 3 for the three focal distances ($f = 5\lambda,\ 10\lambda$, and 20λ). Each of the binary holograms showed an improvement in the results,

Designed Focal Distance $f(\lambda)$	R_A (λ)	$\frac{f}{2R_a}$	Feed N	Directivity (dB)		Maximum Sidelobe (dB)	
				Holo	FZP	Holo	FZP
5	10.91	0.23	2	23.2	25.5	–18.2	–18.6
10	11.18	0.45	6	23.9	26.3	–15.9	–17.1
20	11.36	0.88	20	24.8	27.0	–13.1	–13.5

Table 2. The far-field pattern comparison (Holo is the elementary hologram; FZP is the Fresnel zone plate)

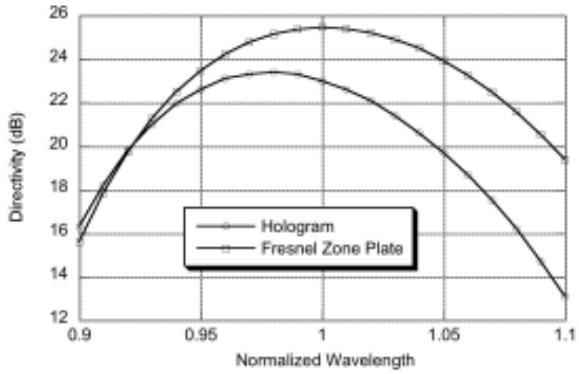

Figure 13. The directivity as a function of wavelength for a focal length of $f = 5\lambda$

with case "d" obtaining the same values as the Fresnel zone plate. In fact, the application of this rule results in a discretized hologram that is identical to the Fresnel zone plate. Based on the results of this limited study, quantization of the hologram using phase quantities results in better directivity performance than quantization based on amplitude levels. Using the 50%-amplitude rule (case "b") offered the best focal field power, slightly higher than that obtained using the Fresnel zone plate.

7. Summary

This study has demonstrated that although the Fresnel zone plate and elementary amplitude hologram exhibit nearly identical bandwidth behavior, the Fresnel zone plate can achieve up to about a 2 dB improvement in both the focal field power and in the directivity. However, at microwave frequencies, amplitude holograms are usually implemented in binary form. Applying a discretization rule based on the phase of the total fields over the hologram's surface appears to offer better directivity performance than rules based on the magnitude of the intensity, while a 50% amplitude discretization rule offers better focusing power.

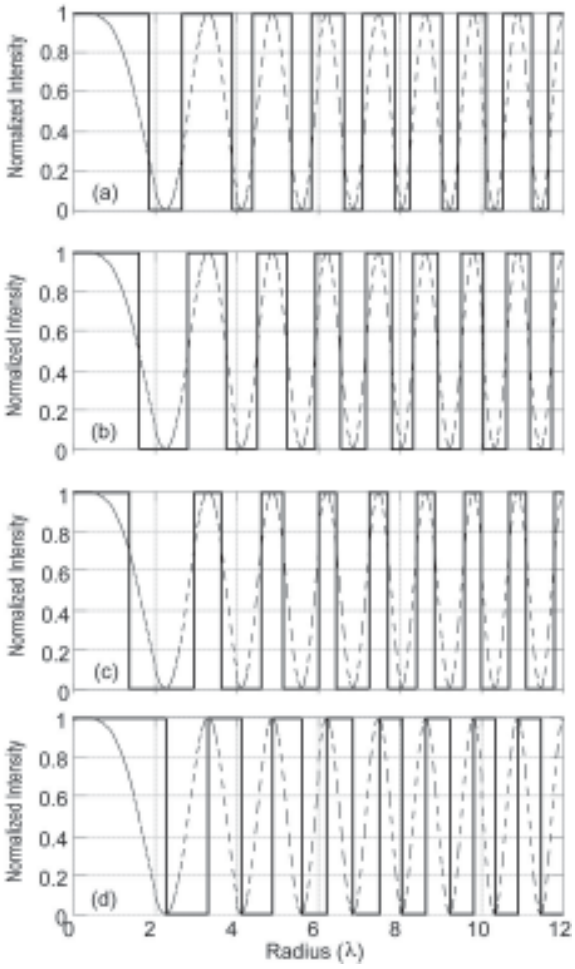

Figure 14. Digitized intensities for the hologram with $f = 5\lambda$ *(see Table 3)*

The appropriate discretization rule should therefore be considered for holograms formed by the interference of more complicated waves, and may lead to their improved performance.

Case	Digitizing Rule	f (λ)	F (λ)	Focal Field Power (dB)	Directivity (dB)
o	$I_d = \lvert I \rvert$	5	4.8	19.3	23.2
		10	9.5	17.6	23.9
		20	18.2	14.5	24.8
a	$I_d = \begin{cases} 1, & \lvert I \rvert \geq 0.25 \\ 0, & \lvert I \rvert < 0.25 \end{cases}$	5	4.7	20.3	24.2
		10	9.4	18.6	25.0
		20	18.0	15.8	26.1
b	$I_d = \begin{cases} 1, & \lvert I \rvert \geq 0.5 \\ 0, & \lvert I \rvert < 0.5 \end{cases}$	5	4.8	21.4	25.2
		10	9.5	19.6	25.9
		20	18.3	16.3	26.7
c	$I_d = \begin{cases} 1, & \lvert I \rvert \geq 0.707 \\ 0, & \lvert I \rvert < 0.707 \end{cases}$	5	4.85	20.6	24.3
		10	9.6	18.6	25.0
		20	18.6	15.2	25.6
d	$I_d = \begin{cases} 1, & \arg(U) < 0 \\ 0, & \arg(U) \geq 0 \end{cases}$	5	5.0	21.2	25.5
		10	9.5	19.2	26.3
		20	20	15.3	27.0

Table 3. The focal field power and directivity for digitized holograms ($I = I(x,y)$, $U = U_r(x,y) + U_o(x,y)$).

8. References

1. D. Gabor, "Holography: 1948-1971," *Proceedings of the IEEE*, **60**, 6, June 1972, pp. 655-668.
2. D. D. Dudley, "Holography: A Survey," NASA SP-5118, NASW-2173, Washington, DC, 1973.
3. W. T. Cathey, *Optical Information Processing and Holography*, New York, John Wiley & Sons, 1974.
4. J. B. DeVelis and G. O. Reynolds, *Theory and Applications of Holography*, Reading, MA, Addison-Wesley Publishing Co., 1967.
5. R. P. Dooley, "X-Band Holography," *Proceedings of the IEEE*, **53**, 11, November 1965, pp.1733-1735.
6. W. E. Kock, "Microwave Holography," *Microwaves*, November 1968, pp. 46-54.
7. N. B. Farhat and W. R. Guard, "Millimeter Wave Holographic Imaging of Concealed Weapons," *Proceedings of the IEEE*, **59**, 9, September 1971, pp. 1383-1384.
8. G. Papi, V. Russo, and S. Sottini, "Microwave Holographic Interferometry," *IEEE Transactions on Antennas and Propagation*, **AP-19**, 6, November 1971, pp. 740-746.
9. L. J. Cutrona, E. N. Leith, L. J. Porcello, and W. E. Vivian, "On the Application of Coherent Optical Processing Techniques to Synthetic-Aperture Radar," *Proceedings of the IEEE*, **54**, 8, August, 1966, pp. 1026-1032.
10. P. F. Checcacci, V. Russo, and A. M. Scheggi, "Holographic Antennas," *Proceedings of the IEEE*, **56**, 12, December 1968, pp. 2165-2167.
11. P. F. Checcacci, V. Russo, and A. M. Scheggi, "Holographic Antennas," *IEEE Transactions on Antennas and Propagation*, **AP-18**, 6, November 1970, pp. 811-813.
12. P. F. Checcacci, G. Papi, and V. Russo, "A Holographic VHF Antenna," *IEEE Transactions on Antennas and Propagation*, **AP-19**, 2, March 1971, pp. 278-292.
13. K. Iizuka, M. Mizusawa, S. Urasaki, and H. Ushigome, "Volume-Type Holographic Antenna," *IEEE Transactions on Antennas and Propagation*, **AP-23**, 6, November 1975, pp. 807-810.
14. N. H. Farhat, "Holographically Steered Millimeter Wave Antennas," *IEEE Transactions on Antennas and Propagation*, **AP-28**, 4, July 1980, pp. 476-480.
15. K. Levis, A. Ittipiboon, A. Petosa, L. Roy, and P. Berini, "Ka-Band Dipole Holographic Antennas," *IEE Proceedings Microwave Antennas Propagation*, **148**, 2, April 2001, pp. 129-132.
16. A. E. Fathy, M. Elsherbiny, A. Rosen, G. Ayers, and S. Perlow, "Experimental Demonstration of a 35 GHz Holographic Antenna," *IEEE MTT-S Microwave Symposium Digest*, 2003, Vol. 3, pp. 1833-1836.
17. M. Elsherbiny, A. E. Fathy, A. Rosen, G. Ayers, and S. M. Perlow, "Holographic Antenna Concept, Analysis, and Parameters," *IEEE Transactions on Antennas and Propagation*, **AP-52**, 3, March, 2004, pp. 830-839.
18. A. Petosa, S. Thirakoune, K. Levis, and A. Ittipiboon, "A Microwave Holographic Antenna with Integrated Printed Dipole Feed," *IEE Electronics Letters*, **40**, 19, September 2004, pp. 1162-1163.
19. T. Quach, D. McNamara, and A. Petosa, "Holographic Antenna Realised Using Interference Patterns Determined in the Presence of the Dielectric Substrate," *IEE Electronics Letters*, **41**, 13, June 2005, pp. 724-725.
20. P. Sooryadevan, D. McNamara, A. Petosa, and A. Ittipiboon, "The Electromagnetic Modelling and Optimisation of a Planar Holographic Antenna," *IET Proceedings Microwaves, Antennas and Propagation*, **1**, 3, June, 2007, pp. 693-699.
21. D. Sievenpiper, J. Colburn, B. Fon, J. Ottusch, and J. Visher, "Holographic Artificial Impedance Surfaces for Conformal Antennas," IEEE International Symposium on Antennas and Propagation *Digest*, Vol. 1B, July 2005, Washington, DC, pp. 256-259.
22. G. L. Rogers, "Gabor Diffraction Microscopy: The Hologram as a Generalized Zone Plate," *Nature*, **166**, August 1950, pp. 237.
23. W. E. Kock, L. Rosen, and J. Rendeiro, "Holograms and Zone Plates," *Proceedings of the IEEE*, **54**, 11, November 1966, pp. 1599-1601.
24. J. W. Goodman, "An Introduction to the Principles and Applications of Holography," *Proceedings of the IEEE*, **59**, 9, September 1971, pp. 1292-1304.
25. A. Vasara, J. Turunen, and A. T. Friberg, "Realization of General Nondiffracting Beams with Computer-Generated Holograms," *Journal of the Optical Society of America A*, **6**, 11, November 1989, pp. 1748-1754.
26. J. C. Urbach and R. W. Meier, "Properties and Limitations of Hologram Recording Materials," *Applied Optics*, **8**, 11, November 1969, pp. 2269-2281.
27. A. Fresnel, "Oeuvres Complete d'Augustin Fresnel," Vol. 1, Note 1, 1866, pp. 365-371.
28. H. Hristov, *Fresnel Zones in Wireless Links, Zone Plate Lenses and Antennas*, Norwood, MA, Artech House, 2000, pp. 38-40.
29. Y. J. Guo and S. K. Barton, *Fresnel Zone Antennas*, Amsterdam, Kluwer Academic Press, 2002, pp. 30-33.
30. O. V. Minin and I. V. Minin, *Diffraction Optics of Millimeter Waves*, Bristol, UK, Institute of Physics Publishing, 2004.
31. J. C. Wiltse and J. E. Garrett, "The Fresnel Zone Plate Antenna," *Microwave Journal,* January 1991, pp. 101-114.
32. L. C. J. Baggen, C. J. J. Jeronimus, and M. H. A. J. Herben, "The Scan Performance of the Fresnel-Zone Plate Antenna: A Comparison with a Parabolic Antenna," *Microwave and Optical Technology Letters*, **6**, 13, October 1993, pp. 769-774.
33. K. Iizuka, "Microwave Hologram by Photoengraving," *IEEE Proceedings*, **57**, 5, May 1969, pp. 813-814.

IUCAF Annual Report for 2007

1. Introduction

The Scientific Committee on Frequency Allocations for Radio Astronomy and Space Science, IUCAF, was formed in 1960 by its sponsoring Scientific Unions, COSPAR, the IAU, and URSI. Its brief is to study and coordinate the requirements of radio frequency allocations for passive (i.e., non-emitting) radio sciences, such as radio astronomy, space research and remote sensing, in order to make these requirements known to the national and international bodies that allocate frequencies. IUCAF operates as a standing inter-disciplinary committee under the auspices of ICSU, the International Council for Science. IUCAF is a Sector Member of the International Telecommunication Union (ITU).

2. Membership

At the end of 2007 the composition of membership for IUCAF was:

URSI	S. Reising (Com F)	USA
	U. Shankar (Com J)	India
	W. Swartz (Com G)	USA
	A. Tzioumis (Com J)	Australia
	W. van Driel (Com J,Chair)	France
IAU	H. Chung	Korea
	D.T. Emerson	USA
	M. Ohishi	Japan
	K.F. Tapping	Canada
COSPAR	J. Romney	USA
at large:	W.A. Baan	Netherlands
	K. Ruf	Germany

No replacement has yet been found for the IAU representative Jim Cohen, who passed away in November 2006.

IUCAF also has a group of Correspondents, in order to improve its global geographic representation and for issues on spectrum regulation concerning astronomical observations in the optical and infrared domains.

3. International Meetings

During the period of January to December 2007, its Members and Correspondents represented IUCAF in the following international meetings:

February	ITU-R Working Party 7D (radio astronomy) in Geneva, Switzerland
	ITU-R Conference Preparatory Meeting in Geneva, Switzerland
September	Space Frequency Coordination Group meeting SFCG-27 in Maspalomas, Spain
October	ITU World Radiocommunication Conference WRC-07 in Geneva, Switzerland

Additionally, many IUCAF members and Correspondents participated in numerous national or regional meetings (including CORF, CRAF, RAFCAP, the FCC etc.), dealing with spectrum management issues, such as the preparation of input documents to various ITU fora.

3.1 IUCAF Business Meetings

During 2007 IUCAF had a face-to-face committee meeting before each of the ITU meetings listed above, with the purpose of discussing issues on the agenda of the meetings in preparation for the public sessions. During these ITU sessions ad-hoc meetings of IUCAF were held to discuss further its strategy. Also discussed were other IUCAF business, such as action plans for future workshops and summer schools or initiatives and future contributions to international spectrum management meetings.

Although such face-to-face meetings have been convenient and effective, throughout the year much IUCAF business is undertaken via e-mail communications between the members and correspondents.

4. Contact with the Sponsoring Unions and ICSU

IUCAF maintains regular contact with its supporting Scientific Unions and with ICSU. The Unions play a strong supporting role for IUCAF and the membership is greatly encouraged by their support.

Pursuing its brief, IUCAF continued its activities towards strengthening its links with other passive radio science communities, in particular in space science, and defining a concerted strategy in common spectrum management issues. For the 2008 COSPAR Scientific Assembly, IUCAF has been organizing Scientific Event E110 on “Spectrum Management and COSPAR: Keeping Passive Radio Observations Free of Interference”.

The IUCAF Chair is a member of the Organizing Committee of IAU Commission 50 on the Protection of Existing and Potential Observatory Sites, IUCAF member A. Tzioumis is Chair of the Working Group on Radio Frequency Interference of IAU Division X (radio astronomy), and IUCAF member M. Ohishi chairs the Working Group on Astrophysically Important Spectral Lines of Division X.

For the 2008 URSI Scientific Assembly, IUCAF has been organizing its open meeting during session J07, and IUCAF members have been actively involved in the organization of the session on Solar Power Satellites. In 2007, IUCAF members also actively participated in national URSI meetings.

5. Protecting the passive Radio Science Services

At the ITU, the work in the various Working Parties of interest to IUCAF was focused largely on the preparations for WRC-07, the ITU World Radiocommunication Conference, which lasted for 4 weeks, from October 22nd to November 16nd, in Geneva, Switzerland. WRC-07 was attended by well over 3000 delegates from over a 180 nations and accredited organizations, including 7 IUCAF members and correspondents, and 9 other astronomers and astronomical spectrum managers.

The main goal of a WRC is the revision of the ITU Radio Regulations, which define the worldwide framework for spectrum management, including protection criteria for the radio astronomy service from unwanted emissions into its allocated frequency bands. WRCs are held every 3 to 4 years, and its agenda items are adopted at the previous WRC.

Of greatest relevance to IUCAF was an agenda item on the protection of the radio astronomy service and the Earth exploration-satellite (passive) service from unwanted emissions of active services in adjacent and nearby bands. This has resulted in an update of the tables of threshold levels used for consultation between the passive and active radio services in Resolutions 738 and 739. Of particular, and long-standing, concern to IUCAF was the case of the 1610.6-1613.8 MHz band, which contains important spectral lines of the interstellar OH molecule. It was decided that "The protection of the radio astronomy service in the 1 610.6-1 613.8 MHz band is ensured and will continue to be in accordance with the bilateral agreement between the Russian Federation, the notifying administration of the GLONASS/GLONASS-M system, and IUCAF, and subsequent bilateral agreements with other administrations."

Among the preliminary agenda items adopted for the next WRC in 2011, the one most relevant to radio astronomy concerns the use of the radio spectrum between 275 and 3000 GHz. No allocations for the use of this frequency band will be made at WRC-11, but the radio astronomy community has to identify a list of specific bands of interest.

IUCAF member M. Ohishi is Chair of ITU-R Working Party 7D (radio astronomy) and in 2007 IUCAF member H. Chung was named Vice-chair of ITU-R Study Group 7 (Science Services).

6. IUCAF-SponsoredMeetings

In 2007, IUCAF worked towards the organization of two future international meetings: Scientific Event E110 on "Keeping Passive Radio Observations Free of Interference" at the 2008 COSPAR Scientific Assembly in Montreal, and the 2009 Summer School on Spectrum Management for Passive Radio Sciences, planned to be held in Korea.

7. Publications and Reports

IUCAF has a permanent web address, http://www.iucaf.org, where the latest updates on the organization's activities are made available. All contributions to IUCAF-sponsored meetings are made available on this website.

8. Conclusion

IUCAF interests and activities range from preserving what has been achieved through regulatory measures or mitigation techniques, to looking far into the future of high frequency use and giant radio telescope use. Current priorities, which will certainly keep us busy through the next years, include the use of satellite down-links close in frequency to the radio astronomy bands, the coordination of the operation in shared bands of radio observatories and powerful transmissions from downward-looking satellite radars, the possible detrimental effects of ultra-wide band (UWB) transmissions and high-frequency power line communications (HF-PLC) on all passive services, and studies on the operational conditions that will allow the successful operation of future giant radio telescopes.

IUCAF is grateful for the moral and financial support that has been given for these continuing efforts by ICSU, COSPAR, the IAU, and URSI during the recent years. IUCAF also recognizes the support given by radio astronomy observatories, universities and national funding agencies to individual members in order to participate in the work of IUCAF.

Wim van Driel, IUCAF Chair
IUCAF website: http://www.iucaf.org
IUCAFcontact:iucafchair@iucaf.org

Radio Science Doctoral Abstracts

Partha Pratim Bhattacharya, ***Optimized Call Handover Strategies for Mobile Cellular Communication***, Department of Electronics and Telecommunication Engineering, Jadavpur University, Kolkata 700032, India, December 2007; E-mail: partha_p_b@yahoo.com
Relevant Commission: C

Abstract

Certain fuzzy-logic-based handover algorithms are proposed and studied. It is seen that the proposed algorithms work efficiently under multipath environments and avoid call dropping and call-quality degradation.

Now, the effect of Rayleigh fading is dependent on mobile velocity. A mobile station (MS) with high velocity may cross the cell boundary before a handover execution, leading to call termination, whereas an MS with low velocity may stop or turn back, which in turn will lead to undue handover. To overcome these problems, a fuzzy logic-based velocity-dependent algorithm is proposed and found to give better response, with a lower number of fluctuations in handover response, and a low rise time.

There may be call dropping due to non-availability of free channels in the target cell, although some of the free channels may be available in the neighboring cells. The proposed algorithm has been modified so that the call may be handed over to any of the surrounding cells, depending on the availability of free channels.

A variable-hysteresis margin-based handover is then proposed and studied, where the hysteresis margin depends on the path-loss exponent (which can vary from two to six) and the user's velocity. The algorithm avoids both call termination and unnecessary handover for high- and low-velocity mobiles, respectively, and hence reduces the Base Station Controller (BSC) and Mobile Switching Center (MSC) processor loading. For interference-limited systems, a signal-to-interference-ratio-based handover algorithm is also proposed.

Since the program software has controlled complexity and it is thoroughly tested, the codes can be burned-in at the system ROM and embedded into application programs.

Sarbani Ray, ***Ionospheric Scintillation and its Effects on the Global Positioning System (GPS)***, S. K. Mitra Center for Research in Space Environment, University of Calcutta, Kolkata, India, December 2007. E-mail: sarbanir@yahoo.com
Relevant Commission: G

Abstract

This thesis presents a long-term study of the effects of equatorial scintillations at L band on GPS and SBAS observed from station Calcutta, located under the northern crest of the equatorial anomaly in the Indian longitude zone. The station provides an excellent platform for studying worst-case scintillation events, even at L band. Scintillations at this location are essentially controlled by solar flux under quiet geomagnetic conditions, and are most intense in the pre-midnight hours of equinoctial months of high-sunspot-number years. The statistics of L-band scintillation occurrence for half of a solar cycle (1996-2000) observed at Calcutta provides a means of estimating the optimum separation between two geostationary satellites for reliable operation of SBAS. The present thesis contains a study of scintillation observed at Calcutta subsequent to seventeen intense storms with sudden commencement, during 1996-2000. The response has been attributed to the prompt penetration of eastward electric field when it occurred within three hours of occurrence of maximum *AE* or *dDst/dt* and southward turning of *Bz*. Scintillations occurring with a time delay of more than ~3 hr after *dDst/dt* maximum may be attributed to the disturbance dynamo effects under an over-shielding condition, which prevails over all longitude sectors and local times. Beyond 12 hr, the scintillation occurrence may be attributed to the long-term ionospheric disturbance electric fields, resulting from storm-induced composition changes. A comparison of scintillation events on the GPS satellites with those on the geostationary links observed from this station shows considerable differences in occurrence patterns. The observations of GPS signal scintillations from the northern crest of the equatorial anomaly in the Indian zone reveal two distinct regions of very intense scintillations: i) near the crest of the equatorial anomaly, and ii) in the southern sky. The northern limit of the equatorial irregularity belt extends up to 35°-40° N magnetic dip in the pre-midnight hours of vernal equinox, and 30°-35° N in the autumnal equinox of high-sunspot-number years. It is shown that the accuracy of position fixing becomes worse during periods of intense scintillations on a number of GPS links. During sunspot-number-maximum years, when intense scintillations are very frequent, the observed deviation is a regular feature at the present location.

Call for Submissions

In order to encourage dialogue with young radio scientists, the *Radio Science Bulletin* publishes the abstracts of relevant doctoral dissertations or theses in the fields of

radio science as soon as they are approved by universities or other degree-awarding institutions.

We thus call upon supervisors or research-group leaders to bring this opportunity to the attention of recently qualified doctoral graduates, asking them to e-mail their abstracts to the address given below. The date of publication should be given, with full details of the address of the awarding institution, and also an e-mail address for the author. It would also be helpful to indicate which URSI Commissions relate most closely to the doctoral work.

Peter Watson
University of Bath
E-mail: rsbursi@bath.ac.uk

Radio-Frequency Radiation Safety and Health

James C. Lin

Tumor Incidence Studies in Lymphoma-Prone Mice Exposed to GSM Mobile-Phone Radiation

The first study of lymphomas in female Em-Pim1 transgenic mice using frequencies and modulations specific to cellular mobile phones was conducted in Australia, in which the incidence was shown to be significantly higher (odds ratio, $OR = 2.4$) in the exposed mice (43%) than in the sham controls (22%) [1]; following 18 months of two 30-min periods per day of exposure to 900 MHz plane-wave radiation repeated at 217 Hz (signals that mimic Global System For Mobile Communication – GSM – digital mobile phones). Lymphomas are a type of cancer that affect the lymphatic system, which is part of the body's immune system. Specifically, the lymphatic system is the body's blood-filtering tissue that helps fight infection and disease. (See [2] for more discussions on lymphomas.) Follicular lymphomas were the major contributor to the increased tumor incidence. At the end of the entire experiment, 53% of the exposed mice had lymphomas, compared to 22% of the unexposed controls. The exposed transgenic mice also recorded a faster onset of lymphomas. In this study, one hundred mice were sham-exposed and 101 were exposed for up to 18 months. The pulse width was 0.6 ms. The average incident power density and SAR were 2.6 to 13 W/m^2 and 0.13 to 1.4 W/kg, respectively.

It should be noted that the Eμ-Pim1 transgenic mice were genetically engineered for a predisposition to lymphoma. Thus, the extrapolation of results found in a very sensitive animal model to possible carcinogenesis in humans is not well established.

Moreover, this study suffered from two general types of identifiable deficiencies. One type was dosimetric in nature. Specifically, the plane-wave-equivalent exposure system used in this study allowed mice to roam and huddle freely during exposure to incident power densities of 2.6 to 13 W/m^2. Consequently, there was a wide variation of SARs (0.008 to 4.2 W/kg, averaging 0.13 to 1.4 W/kg). Only an average response can be inferred from an average SAR, not an individual SAR. Moreover, it is conceivable that the higher incidence of lymphomas was associated with the higher SAR instead of the reported average SAR. Further, mice selected for necropsy during the experiment were not replaced with either other mice or tissue-equivalent phantoms, thus altering dosimetry in the remaining animals. There are also some critical shortcomings concerning the biological assay, methods, and procedures. The study lacked any standardized assessment criteria for deciding which mice would be selected for necropsy, and surviving mice were disposed of without performing necropsy to ascertain whether there were infections and/or other relevant diseases, such as kidney failure, in those animals. Apparently, cage-control animals were not included as part of the experiment.

Subsequently, another study [3] was set up to test the same central hypothesis as that of the earlier study [1], but with refinements to overcome some of the perceived shortcomings. For example, the variation in SAR was reduced by restraining the mice and by using tissue-equivalent phantoms to replace autopsied mice. The new exposure system, supplied by Motorola, consisted of 15 lossy, radial, parallel-plate electromagnetic cavities (the "Ferris wheel"), configured for far-field operation. Each cavity had 40 mice restrained individually in clear Perplex tubes, cylindrically arranged around a dipole antenna. The tubes were constructed to prevent each mouse from changing its orientation relative to the field, to facilitate SAR determination. The exposed groups were divided into four SAR levels: 0.25, 1.0, 2.0, and 4.0 W/kg. A standardized set of criteria (10% reduction in body mass over a week) was used for selecting mice for necropsy, and all surviving animals were necropsied. A total of 120 lymphoma-prone, Em-Pim1 mice and 120 wild-type mice were exposed for 1 h/day, five days/week, at each of the four SAR levels, for up to 24 months. In addition, 120 Eμ-Pim1 and 120 wild-

James C. Lin is with the University of Illinois at Chicago, 851 South Morgan Street (M/C 154), Chicago, Illinois 60607-7053 USA;
Tel: +1 (312) 413-1052 (direct); +1 (312) 996-3423 (main office); Fax: +1 (312) 996-6465;
E-mail: lin@uic.edu.

A version of this column also appeared in *IEEE Antennas and Propagation Magazine*, **50**, 1, February 2008, pp. 217-220; ©2008 IEEE.

type mice were sham-exposed; there was also an unrestrained negative control group.

This paper concluded that the results of the double-blind study did not show an increase in lymphomas, following a two-year exposure to GSM- mobile-phone radiation [3]. Furthermore, there was no significant difference in the incidence of lymphomas between exposed and sham-exposed groups at any of the exposure levels (with one exception). A dose-response effect was not detected. The findings showed that long-term exposures of lymphoma-prone mice to 898.4 MHz (referred to as 900 MHz) GSM RF radiation at SARs of 0.25, 1.0, 2.0, and 4.0 W/kg had no significant effects when compared to sham-irradiated animals. This was in contrast to the previous study, which reported that long-term (18-month) exposure of lymphoma-prone mice significantly increased the incidence of non-lymphoblastic lymphomas when compared to sham-irradiated animals.

Because this study was designed to test the same central hypothesis as that of the earlier study [1], but with refinements to overcome some of the perceived shortcomings, the study deserves close examination.

To be sure, the latter study was not a replication of the earlier study. A replication, as a standard practice of the scientific approach, requires that the same methods and materials are followed as in the earlier study. Given that there are major differences in materials and methods (beyond refinements), the design of the latter study is more appropriately characterized as an attempt to confirm or refute, rather than replicate. More significantly, close examination of the source of mice, exposure regime, animal restraint, and the omission of data from analysis in the later study could lead to a different conclusion than that stated in the publication. It was stated in the paper that the mice were supplied from the same source used in the earlier study, and listed Taconic Farms, New York, as the source. However, mice for the earlier study came from GenPharm International of Mountain View, California. Thus, the Em-Pim1 mice appear not to be the same after all. Even the same strain of mice, from different suppliers, may have different characteristics and may respond differently, a factor to be considered further.

Mice in the later study were exposed to daily 1-h sessions, while those in the earlier study were exposed for two 30-min periods per day. The biological effect of fragmenting exposure duration is not well known. However, diurnal variations and the temporal dependence of physiologic, cellular, and molecular processes are well established. The use of free-roaming versus restrained animals by themselves is not a problem, so long as the effects on these mice are characterized, with appropriate cage controls. Unfortunately, data for the cage-control mice were missing from the publication [3]. Restraining the animal in a tight tube during the exposure session constitutes a continuing stress to the animal, which may lead to significant stress responses that potentially could obscure any effect from the exposure to mobile-phone radiation.

There are also some rather glaring inconsistencies in the published data. For example, some or all of the mice were dead after 18 or 20 months, but had weight gains up to 26 months [3]. The study design included equal numbers of freely moving mice for negative controls (cage controls). However, data for the cage-control group were not given in the paper, and appear to have been excluded from the statistical analyses. By not having the free-moving mice form a part of the statistical-analysis group, the report was deprived of the pathophysiology of cage-control mice for comparison. The cage controls can and should serve as valuable background materials, which potentially might be masked by stress response induced by the restraining tube used for sham control. It is noteworthy that the number of lymphomas among the sham controls (mice are restrained but not exposed) was abnormally high in this study. Specifically, among the transgenic mice, the incidence of lymphomas was 75% for the sham-control group (89 out of 120 mice developed lymphomas: 15 with lymphoblastic lymphomas, 74 with non-lymphoblastic lymphomas). In contrast, the incidence of lymphomas in the earlier study [1] was 22% for the sham-control mice (22 out of 100 mice developed the disease: three with lymphoblastic lymphomas, 19 with non-lymphoblastic lymphomas). The high degree of incidence in the sham controls (75% versus 22%) makes the experimental protocol impractical. It could have masked an effect from mobile phones, or any other agent, for that matter. It is unfeasible to come to any firm conclusions about lymphomas in transgenic mice exposed to mobile-phone radiation. These flaws –possibly in the sourcing or handling of mice, the statistical analysis of the data, or in the fundamental design of the experiment – limit the conclusions that can be drawn for the outcome of the Utteridge et al. [3] study, despite the paper's claim.

Utteridge et al. [4] have published a response to several comments [5-7] on their original article [3]. Unfortunately, acceptability of results of the Utteridge et al. study has not been enhanced, and clear, unambiguous data and information remain elusive for an unequivocal interpretation of the Utteridge et al. study [8]. The need for other investigators to replicate or confirm these two studies [1, 3] and to help appraise the acceptability and reliability of the reported results persisted.

Later, a dosimetric evaluation of the Ferris-wheel exposure system used by Utteridge et al. [1] for exposure of the Eμ-Pim1 transgenic mice to pulsed radiofrequency energy at 898.4 MHz was reported by Faraone et al. [9]. Twin-well calorimetry was used to measure the whole-body SAR of exposed mice. One major conclusion was that since the average lifetime weight was slightly higher than originally projected (30 g), the lifetime exposure received by the mice was somewhat less than anticipated. In particular, the mean lifetime exposure levels were lower by about 18% than the original targets for the wild-type mice, and about

10% for the transgenic mice. Specifically, the lifetime average whole-body SARs were 0.21, 0.86, 1.7, and 3.4 W/kg for the four exposure groups. Infrared thermography showed SAR peaks in the abdomen, neck, and head in thermograms taken over the sagittal plane of mouse cadavers. The peak local SAR (1-g) at these locations, determined by thermometric measurements, showed peak-to-average SAR ratios with typical values around 3:1, but some are close to 6:1. Thus, the average SARs were slightly lower than originally reported in Utteridge et al. [3].

The effect of chronic exposure to GSM-modulated 900 MHz fields and tumor development in mouse strains genetically predisposed to lymphoma development was the subject of a more recent publication [10]. This, too, was intended as a follow-up to the study by Repacholi et al. [1], with improvements in dosimetry and methodology. The exposure system consisted of four "Ferris wheels," and each wheel was composed of two parallel, circular, stainless-steel metal plates with a conical antenna in its center. Dosimetry was improved by restraining the mice in plastic tubes to obtain more uniform exposure. The incident field was adjusted as a function of body mass to obtain an age-independent exposure dose. Tissue-equivalent phantoms were used to replace necropsied mice to maintain a more consistent and symmetrical absorption profile. The study used identical RF signals as the previous study, i.e., animals were exposed to 217 Hz pulsed 900 MHz fields, but at average whole-body SARs of 0.5, 1.4, or 4.0 W/kg. In addition to whole-body dosimetric information about organ and spatial-average-peak SARs, their life-time variations were reported. It is interesting to note that the ratio of organ- or tissue-average SAR to the whole-body average SAR varied between 0.18 and 1.90. Moreover, the spatial peak SAR relative to the whole-body average SAR was as high as 62 and 85 for tissue masses of 5 and 0.5 mg, respectively.

At variance with Repacholi et al. [1] and Utteridge et al. [3], who used only female Eμ-Pim1 transgenic mice in their studies, this blinded study presented data on 500 female and male Eμ-Pim1 mice (250 females and 250 males purchased from Taconic Farms, New York). The mice were trained to the exposure system before exposure started. Fifty female and 50 male mice were randomly selected for exposure at each SAR level (0.5, 1.4, or 4.0 W/kg), for sham exposure, or as cage controls. The exposure was performed 1 h/day, 7 days/week for 18 consecutive months. Necropsy was performed on-site both for animals that died and for those that survived up to termination of the study.

The results of this study showed a large gender difference in the overall incidence of lymphomas in these Eμ-Pim1 transgenic mice. The incidence in females was two to three times higher than in males. However, to compare results with the other two experiments, we will restrict our discussion to female mice. In females, incidence was 52% in cage controls, 44% in sham-exposed controls, 36% at 0.5 W/kg, 60% at 1.4 W/kg, and 40% at 4.0 W/kg. The results for malignant lymphoma (lymphoblastic and non-lymphoblastic) did not show any relationship to GSM-900 exposure. In females, the combined incidence of malignant lymphoma was 46.4% (116/250). Non-lymphoblastic lymphoma (mainly pleomorphic and follicular) was the prevailing type of lymphoma, similar to that of the Repacholi et al. [1] and Utteridge et al. [3] studies.

It was reported that for all tumors, there was no significant difference in the number of animals with tumors (incidence of tumors), regardless of malignancy. However, the number of mice with tumors was about 20% higher in the cage controls than in the sham or any of the exposed groups. The incidence of benign tumors in females did not show any significant differences among the various groups. However, the incidence was reduced by 34% at 4.0 W/kg for females.

At the end of the experiment, the incidence of lymphomas in decedents was 42% (cage controls), 41% (sham controls), 16.6% (0.5 W/kg), 37.5% (1.4 W/kg), and 37.5% (4.0 W/kg) in females. Thus, the data did not show any increase in lymphomas in the exposed animals. In females, the only significant finding on survival was a reduction in time to death at 0.5 W/kg ($P < 0.05$).

Oberto et al. indicated that their study did not confirm the finding of a 2.0-2.4-fold increase in lymphomas by Repacholi et al. Indeed, they consider the finding by Repacholi et al. [1] to be incidental. Oberto et al. [10] claimed that the culprit was the low tumor rates of the female Eμ-Pim1 transgenic mice used for sham controls. In the study by Repacholi et al., only 22% of the sham-control mice had lymphomas, whereas 44% of the sham-control female mice in their 18-month study had lymphomas.

While all three studies used Eμ-Pim1 transgenic female mice and GSM-900 RF fields, they may be characterized at best as attempts to confirm or refute, rather than replicate, the earlier study. First, the exposure systems and protocols were different. Mice were free-roaming, not restrained, in a plane-wave exposure field for the initial study, but the Utteridge et al. and Oberto et al. studies used restrained animals in plastic tubes placed in radial waveguides for exposure. The tumor incidence varied among all three studies. Cage-control data was available only from the Oberto et al. study, which exhibited a tumor incidence of 52%. The reported incidences of lymphomas in the sham controls were 22%, 74%, and 44% for the Repacholi et al., Utteridge et al., and Oberto et al. studies, respectively. (Since sham-control mice in Repacholi et al. were free-roaming, not restrained, it might be reasonably compared to the 52% in cage-controls of Oberto et al.) Clearly, the incidence of lymphomas among the sham controls varied widely. Moreover, the restraining and sham exposure of mice were supposedly the same for the Utteridge et al. and Oberto et al. studies, but they presented totally different rates of tumor incidence, thus rendering a realistic comparison between and among these studies difficult, if not impossible. These flaws – possibly in the sourcing or

handling of mice or in the fundamental design of the experiments – limit the conclusions that can be drawn.

References

1. M. H. Repacholi, A. Basten, V. Gebski, D. Noonan, J. Finnie, and A. W. Harris, "Lymphomas in Eu-Pim1 Transgenic Mice Exposed to Pulsed 900 MHz Electromagnetic Fields," *Radiation Research*, **147**, 1997, pp. 631-640.

2. J. C. Lin "Cellular-Phone Radiation Effects on Cancer in Genetically Modified Mice," *IEEE Antennas and Propagation Magazine*, **44**, 6, December 2002, pp. 165-168.

3. T. D. Utteridge, V. Gebski, J. W. Finnie, B. Vernon-Roberts, and T. R. Kuchel, "Long-Term Exposure of E-mu-Pim1 Transgenic Mice to 898.4 MHz Microwaves does not Increase Lymphoma Incidence," *Radiation Research*, **158**, 2002, pp. 357-364.

4. T. D. Utteridge, V. Gebski, J. W. Finnie, B. Vernon-Roberts, and T. R. Kuchel, "Response to the Letters to the Editor sent by (1) Kundi, (2) Goldstein/Kheifets/van Deventer/Repacholi, and (3) Lerchl (2003)," *Radiation Research*, **159**, 2003, pp. 277-278.

5. M. Kundi, "Comments on 'Long-Term Exposure of Em-Pim1 Transgenic Mice to 898.4 MHz Microwaves does not Increase Lymphoma Incidence' by Utteridge et al., (Radiat. Res. 158, 357-364 2002)," *Radiation Research*, **159**, 2003, p. 274.

6. A. Lerchl, "Comments on the Recent Publication on Microwave Effects on Em-Pim1 Transgenic Mice (Utteridge et al., Radiat. Res. 158, 357-364 2002)," *Radiation Research*, **159**, 2003, p. 276.

7. L. S. Goldstein, L. Kheifets, E. van Deventer, and M. Repacholi, "Comments on 'Long-Term Exposure of Em-Pim1 Transgenic Mice to 898.4 MHz Microwaves does not Increase Lymphoma Incidence' by Utteridge et al.,' (Radiat. Res. 158, 357-364 2002)," *Radiation Research*, **159**, 2003, pp. 275-276.

8. M. Kundi, "Comments on the Responses of Utteridge et al. Radiat. Res. 159, 277-278 (2003) to Letters about their Paper, Radiat. Res. 158, 357-364, (2002)," *Radiation Research*, **160**, 5, November 2003, pp. 613-614.

9. A. Faraone, W. Luengas, S. Chebrolu, M. Ballen, G. Bit-Babik, A. V. Gessner, M. Y. Kanda, T. Babij, M. L. Swicord, and C. K. Chou, "Radiofrequency Dosimetry for the Ferris-Wheel Mouse Exposure System," *Radiation Research*, **165**, 1, 2006, pp. 105-112.

10. G. Oberto, K. Rolfo, P. Yu, M. Carbonatto, S. Peano, N. Kuster, S. Ebert, and S. Tofani, "Carcinogenicity Study of 217 Hz Pulsed 900 MHz Electromagnetic Fields in *Pim1* Transgenic Mice," *Radiation Research,* **168**, 2007, pp. 316-326.

Conferences

CONFERENCE REPORT

2008 Conference on Precision Electromagnetic Measurements (CPEM 2008)

Broomfield, Colorado, USA, 8 - 13 June 2008

Scope

CPEM 2008 will examine the close interrelation between science and metrology. New science and technology often foster major improvements in metrology. Similarly new metrology often leads to vast improvements in scientific understanding. CPEM 2008 will include plenary and invited talks about new science that is likely to have a future impact on metrology as well as still emerging examples such as the Josephson effect, the quantum Hall effect, trapped ions, and frequency combs. This theme will carry thorough to tours of the NIST Boulder Laboratories. Suggestions for topics and speakers will be warmly welcomed.

Topics

A major focus of this conference is quantum devices that relate electrical standards to fundamental constants and the international system of units.

- Electromagnetic metrology standards and techniques ranging from dc through optical frequencies
- Definitions of the SI units
- Advanced instrumentation
- International compatibility of measurement systems.

James K. Olthoff , Chief, Quantum Electrical Metrology Division, is the chairman of the meeting. He can be contacted at james.olthoff@nist.gov. Visit www.icpem.org/2008 for more information.

3rd VERSIM Workshop 2008

Tihany, Hungary, 15 - 20 September 2008

Topics

Scientific focus of the 3nd VERSIM Workshop

- ELF/VLF waves as diagnostic tools for key ionospheric and magnetospheric physical parameters
- Schumann resonances, world wide lightning activity and climate changes
- Triggered Emissions and Nonlinear wave phenomena
- VLF waves and the radiation belts (acceleration and loss)
- Effects of ELF/VLF radiation on the atmosphere (lightning/sprites, etc)
- Instrumentation (as a poster session)

These represent many of the core-scientific areas of the VERSIM Working group:

- Wave propagation in magnetosphere and ionosphere and in Earth-Ionosphere waveguide
- Plasma structures and boundaries - morphology and dynamics
- Wave-particle and nonlinear wave-wave interactions
- Wave-induced particle precipitation
- Sprites and the effects of lightning on the ionosphere

Abstracts

Abstracts of around 200 words should be sent to János Lichtenberger at ELTE-SRG before **Sunday, 8th June 2008**. These will be considered for oral (preferred) or poster (if necessary) presentation, by the Scientific Committee.

The Scientif Committee consists of D. Carpenter, M. Clilverd, Cs. Ferencz, J. Manninen, Y. Omura, O. Santolik and D. Shklyar. We are seeking sponsors to offer grants to PhD students and participants coming from developing countries.

Contact

János Lichtenberger (chairman)
Space Research Group,Eötvös University
Budapest, Pf 32 H-1518 HUNGARY
Tel: +36-1-372 2934, Fax: +36-1-372 2927
Email: versim2008@sas.elte.hu
Web site: http://sas2.elte.hu/versim

URSI CONFERENCE CALENDAR

An up-to-date version of this Conference Calendar, with links to various conference web sites can be found at www.ursi.org/Calendar of supported meetings.

May 2008

META'08, NATO Advanced Research Workshop:Metamaterials for Secure Information and Communication Technologies
Marrakesh, Morocco, 7 - 10 May 2008
cf. Announcement in the Radio Science Bulletin of June 2007, p. 57.
Contact: Prof. Saïd Zouhdi, Laboratoire de Génie Electrique de Paris (LGEP-Supélec), Plateau de Moulon, 91192 Gif-Sur-Yvette Cedex, France, Tel: +33 1 69851660, Fax: +33 169418318, Email: said.zouhdi@supelec.fr, Web site: http://meta.lgep.supelec.fr

9th International Workshop on Finite Elements in Microwave Engineering
Bonn, Germany, 8 - 9 May 2008
cf. Announcement in the Radio Science Bulletin of September 2007, p. 55.
Contact: FEM2008 Secretariat, c/o Theoretische Elektrotechnik, Saarland University, Building C63, P.O. Box 151150, D-66041 Saarbrucken, Germany, Tel: +49 681 302 2551, Fax: +49 681 302 3157, Web: http://www.lte.uni-saarland.de/fem2008

IES2008 - 12th International Ionospheric Effects Symposium
Alexandria, Virginia, USA, 13-15 May 2008
Contact : JMG Associates Ltd., IES Symposium Managers, 8310 Lilac Lane, Alexandria VA 22308, USA, Fax: +1-703-360-3954, Web : http://www.ies2008.com/index.html

ISEA-12 - 12th International Symposium on Equatorial Aeronomy
Crete, Greece, 18 - 24 May 2008
Contact: Christos Haldoupis, Physics Department, University of Crete, Heraklion, Crete 71003, Greece, Tel: +30 2810 394222, Fax: +30 2810 394201, Email: isea12@physics.uoc.gr, chald@physics.uoc.gr, Web: http://isea12.physics.uoc.gr/

June 2008

ClimDiff 2008
Boulder, Colorado, USA, 3-4 June 2008
Contact: Mrs. Carol Wilson, CSIRO ICT Centre, P.O. Box 76, Epping NSW 1710, Australia, Fax: +61 2 9372 4490, Email: carol.wilson@csiro.au, htpp://www.its.bldrdoc.gov/ClimDiff/Climdiff_call_for_papers_v3.pdf

2008 Conference on Precision Electromagnetic Measurements (CPEM 2008)
Broomfield, CO, USA, 8-12 June 2008
cf. Announcement in the Radio Science Bulletin of March 2008, p. 45.
Contact: James K. Olthoff, NIST,100 Bureau Drive, MS 8170, Gaithersubrg, MD 20899 USA, Tel: 301-975-2431 Fax: 3019263972, Email: james.olthoff@nist.gov, Web: http://www.icpem.org/2008.

July 2008

COSPAR 2008 - 37th Scientific Assembly of the Committee on Space Research and Associated Events "50th Anniversary Assembly"
Montreal, Canada, 13 - 20 July 2008
cf. Announcement in the Radio Science Bulletin of March 2007, p. 58.
Contact : COSPAR Secretariat, c/o CNES, 2 place Maurice Quentin, 75039 Paris Cedex 01, France, Tel: +33 1 44 76 75 10, Fax: +33 1 44 76 74 37, E-mail : cospar@cosparhq.cnes.fr, Web : http://www.cospar2008.org

EUROEM 2008 - European Electromagnetics
Lausanne, Switzerland, 21-25 July 2008
Contact : EUROEM'08, EPFL-STI- LRE, Station 11, CH-1015 Lausanne, Switzerland, Tel : +41-21-693 26 20, Fax : +41-21-693 46 62, E-mail: information@euroem.org, Web : http://www.euroem.org

August 2008

URSI GA08 - XXIXth URSI General Assembly
Chicago, IL, USA, 9-16 August 2008
Contact : URSI Secretariat, c/o INTEC, Ghent University, Sint-Pietersnieuwstraat 41, B-9000 Ghent, Belgium, Tel. : +32 9 264 3320, Fax : +32 9 264 4288, E-mail : info@ursi.org

ICWCUCA - Second International Conference on Wireless Communications in Underground and Confined Areas
Val-d'Or, Canada, 25-27 August 2008
Contact: Laboratoire de recherche Télébec Mobilité en communications souterraines (LRTCS), International Conference on Wireless Communications in Underground and Confined Areas (ICWCUCA), 450, 3e avenue, local 103, Val-d'Or (Québec) J9P 1S2, Canada, TEl: +1 819 874 7400, Fax: +1 819 874 7166, Email: lrcs@uqat.ca, Web: http://www.icwcuca.ca

September 2008

EMC Europe 2008
Hamburg, Germany, 8 - 12 September 2008
Contact: EMC Europe 2008, Harburger Schlossstrasse 6 - 12, 21079 Hamburg, Germany, Tel: +49 40 76629 6551, Fax: +49 4076629 6559, Email: info@emceurope2008.org, Web: http://www.emceurope2008.org

Metamaterials 2008 - 2nd International Congress on Advanced Electromagnetic Materials in Microwaves and Optics
Pamplona, Spain, 21-26 September 2008
Contact: http://congress2008.metamorphose-vi.org

November 2008

Microwave 2008 - International Conference on Recent Advances in Microwave Theory and Applications
Jaipur, India, end of November 2008
Contact: Dr. Deepak Bhatnagar, Department of Physics, University of Rajasthan, Jaipur, 302004, India, Fax: +91 1412 702645, Email: dbhatnagar_2000@rediffmail.com, Web: http://www.uniraj.ernet.in

URSI cannot be held responsible for any errors contained in this list of meetings

News from the URSI Community

NEWS FROM A MEMBER COMMITTEE

INDIA

National Conference on Engineering Education

Dedicated to the Memory of Dr. A.P. Mitra

AdisaptagramWest Bengal, India, 9 - 10 February 2008

The National Conference on Engineering Education (NCEE-2008) was held in the campus of the Academy of Technology, Adisaptagram, West Bengal, INDIA, during 09-10 February 2008. The National Organizing Committee organized the Conference. There were 72 registered participants from all over India, 40 papers were presented and 110 graduate students attended. The NCEE- 2007 was held in the same campus and Dr. A.P. Mitra inaugurated it on 10 February 2007. Dr Mitra also inaugurated the B.N. Biswas Centre for Information and Communication Technology of the Academy of Technology during that period. We lost him on 03 September 2007, an unforgettable and irreparable loss to all of us.

The Conference was opened in the morning of 09 February 2008. In his welcome address, Professor Dilip Bhattacharya Director of Academy of Technology touched upon the challenges of the engineering education confronted with and stressed the need for sustained efforts through seminars, conference, debates plenary sessions for meeting the changing requirements and developmental challenges. Professor Bhattacharya acquainted the participants about the infrastructures and facilities available at this Institute and further mentioned the achievements of the students and faculty of the institute, noteworthy among them was Young Scientist Award (2005) of URSI won by Dr. Apala Bhattacharya and Mr. S.Chatterjee. Professor J. Banerjee CEO expressed his imagination in establishing this institute as a centre of excellence to impart leadership in research and recalled Michael Faraday's definition for centre of excellence as "a place where second class people may perform first class work".

Professor B.N. Biswas, Chairman of the NCEE-2008 stressed the need of organizing a national He said "Reading is not learning, /Learning is not teaching, /Teaching is not following a familiar routine, /Following a familiar routine is not an understanding, /Understanding is the best." In support of this he quoted famous experiment with a group of caterpillars by the renowned naturalist Jean Henri Fabri. He advised the young participants not to risk becoming like caterpillars and consequently become victims of following a familiar routine.

Dr K.N. Shankara, Padmashree, Director, ISRO Satellite Centre, Bangalore, delivered the inaugural speech. Dr Shankara highlighted Indian Space Programme for National Development. This was followed by a keynote address by Professor R. Mukherjee, former Vice-Chancellor and Vivekananda Professor, Ramakrishna Mission Institute of Culture, Kolkata. Professor Mukherjee explained the role of humanities in engineering education. He referred to the advice of the great Swami Vivekananda to the society to study the 'within' and 'without' of nature.

A special session to the memory Dr A P Mitra, chaired by Professor R Mukherji, was organized. Professor N B Chakrabarti, Kharagpur IIT, Professor S.C. Dutta Roy, Delhi IIT and Dr P Banerjee, National Physical Laboratory, New Delhi discussed various aspects on the life and works of Dr. A.P. Mitra. In this occasion a student-paper contest was held. Fourteen papers were presented which a team of experts adjudicated. Certificates of merit were awarded to first three papers.

The entire schedule of the conference was divided into: Special Lectures, Tutorial Lecture, Session-I, Session-II, Session-III and Session-IV. These sessions were equally divided during the two days of the conference. Among the special lectures reference may be made to: Software Defined Radio by Professor N.B. Chakrabarti of Kharagpur IIT. This topic assumed a special significance in view of the XXIX GA of URSI's thrust on Cognitive Radio. In view of the country's shortage of teaching personnel the lecture on Teaching and Research as Career Options by Professor S.C. Dutta Roy of Delhi IIT is timely and important. Two special lectures on engineering educations, namely, Industry Academic Convergence to bridge Skills Gap and meet the Shortage in the Manufacturing and Services Sector by Professor A Chakraborty Kharagpur, IIT, and Engineering Education in 21st Century: The Changing Scenario & Some Suggestions, by Professor B. Gupta of Jadavpur University, were presented. Was organized another session of special lectures on frontier areas with the following topics: Governance and Mobile Communication by Dr S Gupta of West Bengal Industrial Development Corporation, Surface Plasmon Polariton and Sub-wave Length Photonics by Professor P K Saha of Calcutta University, Role of Engineering College students and Teachers in Microwave Tube Research in the Country by Professor B N Basu of Beneras Hidu University, Accuracy of GPS Time by Dr P Banerjee of National Physical Laboratory, Recent Development in Integrated Circuit Technology by Professor C Sarkar of The of Quantum Dots for Seeing in the Dark by Professor N R Das of Calcutta University.

Professor S C Dutta Roy of Delhi IIT delivered a tutorial lecture on Fun with Circuit Theory inviting attention to few fundamental unsolved paradoxes in network theory.

In order to provide a kind of "dramatic relief" to the participants at the end of the first day's schedule a cultural program was organized by the students of the Academy of Technology for the pleasure of the invited guests, participants and the members of the Academy. The conference was successful in focusing on the need and modalities of attracting the brightest young minds to the teaching and research profession – pinpointing the positive points of this profession as compared to others. The deliberation in the different sessions encouraged students and faculties to appreciate the need of innovation and creativity in engineering education and pleasure of working in the frontier areas. It also successfully established the fact that conference is the ideal screen on which academic activities of the past and present can be projected and viewed. National organizing Committee is thankful to different sections of IEEE (Kolkata Chapters) to AICTE, ISRO, CSIR and IETE (Kolkata) for sponsoring the conference. The Committee is immensely grateful to URSI for giving moral support in holding this conference. For more about the information of the Academy of technology and to access institute material please visit, www.actechindia.org.

Professor B N Biswas
baidyanathbiswas@yahoo.com

IN MEMORIAM

Wilbur Norman Christiansen
1913 - 2007

W. N. Christiansen (Chris) was an innovative and influential pioneer in world radio astronomy. He died April 26, 2007.

Born in Melbourne, Australia on August 9, 1913, Chris graduated BSc in 1934 and MSc with First Class Honors in 1935 from the University of Melbourne. He was awarded the Dwight Prize in Physics in 1931 and the Kernot Prize in 1934. He graduated Doctor of Science at Melbourne University in 1953.

While a graduate student at Melbourne in 1935, he discovered, with Crabtree and Laby, that "light" and "heavy" water could be separated by fractional distillation, indicating that special measures must be taken in purifying water prior to analyzing its isotopic content.

In 1937, after a two-year appointment with the Commonwealth X-ray and Radium Laboratory, he joined Builder and Green, pioneers in ionospheric research, at the AWA Ltd. Research Laboratory in Sydney, where his major work was concentrated on the design of stacked rhombic antennas for overseas short-wave communications. Published in the *AWA Technical Review*, this work appeared subsequently in the CCIR "High Frequency Directional Antennae" Handbook and was widely referenced. The Overseas Telecommunications Commission, AWA's successor in operating the shortwave services, made extensive use of the designs.

In 1948, Christiansen joined Joe Pawsey's radio astronomy group at the Radiophysics Division of CSIRO. He became involved in solar radio astronomy, and organized observations of two partial solar eclipses at a wavelength of 50 cm. These observations showed that regions of the sun of high radio emission (associated with sunspots) had dimensions about one-tenth of the solar diameter. The discovery led to the development of the "grating array," which achieved high resolution from its length, and produced multiple responses on the sky separated by a number of solar diameters. The first grating telescope (1951) at Potts Hill allowed the distribution of radio brightness across the sun to be studied as the sun drifted through the responses during the day. It was found that the enhanced emissions came from regions in the lower corona of the sun. Their dimensions and height above the photosphere could be determined for the first time.

A second investigation concerned the background or "quiet sun" radiation. Christiansen, with Warburton, made use of two gratings, one in an east-west and one in a north-south direction, to observe the sun from dawn until dusk. They obtained the two-dimensional brightness distribution from these observations. This approach was an early application of Earth-rotational synthesis to produce, for the first time, a radio map with a resolution as fine as four minutes of arc.

A new instrument, which combined the grating with the Mills Cross principle, was subsequently built at the Fleurs field station. Known as the "Chris Cross," the telescope provided daily two-dimensional maps of the sun with a resolution of 3 arc minutes, from 1957 onwards. It was the first of a number of similar instruments built around the world.

In 1952, Christiansen and Hindman confirmed the discovery by Ewen of 21 cm line radiation from ground-state hydrogen in space, and went on to make the first survey of H-line emission from space, obtaining the first radio evidence of the existence of spiral arms in our galaxy.

During this period at CSIRO (1948-59), Chris was awarded the Syme Prize for Research by the University of Melbourne. A paper describing the design of the Grating Cross received the Fleming Premium of the Institution of Electrical Engineers in 1961.

In 1960, Chris was appointed to the Chair of Electrical Engineering at the University of Sydney. He did not take up his post immediately, but spent 15 months at Leiden University as the leader of an international design team for the "Benelux Cross Project." This project was abandoned, but Chris maintained an active collaboration with the Dutch group, developing the Westerbork Telescope.

Back in Sydney, he attempted, unsuccessfully, to gain financial support to build a 30 m diameter "hole-in-the-ground" spherical reflecting telescope for use at millimeter wavelengths. He then requested that CSIRO donate its field

station at Fleurs, where his grating cross was situated, to the University of Sydney. This was agreed to, and he set about changing this instrument from a low-sensitivity, 3-arc-min resolving power instrument, designed for solar observations, into a high-resolution rotational-synthesis telescope. As the Fleurs Synthesis Telescope, it would be used for galactic and extra-galactic astronomical observations. Over a period of more than 15 years, it was to be an important test bed for electrical engineering PhDs, and a critical training ground for the next generation of engineers in Australian radio astronomy. These engineers played key roles the design of the Australia Telescope and the SKA, as well as a number of overseas instruments. Chris had a strong belief in the benefit for students of working on large complex projects in a team environment.

In addition to the work in radio astronomy, Chris established a research group to tackle problems in the radio navigation of civil aircraft. This group earned a considerable reputation internationally.

From the mid-sixties, Chris was involved with the design and construction of a large grating telescope (later to become a rotational-synthesis instrument) in Peking. He spent many months with the young radio astronomy group of the Peking Observatory, and also, at various stages, had groups of Chinese radio astronomers working with him in Sydney.

In 1969, Chris published a book called *Radiotelescopes* with Swedish astronomer Jan Högbom, who had worked with him in Leiden. It was published by Cambridge University Press. A Russian translation appeared in 1971.

He was awarded the Peter Nicol Russell Medal, the premium award of the Institution of Engineers Australia, in 1970, and the medal of ADION from the Nice Observatory in France, in 1976.

He took on significant roles with the international scientific unions. He served as a Vice President of the International Astronomical Union (IAU) from 1964 to 1970, President of the Radio Astronomy Commission of the International Union for Radio Science (URSI) from 1963 to 1966, Vice President of URSI from 1972 to 1978, and then President, from 1978 to 1981. He was a member of the General Committee of the International Council of Scientific Unions from 1978 to 1981.

In Australia, he served on a number of Committees. In the Academy of Science, he was Foreign Secretary (1981-85), had served on the Council for two terms, was Chairman of several committees of the Academy, including Chairman of the National Committee for Radio Science from 1962-70. He was President of the Astronomical Society of Australia 1977-79.

He was the Independent Technical Advisor to the Committee of Inquiry into Radio Australia, and was a member of the Australia-China Council of the Department of Foreign Affairs. He was a UNESCO Consultant in India on the Project for the construction of a "Giant Equatorial Radiotelescope."

Chris was an Honorary Fellow of the Institution of Engineers, Australia, and a Fellow of the Institution of Electrical Engineers (UK), the Institution of Radio and Electronic Engineers (Australia), the Institute of Physics (UK), the Australian Institute of Physics, and the Royal Astronomical Society (UK).

On retirement in 1979 from the Chair of Electrical Engineering at the University of Sydney, Chris was given the title of Professor Emeritus, and later awarded the degree of Doctor of Science in Engineering, honoris causa. He was a visiting Fellow at the Mount Stromlo Observatory of the Australian National University from 1980 to 1985. He also received honorary degrees from the University of Melbourne (1982) and the University of Western Sydney (1994), and was elected a Fellow of the Chinese Academy of Science in 1996.

Chris Christiansen is survived by his sons, Steve and Tim. His wife, Elspeth, died in 2001. Their son Peter died in 1992.

Bob Frater
ResMed Ltd.
1 Elizabeth Macarthur Drive
Bella Vista NSW 2153 Australia
E-mail: BobF@resmed.com.au

Wireless Networks

The journal of mobile communication, computation and informa-

The Journal of Atmospheric and Solar-Terrestrial Physics

SPECIAL OFFER TO URSI RADIOSCIENTISTS

AIMS AND SCOPE

The *Journal of Atmospheric and Terrestrial Physics* (JASTP) first appeared in print in 1951, at the very start of what is termed the "Space Age". The first papers grappled with such novel subjects as the Earth's ionosphere and photographic studies of the aurora. Since that early, seminal work, the Journal has continuously evolved and expanded its scope in concert with - and in support of - the exciting evolution of a dynamic, rapidly growing field of scientific endeavour: the Earth and Space Sciences. At its Golden Anniversary, the now re-named *Journal of Atmospheric and Solar-Terrestrial Physics* (JASTP) continues its development as the premier international journal dedicated to the physics of the Earth's atmospheric and space environment, especially the highly varied and highly variable physical phenomena that occur in this natural laboratory and the processes that couple them. The *Journal of Atmospheric and Solar-Terrestrial Physics* is an international journal concerned with the inter-disciplinary science of the Sun-Earth connection, defined very broadly. The journal referees and publishes original research papers, using rigorous standards of review, and focusing on the following: The results of experiments and their interpretations, and results of theoretical or modelling studies; Papers dealing with remote sensing carried out from the ground or space and with in situ studies made from rockets or from satellites orbiting the Earth; and, Plans for future research, often carried out within programs of international scope. The Journal also encourages papers involving: large scale collaborations, especially those with an international perspective; rapid communications; papers dealing with novel techniques or methodologies; commissioned review papers on topical subjects; and, special issues arising from chosen scientific symposia or workshops. The journal covers the physical processes operating in the troposphere, stratosphere, mesosphere, thermosphere, ionosphere, magnetosphere, the Sun, interplanetary medium, and heliosphere. Phenomena occurring in other "spheres", solar influences on climate, and supporting laboratory measurements are also considered. The journal deals especially with the coupling between the different regions. Solar flares, coronal mass ejections, and other energetic events on the Sun create interesting and important perturbations in the near-Earth space environment. The physics of this subject, now termed "space weather", is central to the Journal of Atmospheric and Solar-Terrestrial Physics and the journal welcomes papers that lead in the direction of a predictive understanding of the coupled system. Regarding the upper atmosphere, the subjects of aeronomy, geomagnetism and geoelectricity, auroral phenomena, radio wave propagation, and plasma instabilities, are examples within the broad field of solar-terrestrial physics which emphasise the energy exchange between the solar wind, the magnetospheric and ionosphericplasmas, and the neutral gas. In the lower atmosphere, topics covered range from mesoscale to global scale dynamics, to atmospheric electricity, lightning and its effects, and to anthropogenic changes. Helpful, novel schematic diagrams are encouraged. Short animations and ancillary data sets can also be accommodated. Prospective authors should review the *Instructions to Authors* at the back of each issue.

Complimentary Information about this journal:
http://www.elsevier.com/locate/JASTP?
http://earth.elsevier.com/geophysics

Audience:
Atmospheric physicists, geophysicists and astrophysicists.

Abstracted/indexed in:
CAM SCI Abstr
Curr Cont SCISEARCH Data
Curr Cont Sci Cit Ind
Curr Cont/Phys Chem & Sci
INSPEC Data
Meteoro & Geoastrophys Abstr
Res Alert

Editor-in-Chief:
T.L. Killeen, National Centre for Atmospheric Research, Boulder, Colorado, 80307 USA

Editorial Office:
P.O. Box 1930, 1000 BX Amsterdam, The Netherlands

Special Rate for URSI Radioscientists 2003:
Euro 149.00 (US$ 149.00)
Subscription Information
2002: Volume 65 (18 issues)
Subscription price: Euro 2659 (US$ 2975)
ISSN: 1364-6826

CONTENTS DIRECT:
The table of contents for this journal is now available pre-publication, via e-mail, as part of the free ContentsDirect service from Elsevier Science. Please send an e-mail message to cdhelp@elsevier.co.uk for further information about this service.

For ordering information please contact Elsevier Regional Sales Offices:

Asia & Australasia/ e-mail: asiainfo@elsevier.com
Europe, Middle East & Africa: e-mail: nlinfo-f@elsevier.com
Japan: Email: info@elsevier.co.jp
Latin America : e-mail: rsola.info@elsevier.com.br
United States & Canada : e-mail: usinfo-f@elsevier.com

Information for authors

Content

The *Radio Science Bulletin* is published four times per year by the Radio Science Press on behalf of URSI, the International Union of Radio Science. The content of the *Bulletin* falls into three categories: peer-reviewed scientific papers, correspondence items (short technical notes, letters to the editor, reports on meetings, and reviews), and general and administrative information issued by the URSI Secretariat. Scientific papers may be invited (such as papers in the *Reviews of Radio Science* series, from the Commissions of URSI) or contributed. Papers may include original contributions, but should preferably also be of a sufficiently tutorial or review nature to be of interest to a wide range of radio scientists. The *Radio Science Bulletin* is indexed and abstracted by INSPEC.

Scientific papers are subjected to peer review. The content should be original and should not duplicate information or material that has been previously published (if use is made of previously published material, this must be identified to the Editor at the time of submission). Submission of a manuscript constitutes an implicit statement by the author(s) that it has not been submitted, accepted for publication, published, or copyrighted elsewhere, unless stated differently by the author(s) at time of submission. Accepted material will not be returned unless requested by the author(s) at time of submission.

Submissions

Material submitted for publication in the scientific section of the *Bulletin* should be addressed to the Editor, whereas administrative material is handled directly with the Secretariat. Submission in electronic format according to the instructions below is preferred. There are typically no page charges for contributions following the guidelines. No free reprints are provided.

Style and Format

There are no set limits on the length of papers, but they typically range from three to 15 published pages including figures. The official languages of URSI are French and English: contributions in either language are acceptable. No specific style for the manuscript is required as the final layout of the material is done by the URSI Secretariat. Manuscripts should generally be prepared in one column for printing on one side of the paper, with as little use of automatic formatting features of word processors as possible. A complete style guide for the *Reviews of Radio Science* can be downloaded from http://www.ips.gov.au/IPSHosted/NCRS/reviews/. The style instructions in this can be followed for all other *Bulletin* contributions, as well. The name, affiliation, address, telephone and fax numbers, and e-mail address for all authors must be included with all submissions.

All papers accepted for publication are subject to editing to provide uniformity of style and clarity of language. The publication schedule does not usually permit providing galleys to the author.

Figure captions should be on a separate page in proper style; see the above guide or any issue for examples. All lettering on figures must be of sufficient size to be at least 9 pt in size after reduction to column width. Each illustration should be identified on the back or at the bottom of the sheet with the figure number and name of author(s). If possible, the figures should also be provided in electronic format. TIF is preferred, although other formats are possible as well: please contact the Editor. Electronic versions of figures *must* be of sufficient resolution to permit good quality in print. As a rough guideline, when sized to column width, line art should have a minimum resolution of 300 dpi; color photographs should have a minimum resolution of 150 dpi with a color depth of 24 bits. 72 dpi images intended for the Web are generally *not* acceptable. Contact the Editor for further information.

Electronic Submission

A version of Microsoft *Word* is the preferred format for submissions. Submissions in versions of T_EX can be accepted in some circumstances: please contact the Editor before submitting. *A paper copy of all electronic submissions must be mailed to the Editor, including originals of all figures.* Please do *not* include figures in the same file as the text of a contribution. Electronic files can be send to the Editor in three ways: (1) By sending a floppy diskette or CD-R; (2) By attachment to an e-mail message to the Editor (the maximum size for attachments *after* MIME encoding is about 7 MB); (3) By e-mailing the Editor instructions for downloading the material from an ftp site.

Review Process

The review process usually requires about three months. Authors may be asked to modify the manuscript if it is not accepted in its original form. The elapsed time between receipt of a manuscript and publication is usually less than twelve months.

Copyright

Submission of a contribution to the *Radio Science Bulletin* will be interpreted as assignment and release of copyright and any and all other rights to the Radio Science Press, acting as agent and trustee for URSI. Submission for publication implicitly indicates the author(s) agreement with such assignment, and certification that publication will not violate any other copyrights or other rights associated with the submitted material.

APPLICATION FOR AN URSI RADIOSCIENTIST

I have not attended the last URSI General Assembly, and I wish to remain/become an URSI Radioscientist in the 2006-2008 triennium. Subscription to *The Radio Science Bulletin* is included in the fee.

(please type or print in BLOCK LETTERS)

Name: Prof./Dr./Mr./Mrs./Ms. _____
Family Name *First Name* *Middle Initials*

Present job title: _____

Years of professional experience: _____

Professional affiliation: _____

I request that all information, including the bulletin, be sent to my ☐ home ☐ business address, i.e.:

Company name: _____

Department: _____

Street address: _____

City and postal / zip code: _____

Province / State: _____ Country: _____

Phone: _____ ext: _____ Fax: _____

E-mail: _____

Areas of interest (please tick)

☐ A Electromagnetic Metrology
☐ B Fields and Waves
☐ C Signals and Systems
☐ D Electronics and Photonics
☐ E Electromagnetic Noise & Interference
☐ F Wave Propagation & Remote Sensing
☐ G Ionospheric Radio and Propagation
☐ H Waves in Plasmas
☐ J Radio Astronomy
☐ K Electromagnetics in Biology & Medicine

The fee is 50 Euro.
(The URSI Board of Officers will consider waiving of the fee if the case is made to them in writing)

Method of payment: VISA / MASTERCARD (we do not accept cheques)

Credit Card No ☐☐☐☐ ☐☐☐☐ ☐☐☐☐ ☐☐☐☐ Exp. date: _____

Date: _____ Signed _____

Please return this signed form to:

The URSI Secretariat
c /o Ghent University / INTEC
Sint-Pietersnieuwstraat 41
B-9000 GENT, BELGIUM
fax (32) 9-264.42.88